

A New Spatio-Temporal Model Exploiting Hamiltonian Equations

Satyaki Mazumder¹, Sayantan Banerjee², and Sourabh Bhattacharya³

¹DMS, IISER Kolkata, Mohanpur

²Operations Management & Quantitative Techniques Area, IIM Indore

³Interdisciplinary Statistical Research Unit, ISI Kolkata

December 10, 2024

¹email: satyaki@iiserkol.ac.in

Contents

1	Introduction	1
2	Modified Hamiltonian equations and the proposed model	9
2.1	Modified Hamiltonian equations and the corresponding leap-frog algorithm	10
2.2	Proposed model	12
2.3	Completion of specification of the proposed spatio-temporal process and investigation of its theoretical properties	13
3	Calculation of likelihood functions	19
3.1	Joint conditional density of the observed data	20
3.2	Joint conditional density of latent data	21
3.3	Complete likelihood combining observed and latent data	21
4	Prior distributions	22
5	Full conditional distributions	23
6	Simulation Studies	26
6.1	Mixture of three Gaussian Processes	27
6.1.1	Data generation	27
6.1.2	Results from our model	28
6.2	Comparative study with nonstationary GP model	30
6.3	Mixture of two GQNs	31
6.3.1	Data generation	34
6.3.2	Results from our model	35
6.3.3	Comparative study with non-stationary GP model	39
7	Real data analysis	41
7.1	Alaska temperature data	42
7.1.1	Prior choices for the Alaska temperature data	44
7.1.2	Results of the Alaska temperature data	45
7.2	Sea surface temperature data	47
7.2.1	Prior choices for sea surface temperature data	49
7.2.2	Controlling M_s	50
7.2.3	Results of the sea surface temperature data	50
8	Summary and conclusion	52
A	Proofs of the theorems	53
B	Calculation of joint conditional density of the observed data	70
C	Calculation of the conditional joint density of latent data	71

D	Calculation of full conditional distributions of the parameters and the latent variables, given the observed data	73
D.1	Full conditional distribution of β^*	73
D.2	Full conditional distribution of α^*	74
D.3	Full conditional distribution of σ_θ^2	74
D.4	Full conditional distribution of σ_p^2	75
D.5	Full conditional distribution of σ^2	75
D.6	Full conditional distributions of η_1^* , η_2^* , and η_3^*	76
D.7	Full conditional distribution of \mathbf{x}_0	77
E	Algorithm for temporal prediction	77
F	Algorithm for prediction of time series at a spatial point	79
G	Supplementary plots for 3 component mixture of GPs	80
G.1	Trace plots	80
G.2	Posterior densities of the complete time series of the latent variables	81
H	Supplementary plots for mixture of GQNs	81
I	Supplementary plots for Alaska temperature data	85
I.1	Trace plots	85
I.2	Posterior densities of the complete time series of the latent variables	85
I.3	Posterior predictive densities for the year 2015 at 26 locations	85
I.4	Posterior predictive densities for the years 2016–2021 at 16 locations	85
J	Supplementary plots for sea temperature data	85
J.1	Trace plots	85
J.2	Predictive densities: latent variables	85
J.3	Predictive densities for 100th month for 30 locations	89
K	Stationarity, convergence of lagged correlations to zero and non-Gaussianity of the detrended Alaska data process	91
K.1	Stationarity of the detrended Alaska data process	91
K.2	Convergence of lagged spatio-temporal correlations to zero for the Alaska data	93
K.3	Non-Gaussianity of the Alaska data	93

Abstract

The solutions of Hamiltonian equations are known to describe the underlying phase space of a mechanical system. In this article, we propose a novel spatio-temporal model using a strategic modification of the Hamiltonian equations, incorporating appropriate stochasticity via Gaussian processes. The resultant spatio-temporal process, continuously varying with time, turns out to be nonparametric, non-stationary, non-separable, and non-Gaussian. Additionally, the lagged correlations converge to zero as the spatio-temporal lag goes to infinity. We investigate the theoretical properties of the new spatio-temporal process, including its continuity and smoothness properties. We derive methods for complete Bayesian inference using MCMC techniques in the Bayesian paradigm. The performance of our method has been compared with that of a non-stationary Gaussian process (GP) using two simulation studies, where our method shows a significant improvement over the non-stationary GP. Further, applying our new model to two real data sets revealed encouraging performance.

Keywords: Continuously varying time and space, Hamiltonian dynamics, Markov Chain Monte Carlo, Non-stationarity, Non-Gaussianity, Spatio-temporal modeling

1 Introduction

Modeling spatially and spatio-temporally dependent data has drawn much attention within the statistics community in the last few decades. A wide array of scientific areas produce spatio-temporal data, including meteorology, environment, and ecology. A significant amount of work has been done on spatial modeling, including hierarchical Bayesian models with applications to climate data, for example, see Jun et al. [2008], Furrer and Sain [2009], Tebaldi and Sansó [2009], Sain et al. [2011] among others. Results of different climate models concerning the increase in temperature for 22 different regions have been combined by Smith et al. [2009] using Bayesian methods, and Sang et al. [2011] built a hierarchical statistical model to combine multiple climate errors. Many spatio-temporal models are available for analyzing climate data. To provide a few examples, spatio-temporal models aiming at analyzing rainfall data have been proposed by Cox and Isham [1988], Sanso and Guenni [1999]. Sahu et al. [2010] proposed a hierarchical Bayesian space-time model with an application to wet deposition.

There is a wide body of literature that describes the use of several spatial and spatio-temporal models in environmental data, such as ozone level, particulate matter, sulfur dioxide, nitrogen oxide etc. Guttorp et al. [1994] did notable work in space-time analysis of ground level ozone data. A spatio-temporal model for interpolating and predicting ozone concentration in Mexico City was proposed by Huerta et al. [2004]. A simple yet popular non-stationary and non-separable spatio-temporal model for analyzing ozone data was proposed by Bruno et al. [2009]. Dou et al. [2010] compared two competing models in explaining hourly ozone concentration fields. The article by Paciorek et al. [2009] is one of the fundamental works in analyzing particulate matter concentration using a spatio-temporal model. Two notable works on sulfur dioxide con-

centration under the paradigm of spatio-temporal structure are Holland et al. [2000] and Giannitrapani et al. [2006]. Quite a few works are also done in explaining nitrogen oxide concentration via spatial and spatio-temporal models; see, for example, Beelen et al. [2013], Amini et al. [2016], and the references therein. Apart from the above applications, Deng et al. [2009] and Chakraborty et al. [2010] dealt with spatio-temporal models explaining ecological data. The above references are only a few amongst plenty of statistical works done on spatio-temporal modeling with application to varied fields.

There are two common assumptions that are employed while analyzing spatio-temporal data: (i) separability of the covariance function in space and time (for the definition of separability, see Chapter 11 of Banerjee et al. [2014]), and (ii) covariance stationarity. By covariance stationarity, we mean that the covariance of the observations at any two locations and time points is a function of the separation vector between the two locations and time points (Chapters 2 and 11 of Banerjee et al. [2014]). A special case of covariance stationarity, known as isotropic stationarity, is also typically assumed while analyzing spatial and spatio-temporal data. By isotropic stationarity, one implies that the covariance between two spatio-temporal observations is a function of the distance between the corresponding locations and time points (Chapters 2 and 11 of Banerjee et al. [2014]). However, in reality, assumptions of any stationarity can be artificial if there is local influence on the correlation structure (see, for example, Sampson and Guttorp [1992]). Indeed, the scenario of local influence is not uncommon in practice. Das and Bhattacharya [2023] and Roy and Bhattacharya [2020] showed that the PM10 pollution data set, analyzed by Paciorek et al. [2009], is not stationary. The same finding was established for a sea-temperature data set by Bhattacharya [2021]. Furthermore, Paciorek [2003] demonstrated that the erroneous assumption of a stationary covariance function would lead to an overly smoothed or inadequately

smoothed process. For a short review on the necessity of nonstationarity for modeling spatio-temporal data, we refer the readers to Chapter 9 of Gelfand et al. [2010].

Recently, several attempts have been made to incorporate nonstationarity in the underlying spatio-temporal process. Sampson and Guttorp [1992] first significantly contributed to capturing nonstationarity of the covariance function based on the idea of spatial deformation. This idea has been further exploited in the Bayesian paradigm by Damian et al. [2001] and Schmidt and O’Hagan [2003]. Kernel convolution technique was used by Higdon [1998], Higdon et al. [1999], Fuentes and Smith [2001], Higdon [2002], Fuentes [2002], Paciorek and Schervish [2006] to model nonstationarity of the underlying processes. Nonlinear, non-stationary, although parametric spatio-temporal models, were considered in Wikle and Hooten [2010]. A general framework, called a general nonlinear spatio-temporal framework, has been developed by Wikle and Hooten [2010], where a hierarchical Bayesian structure was provided with applications to ecology and oceanology. A significant amount of work has been done towards formulating non-stationary processes via the stochastic partial differential equation (SPDE) approach. The SPDE approach in modeling spatial data was first proposed by Lindgren et al. [2011]. Lindgren et al. [2011] proposed a continuous spatial process, a Gaussian field (GF) as a Gaussian Markov random field (GMRF), a discretely indexed spatial random field. The key ingredient was to use the fact that a GF with Matérn covariance kernel is the solution of a fractional SPDE (Chapter 6 of Blangiardo and Cameletti [2015]). Within the framework of the SPDE approach, the extension to the non-stationary covariance function can easily be done by varying the parameters of Matérn covariance kernel with the locations (Lindgren et al. [2011], Bolin and Lindgren [2011], Ingebrigtsen et al. [2014] and Blangiardo and Cameletti [2015]). A lucid review of the SPDE approach in modeling spatial and spatio-temporal data is provided

in Lindgren et al. [2022]. One major advantage of using the SPDE approach is the availability of INLA package in the statistical software R[Lindgren and Rue, 2015]. The INLA package can efficiently analyze spatial and spatio-temporal data using stationary and non-stationary processes via SPDE approach. The books Blangiardo and Cameletti [2015], Gómez-Rubio [2020] and the website r-inla.org/home provide a detailed overview of the package INLA. Another advantage of the SPDE approach is that it can be applied to data sets with large number of locations and time points as it deals with sparse matrices (see Chapter 6 of Blangiardo and Cameletti [2015]). In a different direction, with the help of Dirichlet process, Gelfand et al. [2005] attempted to model the underlying spatial process nonparametrically along with “conditional” non-stationarity. Furthermore, a nonparametric and non-stationary model was proposed by Fuentes and Reich [2013] using kernel process mixing. A discretized version of a stochastic differential equation was considered by Duan et al. [2009] to model spatio-temporal nonstationarity. Recently, Driver and Voelkle [2018] proposed a hierarchical Bayesian approach for estimating continuous time dynamic but parametric models via stochastic differential equations.

In the above-mentioned works, the following aspects can be noticed. The underlying process is Gaussian (may be non-stationary) or parametric, or the correlation between the two spatio-temporal points do not converge to zero as the distance between the two points (locations and/or time points) increases to infinity (as also borne out by our simulation studies not detailed here for brevity) or both. It is not very unlikely to realize spatio-temporal data that are not Gaussian; see, for example, Fuentes and Reich [2013], Das and Bhattacharya [2023], Bhattacharya [2021]. Moreover, in many real-life applications often, it is observed that the sample correlation goes to zero as the distance between two spatial locations and/or two time points goes to infinity; see,

for example, Bhattacharya [2021]. Since many stationary spatio-temporal processes are ergodic, this property follows naturally from the structure of the covariance function in such cases. However, this does not hold for non-stationary processes in general. Hence, while proposing a non-stationary spatio-temporal process, it is desirable to take special care to ensure convergence of the correlation to zero as the distance between two locations and/or time points increases to infinity.

Very recently, Das and Bhattacharya [2023] proposed a nonparametric, non-separable, non-stationary, and non-Gaussian spatio-temporal model based on order-based dependent Dirichlet process, where they showed that the underlying covariance function goes to zero as the distance between the two locations and/or time points increases to infinity. While modeling spatio-temporal data, Das and Bhattacharya [2023] also assumed that time and space vary continuously in their respective domains. Although Das and Bhattacharya [2023] made a successful attempt at building the nonparametric, non-stationary, non-Gaussian model with the desirable properties of covariance, their model did not impart dynamic properties to the temporal part, either directly or via any latent process. It is well known that a statistical model intended for explaining temporal variability should evolve dynamically (Chapter 1 of Cressie and Wikle [2015]). On the other hand, Guha [2017] introduces a nonparametric spatio-temporal model, which, through a nonparametric dynamic latent process, induces desirable dynamic properties in the temporal part. In addition, the model of Guha [2017] is non-stationary, and time does not vary continuously on the respective domain.

In a nutshell, there does not seem to exist any nonparametric, non-stationary, non-separable, non-Gaussian, dynamic spatio-temporal model, which is continuous in time and space with an underlying structured latent process, and with the property that the correlation between two spatio-temporal variables goes to zero as the spatial/temporal

lag goes to infinity. To fill this gap, we propose a dynamic spatio-temporal nonparametric, non-Gaussian model, where the underlying process is non-stationary. A structured latent process is incorporated into the proposed model. The time and space in our proposed spatio-temporal model vary continuously over their respective domains. Further, the underlying process enjoys the property that the covariance goes to zero as the spatial/temporal lag tends to infinity.

To construct the model proposal, we invoke the concept of Hamiltonian dynamics from Physics. Hamiltonian equations have been used in Bayesian statistics for formulating Hamiltonian Monte Carlo Betancourt [2017], Cheung and Beck [2009]. The solutions of the Hamiltonian equations describe the phase-space of a mechanical space. Moreover, the solutions, which are interdependent, continuously vary with respect to time. These properties motivate us to construct a spatio-temporal model based on the solutions of Hamiltonian equations. There are some instances of generalization of deterministic Hamiltonian equations to stochastic Hamiltonian equations (ordinary or partial); (see Lázaro-Camí and Ortega [2007], Hong et al. [2022] and the reference therein), but no temporal or spatio-temporal modeling has been attempted with respect to such generalizations. In any case, the equations are parametric in nature, since the functional forms in the equations are assumed to be deterministically known. The common practice is to add a Brownian motion to one of the two deterministic Hamiltonian equations to build stochastic Hamiltonian ordinary differential equations and the stochastic Hamiltonian partial differential equations are generalizations of the stochastic Hamiltonian ordinary differential equations. Since it is difficult to see how these stochastic equations with deterministic functional forms and (finite or infinite-dimensional) Brownian motions may be useful for constructing realistic temporal or spatio-temporal models with desirable properties, we do not pursue these in this work.

Formulation of spatio-temporal model exploiting the idea of the Hamiltonian dynamics via the leap-frog algorithm (Young [2014]) has not been considered earlier. Adaptation and exploitation of the leap-frog algorithm with appropriate choice of Gaussian process priors make the proposed model non-parametric. To be precise, in this article, we propose a modified leap-frog algorithm associated with modification of the Hamiltonian equations to build our spatio-temporal model incorporating the latent and observed processes, which continuously depend on time t . Moreover, since the leap-frog algorithm exploits the presence of derivative, our proposed spatio-temporal model also enjoys dynamic property with respect to time t through its previous time point $t - \delta t$. The Bayesian nonparametric flavor of our approach is due to modeling functions with unknown forms in the Hamiltonian equations by appropriate Gaussian processes. *In turn, it is observed that the desirable properties, non-stationarity, non-separability, non-Gaussianity are satisfied.* Further analysis shows that the covariance function of the proposed process goes to zero as the spatial and/or temporal lag tends to infinity. In addition to these, we show that the proposed stochastic process under certain regularity conditions, has continuous paths in almost sure and mean square sense. The almost sure differentiability and mean square differentiability of the sample paths are also established. While demonstrating the mean square differentiability of the sample paths of our model with respect to location, we prove a lemma that provides a set of sufficient conditions under which the composition of a random spatial process and a Gaussian spatial process becomes mean square differentiable. The result seems to be significant in its own right.

The remaining part of the article is planned in the following manner. In Section 2, we propose our new spatio-temporal process based on modified Hamiltonian equations and a modified leap-frog algorithm. Section 2 also presents the important and necessary

properties of the proposed observed and latent processes. The proofs of the lemmas, theorems, and corollaries discussed in Section 2, are given in Appendix A. The likelihood function of the parameter vector involved in the model is provided in Section 3. In that section we first find out the joint conditional density of the data given the latent variables and the parameters (Subsection 3.1 and Appendix B) and then obtain the joint density of latent variables given the observed data and the parameters (Subsection 3.2 and Appendix C), before presenting the complete likelihood of the parameter vector (Subsection 3.3). Section 4 deals with the choice of prior distributions for the parameter vectors. A plausible justification of the choice of the prior distributions is also discussed in that section. For applying Gibbs sampling, we evaluate the full conditional densities of all parameters along with the latent variables in Section 5. The detailed calculation of the full conditional densities is given in Appendix D. In Section 6, we provide the results of two simulation studies. The findings of our model for these simulation experiments are compared with those of a non-stationary Gaussian process, which was fitted using the SPDE approach following Lindgren et al. [2011] using INLA Lindgren and Rue [2015]. In Section 7, two real data sets are analyzed to show the performance of the newly proposed spatio-temporal model. Among these two real data sets, one of the data sets corresponds to a non-stationary and non-Gaussian process, while another is associated with a stationary non-Gaussian spatio-temporal process. Finally, in Section 8, we summarize our contributions and make concluding remarks.

2 Modified Hamiltonian equations and the proposed model

We first briefly describe the notion of Hamiltonian dynamics and the associated equations. Thereafter, we shall connect the idea of the proposed spatio-temporal model to Hamiltonian dynamics. Let $(\mathcal{M}, \mathcal{L})$ be a mechanical system, where \mathcal{M} is the configuration space and \mathcal{L} is the smooth Lagrangian. The coordinate system of \mathcal{M} is determined by $(\theta, \dot{\theta})$, where θ is the position of a particle at time t and the $\dot{\theta}$ is the derivative vector with respect to time, thus representing the velocity. The partial derivative of \mathcal{L} with respect to $\dot{\theta}$, known as momenta, is denoted by p , which is a function of time t , the position θ , and velocity $\dot{\theta}$. Now the Hamiltonian, a function of p , θ and t , is defined as

$$H(p, \theta, t) = \sum_i p_i \dot{\theta}_i - \mathcal{L}(\theta, \dot{\theta}, t),$$

which is the energy function of the mechanical system. Here p_i and $\dot{\theta}_i$ are the i th component of p and $\dot{\theta}$. The pair (θ, p) is called phase space coordinates. Now assume that $H(p, \theta, t) = V(\theta, t) + W(p, t)$, where $V(\theta, t)$ is the potential energy, $W(p, t)$ is the kinetic energy given as $W(p, t) = p^T M^{-1} p / 2$, with M being a chosen matrix (mass), and (θ, p) are phase space coordinates (depend on time t) Cheung and Beck [2009]. The Hamiltonian equations are given by

$$\begin{aligned} \frac{dp}{dt} &= \frac{-\partial H}{\partial \theta} = -\nabla V(\theta) \text{ and} \\ \frac{d\theta}{dt} &= \frac{\partial H}{\partial p} = M^{-1} p, \end{aligned}$$

where by $\nabla V(\theta)$ we mean gradient of V with respect to θ . Thus, the phase space coordinates are the solution of the Hamiltonian equations. We note here that the solution θ , which describes the position of a particle at time t and depends on p , the other coordinate of the phase-space, varies continuously with respect to time. Further, p is also dependent on θ at time t , and varies continuously with respect time t . To get the solution (p, θ) numerically, leap-frog algorithm is used and is given by

$$\begin{aligned}\theta(t + \delta t) &= \theta(t) + \delta t M^{-1} \left\{ p(t) - \frac{1}{2} \delta t \nabla V(\theta(t)) \right\} \text{ and} \\ p(t + \delta t) &= p(t) - \frac{1}{2} \delta t [\nabla V(\theta(t)) + \nabla V(\theta(t + \delta t))].\end{aligned}$$

In our case, we introduce $p(t)$ as the latent and $\theta(t)$ as the observed spatio-temporal processes with the hope that the solution to Hamilton's equations will best describe the underlying state-space as done in the phase-space of the mechanical space.

2.1 Modified Hamiltonian equations and the corresponding leap-frog algorithm

We modify the original Hamiltonian equations so that the rate of change of p and θ with respect to t depends on both p and θ . One way to do so is to incorporate p and θ linearly in the equation of $\frac{dp}{dt}$ and $\frac{d\theta}{dt}$, respectively. That is, Hamiltonian equations are modified to

$$\begin{aligned}\frac{dp}{dt} &= \alpha^* p - \nabla V(\theta) \text{ and} \\ \frac{d\theta}{dt} &= \beta^* \theta + M^{-1} p.\end{aligned}$$

Accordingly, the leap-frog algorithm is modified and is given below. Using Leap-frog algorithm for θ [Young, 2014], we have

$$\begin{aligned}
\theta(t + \delta t) &= \theta(t) + \beta^* \theta(t) \delta t + \delta t M^{-1} p(t + \delta t/2) \\
&= \theta(t) (1 + \beta^* \delta t) + \delta t M^{-1} p(t + \delta t/2) \\
&= \beta \theta(t) + \delta t M^{-1} p(t + \delta t/2),
\end{aligned} \tag{1}$$

where $\beta = (1 + \beta^* \delta t)$. We set $|\beta| < 1$, which implies $-2 < \beta^* \delta t < 0$. As will be seen subsequently, this restriction is necessary for the lagged correlations between the observations to tend to zero as the space-time lag tends to infinity. Now, for p , a numerical approximation can be done as

$$\begin{aligned}
p\left(t + \frac{\delta t}{2}\right) &= p(t) + \alpha^* p(t) \frac{\delta t}{2} - \nabla V(\theta(t)) \frac{\delta t}{2} \\
&= p(t) \left(1 + \alpha^* \frac{\delta t}{2}\right) - \nabla V(\theta(t)) \frac{\delta t}{2} \\
&= \alpha p(t) - \nabla V(\theta(t)) \frac{\delta t}{2},
\end{aligned} \tag{2}$$

where $\alpha = (1 + \alpha^* \delta t/2)$. We set $|\alpha| < 1$ implying $-2 < \alpha^* \delta t/2 < 0$. Restricting α on $(-1, 1)$ led to good MCMC mixing in our Bayesian applications. Replacing equation (2) into equation (1), we obtain

$$\theta(t + \delta t) = \beta \theta(t) + \delta t M^{-1} \left(\alpha p(t) - \nabla V(\theta(t)) \frac{\delta t}{2} \right) \tag{3}$$

Again, invoking leap-frog algorithm for p [Young, 2014], we obtain

$$p(t + \delta t) = p\left(t + \frac{\delta t}{2}\right) + \alpha^* p\left(t + \frac{\delta t}{2}\right) \frac{\delta t}{2} - \nabla V(\theta(t + \delta t)) \frac{\delta t}{2}$$

$$\begin{aligned}
&= p \left(t + \frac{\delta t}{2} \right) \left(1 + \alpha^* \frac{\delta t}{2} \right) - \nabla V(\theta(t + \delta t)) \frac{\delta t}{2} \\
&= \alpha p \left(t + \frac{\delta t}{2} \right) - \nabla V(\theta(t + \delta t)) \frac{\delta t}{2} \\
&= \alpha \left(\alpha p(t) - \nabla V(\theta(t)) \frac{\delta t}{2} \right) - \nabla V(\theta(t + \delta t)) \frac{\delta t}{2} \\
&= \alpha^2 p(t) - \frac{\delta t}{2} \{ \alpha \nabla V(\theta(t)) + \nabla V(\theta(t + \delta t)) \}, \tag{4}
\end{aligned}$$

where the fourth equality of equation (4) follows from equation (2). Equations (3) and (4) constitute the modified leap-frog equations and are the key ingredients of our proposed spatio-temporal process.

2.2 Proposed model

We now propose the spatio-temporal model via equations (3) and (4). Let $y(s, t)$ be a realization of the stochastic process $\{Y(s, t) : s \in S, t \geq 0\}$, where $S \subset \mathbb{R}^2$ is non-empty, containing a rectangle of positive volume. Also, assume that corresponding to $y(s, t)$ there is a latent variable $x(s, t)$, which is a realization of a process $\{X(s, t) : s \in S, t \geq 0\}$. However, unlike $y(s, t)$, $x(s, t)$ is not observed. For location $s \in S$, replacing $\theta(t)$, $p(t)$, M and $\nabla V(\theta(t))$ by $y(s, t)$, $x(s, t)$, M_s and $\left. \frac{d}{dx} V(x) \right|_{x=y(s,t)}$ in equations (4) and (3), we propose the spatio-temporal model as

$$y(s, t + \delta t) = \beta y(s, t) + \delta t M_s^{-1} \left(\alpha x(s, t) - \frac{\delta t}{2} \left. \frac{dV}{du}(u) \right|_{u=y(s,t)} \right), \tag{5}$$

$$x(s, t + \delta t) = \alpha^2 x(s, t) - \frac{\delta t}{2} \left(\alpha \left. \frac{dV}{du}(u) \right|_{u=y(s,t)} + \left. \frac{dV}{du}(u) \right|_{u=y(s,t+\delta t)} \right), \tag{6}$$

where (5) corresponds to observation equation and (6) deals with the dynamics of the latent variable. The parameters α , β are such that $|\alpha| < 1$ and $|\beta| < 1$, and M_s is a function of s . The function $V(\cdot)$ is modeled as random function. Note that equation

(6) is not the latent equation *per se*, since it involves the observed variable as well. Integrating the conditional distribution of the latent variable (equation (6)) over the observed variable would give us the latent distribution.

To complete the specification of our spatio-temporal process, we need to model the function $V(\cdot)$ as some appropriate stochastic process; we consider the Gaussian process for our purpose. The choice of Gaussian process for $V(\cdot)$, under suitable assumptions, makes $V(\cdot)$ Gaussian as well (Stein [1999a], Rasmussen and Williams [2006]). Due to this fact, the conditional likelihoods become available in closed forms (see Section 3). Specification of the proposed processes also requires an appropriate form for M_s . Details on these, along with an investigation of the theoretical properties of our spatio-temporal processes, are provided in the next subsection.

2.3 Completion of specification of the proposed spatio-temporal process and investigation of its theoretical properties

Let $s \in S$, a compact subset of \mathbb{R}^2 , and $\|\cdot\|$ denote the Euclidean norm. We put the following assumptions on the processes $X(s, 0), Y(s, 0)$, $s \in S$ and the random function $V(\cdot)$.

A1. $X(s, 0)$, $s \in S$ is assumed to be a centered Gaussian process with a symmetric, positive definite covariance function having bounded partial derivatives. For instance, the Matérn covariance function with $\nu > 1$ has bounded partial derivatives and could be employed. In particular, we consider the squared exponential covariance between $X(s_1, 0)$ and $X(s_2, 0)$, of the form $\sigma_p^2 \exp\{-\eta_1 \|s_1 - s_2\|^2\}$, $s_1, s_2 \in S$.

A2. $Y(s, 0)$, $s \in S$ is also assumed to be a centered Gaussian process with a symmetric,

positive definite covariance function with bounded partial derivatives. Again, we consider the squared exponential covariance function of the form $\sigma_\theta^2 \exp\{-\eta_2 \|s_1 - s_2\|^2\}$.

A3. The function $V(\cdot)$ is assumed to be a Gaussian random function with zero mean and covariance function $c_v(x_1, x_2) = \sigma^2 \exp\{-\eta_3 \|x_1 - x_2\|^2\}$. As for the other cases, different choices of covariance structure can be assumed with the assumption that the covariance function is continuously twice differentiable and the mixed partial derivatives are Lipschitz continuous. If the covariance function has third bounded partial derivatives, then the function will be Lipschitz. In our example, the covariance function is infinitely differentiable and the derivatives are bounded. Other choices may include rational quadratic covariance function, Matérn covariance function with $\nu > 2$ among many others.

The above assumptions need well-behaved covariance functions in the sense of smoothness. For a list of such covariance functions, one may see Banerjee et al. [2014]. Smoothness properties along with other important properties of Matérn covariance functions have been covered in Stein [1999b] (Chapter 2).

Remark 1 *The assumptions A1 and A2 imply that the covariance functions of $X(s, 0)$ and $Y(s, 0)$ are symmetric, positive definite, and Lipschitz continuous, and thus $X(s, 0)$ and $Y(s, 0)$ will have continuous sample paths with probability 1. If the covariance functions are taken to be the Matérn covariance function with $\nu > 1$ or the squared exponential covariance function, then $X(s, 0)$ and $Y(s, 0)$ will have differentiable sample paths in s .*

Remark 2 *Assumption A3 implies that the derivative process of $V(\cdot)$ is also a Gaussian process with continuous sample paths almost surely. In fact, if the squared exponential covariance function is assumed, then all the derivatives of $V(\cdot)$ will be Gaussian*

processes. In particular, the differential of $V(\cdot)$ will have differentiable sample paths. Also note that for Matérn covariance function with $\nu > 2$, the random function $V(\cdot)$ is differentiable and the corresponding covariance function is the mixed partial derivative of the covariance function of $V(\cdot)$. Moreover, the differential of $V(\cdot)$ will have differentiable sample paths as ν is assumed to be more than 2 for Matérn covariance function (refer to Rasmussen and Williams [2006] along with Stein [1999b]).

Now we propose a form of M_s which is continuous and infinitely differentiable when defined on a compact set $S \subset \mathbb{R}^2$.

Definition 1 (Definition of M_s) Let S be a compact subset of \mathbb{R}^2 . Define $M_s = \exp(\max\{\|s^2 - u^2\|^2 : u \in S\})$, where by \mathbf{v}^2 we mean $\mathbf{v}^2 = (v_1^2, v_2^2)^T$, for $\mathbf{v} \in S$.

Remark 3 It can be argued that $M_s \rightarrow \infty$ and $M_{s'} \rightarrow \infty$ as $\|s - s'\| \rightarrow \infty$ in the following fashion. Let $\|s - s'\| \rightarrow \infty$ as S also grows in the sense $S_1 \subset S_2 \subset \dots$, such that at each stage i , S_i remains compact. Under this limiting situation, $M_s = \exp(\max\{\|s^2 - u^2\|^2 : u \in S\}) \geq \exp(\|s^2 - s'^2\|^2) \rightarrow \infty$ and $M_{s'} = \exp(\max\{\|s'^2 - u^2\|^2 : u \in S\}) \geq \exp(\|s'^2 - s^2\|^2) \rightarrow \infty$.

Further, it can be shown that M_s is infinitely smooth in S . The following lemma proves the claim. We provide the proof in Appendix A.

Lemma 2.1 M_s is infinitely differentiable in $s \in S$.

The next results show that the covariance function of $Y(s, t)$ goes to 0 as the distance between two time points and two spatial locations increases to infinity. The distances between any two time points and any two spatial locations are measured with respect to their corresponding distance metrics.

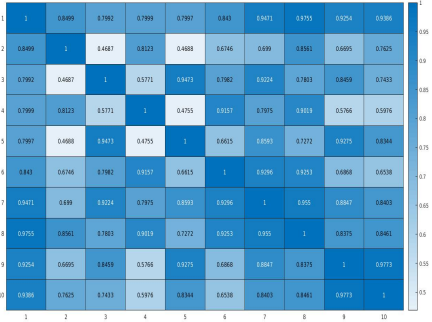
Theorem 2.1 *Under the assumptions A1 to A3, $\text{cov}(Y(s, h\delta t), Y(s', h'\delta t))$ converges to 0, as $\|s - s'\| \rightarrow \infty$ and/or $|h - h'| \rightarrow \infty$.*

In Theorem 2.1, δt in $h\delta t$ and $h'\delta t$ make the time points continuous for continuous δt . However, discrete values of δt are also allowed.

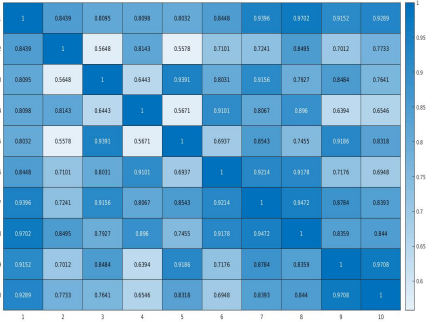
Remark 4 *The closed form of the covariance functional of our proposed process $Y(s, t)$ is unavailable. However, we can argue in the following way that covariance is non-stationary. Conditional on the latent variables, the covariance depends upon the latent variable. For simplicity, let us assume that the latent process is supported on a compact set. Then, by the mean value theorem for integrals, unconditional covariance is a function of a specific value of the latent variables. Moreover, the latent variables are almost surely nonlinear in locations and times, implying that the unconditional covariance is a nonlinear function of space and time. Therefore, it must be non-stationary.*

To complete the discussion on correlation analysis, we provide an illustration to give us an idea regarding the spatial correlation matrix of our model and how it is different from the squared exponential or Matérn covariance. In particular, this illustration shows that the spatial correlation of the proposed model can be negative, whereas the correlation of squared exponential or Matérn will always be positive (see Figure 1). We simulated spatio-temporal observations 1000 times from our model taking $\eta_1 = \eta_2 = \eta_3 = 1$, $\sigma^2 = \sigma_\theta^2 = \sigma_p^2 = 1$, $\alpha = \beta = 0.9$. The number of locations and time points are taken to be 10 and 4, respectively. Based on 1000 simulations we have calculated the sample spatial correlation matrix. Similarly, we simulated spatio-temporal observations from a Gaussian process with zero mean and squared exponential kernel with the variance and the decaying parameter to be 1. The corresponding sample spatial correlation matrix is calculated based on the 1000 repetitions. The same exercise

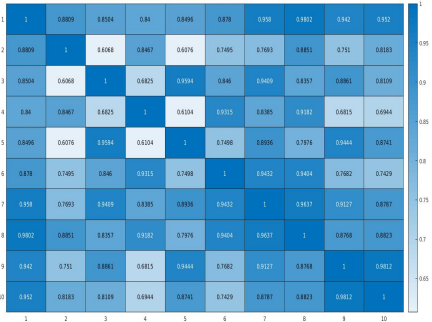
has been done by replacing the squared exponential kernel with two Matérn covariance kernels, namely, Matérn(3/2) and Matérn(5/2), respectively. The range parameter for Matérn covariance kernel is taken as 1 for both cases. The sample spatial correlations are provided in Figure 1.



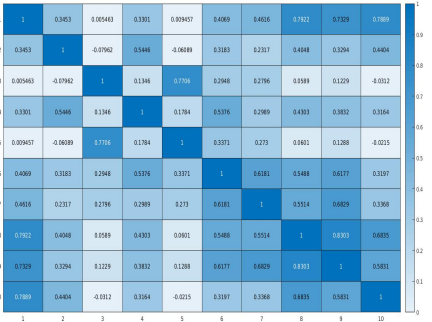
(a) Spatial correlation matrix for squared exponential.



(b) Spatial correlation matrix for Matérn(3/2).



(c) Spatial correlation matrix for Matérn(5/2).



(d) Spatial correlation matrix for model.

Figure 1: The figure depicts examples of spatial correlation matrices for four different models. The x-axis and the y-axis represents the indices of the locations. The higher intensity of the colour represents the higher correlation. Our model can have negative entries in a correlation matrix whereas the correlation matrices for the other models are always positive.

Next we show that $Y(s, t)$ and $X(s, t)$ are continuous in s with probability 1 and in the mean square sense. Since the (modified) Hamiltonian equations already imply that $Y(s, t)$ and $X(s, t)$ are path-wise differentiable with respect to t , we focus on their smoothness properties with respect to s .

Theorem 2.2 *If the assumptions A1-A3 hold true, then $Y(s, h\delta t)$ and $X(s, h\delta t)$ are continuous in s , for all $h \geq 1$, with probability 1.*

Theorem 2.3 *Under assumptions A1-A3, $Y(s, h\delta t)$ and $X(s, h\delta t)$ are continuous in s in the mean square sense, for all $h \geq 1$.*

The next two results deal with the differentiability of the processes $Y(s, t)$ and $X(s, t)$.

Theorem 2.4 *Under assumptions A1-A3, $Y(s, h\delta t)$ and $X(s, h\delta t)$ have differentiable sample paths with respect to s , almost surely.*

Remark 5 *Theorem 2.4 is about once differentiability, however, it can be extended to k times differentiability depending on the structure of the covariances assumed on the processes $Y(s, 0)$, $X(s, 0)$ and the random function $V(\cdot)$. For example, if we assume squared exponential covariance functions on each process, then $Y(s, h\delta t)$ and $X(s, h\delta t)$ will have k times differentiable sample paths in s , for any $k \in \mathbb{N}$.*

To prove that the processes $Y(s, t)$ and $X(s, t)$ are mean square differentiable in s , we need a lemma, stated below, which may be of independent interest.

Lemma 2.2 *Let $f : \mathbb{R} \rightarrow \mathbb{R}$ be a zero mean Gaussian random function with covariance function $c_f(x_1, x_2)$, $x_1, x_2 \in \mathbb{R}$, which is four times continuously differentiable. Let $\{Z(s) : s \in S\}$ be a random process with the following properties*

1. $E(Z(s)) = 0$,
2. covariance function $c_Z(s_1, s_2)$, $s_1, s_2 \in S$, where S is a compact subspace of \mathbb{R}^2 , is four times continuously differentiable, and
3. $\frac{\partial Z(s)}{\partial s_i}$ has finite fourth moment.

Then the process $\{g(s) : s \in S\}$, where $g(s) = f(Z(s))$, is mean square differentiable in s .

Theorem 2.5 *Let A1-A3 hold true, with the covariance functions of all the assumed Gaussian processes being squared exponential. Then $Y(s, h\delta t)$ and $X(s, h\delta t)$ are mean square differentiable in s , for every $h \geq 1$.*

3 Calculation of likelihood functions

In this section, we will derive the data and process models under assumptions A1-A3. We assume here that the random function $V(\cdot)$ is a Gaussian process with mean 0 and squared exponential function as covariance function for simplicity of calculations. In particular, we assume that the covariance function of $V(\cdot)$ takes the form $\text{cov}(V(x), V(y)) = k(h) = \sigma^2 e^{-\eta_3 h^2}$, where $h = \|x - y\|$. Then $V'(\cdot)$ will be a Gaussian random function with mean 0 and covariance function

$$\text{cov}(V'(x), V'(y)) = 2\eta_3 \sigma^2 e^{-\eta_3 h^2} (1 - 2\eta_3 h^2), \quad (7)$$

(see Stein [1999b], Chapter 2).

Before moving forward, we introduce a few notations that will be used for calculations of different distributions. Suppose s_1, \dots, s_n denote the n locations, where $s_i \in \mathbb{R}^2$, for $i = 1, \dots, n$. Let observed data and the corresponding latent variables be given as

$$\mathbb{D} = \{\mathbf{y}_1^T, \mathbf{y}_2^T, \dots, \mathbf{y}_T^T\},$$

$$\mathbb{L} = \{\mathbf{x}_1^T, \mathbf{x}_2^T, \dots, \mathbf{x}_T^T\},$$

respectively, where $\mathbf{y}_t = (y(s_1, t), y(s_2, t), \dots, y(s_n, t))^T$ and $\mathbf{x}_t = (x(s_1, t), x(s_2, t), \dots, x(s_n, t))^T$ for $t = 1, \dots, T$. Assuming $i \in \{1, \dots, n\}$, $m \in \{0, \dots, T\}$ and $r \in \{1, \dots, T\}$, we define

$$\begin{aligned}
h_{ij}(m) &= |y(s_i, m) - y(s_j, m)|, \mu_i(m) = \beta y(s_i, m) + \frac{\alpha x(s_i, m)}{M_{s_i}}, \\
\boldsymbol{\mu}_m &= (\mu_1(m), \dots, \mu_n(m))^T, \mathbf{W}_r = (V'(y(s_1, r)), \dots, V'(y(s_n, r)))^T, \\
\mathbb{W}_{r-1} &= \begin{pmatrix} \alpha \mathbf{W}_{r-1} \\ \mathbf{W}_r \end{pmatrix}, \ell_{ik}(r-1, r) = |y(s_i, r-1) - y(s_k, r)|, \\
\Theta &= (\alpha, \beta, \sigma^2, \sigma_\theta^2, \sigma_p^2, \eta_1, \eta_2, \eta_3).
\end{aligned}$$

By \mathbf{a}^T , we mean transpose of a vector \mathbf{a} and by f' we mean derivative of f .

3.1 Joint conditional density of the observed data

The joint conditional density of the data given the latent variables $\mathbf{x}_0, \mathbf{x}_1, \dots, \mathbf{x}_T$ and the parameter vector Θ is given by

$$\begin{aligned}
& [\mathbb{D} | \mathbf{x}_0; \dots; \mathbf{x}_{T-1}; \mathbf{y}_0; \Theta] \\
& \propto [\mathbf{y}_1 | \mathbf{y}_0; \mathbf{x}_0; \Theta] \dots [\mathbf{y}_T | \mathbf{y}_{T-1}, \dots, \mathbf{y}_0; \mathbf{x}_{T-1}, \dots, \mathbf{x}_0; \Theta] \\
& \propto \frac{(\sigma^2)^{-nT/2}}{\prod_{t=1}^T |\Sigma_{t-1}|^{1/2}} \exp \left\{ -\frac{2}{\sigma^2} \sum_{t=1}^T (\mathbf{y}_t - \boldsymbol{\mu}_{t-1})^T \Sigma_{t-1}^{-1} (\mathbf{y}_t - \boldsymbol{\mu}_{t-1}) \right\}, \quad (8)
\end{aligned}$$

where, for $j = 1, 2, \dots, T$, the (k, ℓ) th element of Σ_{j-1} is $2\eta_3 e^{-\eta_3 h_{k\ell}^2(j-1)} (1 - 2\eta_3 h_{k\ell}^2(j-1)) / (M_{s_k} M_{s_\ell})$.

The details of the calculation of the joint density are provided in Appendix B.

3.2 Joint conditional density of latent data

It can be shown that (see Appendix C for the detailed calculation)

$$\begin{aligned} & \left[\mathbb{L} \left| \mathbf{y}_0; \dots; \mathbf{y}_T; \mathbf{x}_0; \Theta \right. \right] \propto [\mathbf{x}_1 | \mathbf{x}_0; \mathbf{y}_0; \mathbf{y}_1; \Theta] \dots [\mathbf{x}_T | \mathbf{x}_{T-1}; \dots; \mathbf{x}_0; \mathbf{y}_0; \dots; \mathbf{y}_T; \Theta] \\ & \propto \frac{(\sigma^2)^{-nT/2}}{\prod_{t=1}^T |\Omega_t|^{1/2}} \exp \left\{ -\frac{2}{\sigma^2} \sum_{t=1}^T (\mathbf{x}_t - \alpha^2 \mathbf{x}_{t-1})^T \Omega_t^{-1} (\mathbf{x}_t - \alpha^2 \mathbf{x}_{t-1}) \right\}, \end{aligned} \quad (9)$$

where, for $m \in \{1, 2, \dots, T\}$, $\Omega_t = \alpha^2 \Sigma_{t-1, t-1} + \alpha \Sigma_{t-1, t} + \alpha \Sigma_{t, t-1} + \Sigma_{t, t}$, where the (i, k) th element of Σ_{jj} , for $j = t-1, t$, is $2\eta_3 e^{-\eta_3 h_{ik}^2(j)} (1 - 2\eta_3 h_{ik}^2(j))$, and the (i, k) th element of $\Sigma_{t-1, t} = \Sigma_{t, t-1}^T$ is $2\eta_3 e^{-\eta_3 \ell_{ik}^2(t-1, t)} (1 - 2\eta_3 \ell_{ik}^2(t-1, t))$.

3.3 Complete likelihood combining observed and latent data

Next we will find the joint distribution of Data and Latent observations given $\mathbf{x}_0, \mathbf{y}_0$ and Θ . Finally, using the prior distributions on $Y(s, 0)$ and $X(s, 0)$ as mentioned in A1-A2, we shall obtain the complete joint distribution of $(\mathbf{y}_T, \dots, \mathbf{y}_1, \mathbf{y}_0)$ and $(\mathbf{x}_T, \dots, \mathbf{x}_1, \mathbf{x}_0)$, given the parameter Θ . The joint distribution of $(\mathbf{y}_T, \dots, \mathbf{y}_1)$ and $(\mathbf{x}_T, \dots, \mathbf{x}_1)$ given $(\mathbf{x}_0, \mathbf{y}_0, \Theta)$, using equations (9) and (8), is given by

$$\begin{aligned} & \left[\mathbb{D}, \mathbb{L} \left| \mathbf{y}_0, \mathbf{x}_0, \Theta \right. \right] = \prod_{t=1}^T \left[\mathbf{y}_t \left| \mathbf{x}_{t-1}, \mathbf{y}_{t-1}, \Theta \right. \right] \left[\mathbf{x}_t \left| \mathbf{x}_{t-1}, \mathbf{y}_{t-1}, \mathbf{y}_t, \Theta \right. \right] \\ & \propto \frac{(\sigma^2)^{-nT}}{\prod_{t=1}^T |\Sigma_{t-1}|^{1/2} |\Omega_t|^{1/2}} \exp \left\{ -\frac{2}{\sigma^2} \sum_{t=1}^T (\mathbf{y}_t - \boldsymbol{\mu}_{t-1})^T \Sigma_{t-1}^{-1} (\mathbf{y}_t - \boldsymbol{\mu}_{t-1}) + (\mathbf{x}_t - \alpha^2 \mathbf{x}_{t-1})^T \Omega_t^{-1} (\mathbf{x}_t - \alpha^2 \mathbf{x}_{t-1}) \right\} \end{aligned} \quad (10)$$

Let $\text{cov}(Y(s_1, 0), Y(s_2, 0)) = \sigma_\theta^2 \exp\{-\eta_2 k^2\}$ (see assumption A2), and $\text{cov}(X(s_1, 0), X(s_2, 0)) = \sigma_p^2 \exp\{-\eta_1 k^2\}$ (see assumption A1), where $k = \|s_1 - s_2\|$. Therefore, $[\mathbf{y}_0 | \Theta] \sim$

$N_n(\mathbf{0}, \sigma_\theta^2 \Delta_0)$ and $[\mathbf{x}_0 | \Theta] \sim N_n(\mathbf{0}, \sigma_p^2 \Omega_0)$, where the (i, j) th element of Δ_0 and Ω_0 are $\exp\{-\eta_2 k_{ij}^2\}$ and $\exp\{-\eta_1 k_{ij}^2\}$, respectively, with $k_{ij} = |s_i - s_j|$. Thus,

$$\begin{aligned} \left[\mathbf{y}_T, \mathbf{x}_T, \dots, \mathbf{y}_1, \mathbf{x}_1, \mathbf{y}_0, \mathbf{x}_0 \mid \Theta \right] &\propto \left[\mathbb{D}, \mathbb{L} \mid \mathbf{y}_0, \mathbf{x}_0, \Theta \right] \frac{(\sigma_\theta^2)^{-n/2} (\sigma_p^2)^{-n/2}}{|\Delta_0|^{1/2} |\Omega_0|^{1/2}} \exp \left\{ -\frac{1}{2\sigma_\theta^2} \mathbf{y}_0^T \Delta_0^{-1} \mathbf{y}_0 \right\} \\ &\quad \exp \left\{ -\frac{1}{2\sigma_p^2} \mathbf{x}_0^T \Omega_0^{-1} \mathbf{x}_0 \right\}, \end{aligned} \quad (11)$$

where $\left[\mathbb{D}, \mathbb{L} \mid \mathbf{y}_0, \mathbf{x}_0, \Theta \right]$ is obtained from (10).

4 Prior distributions

In this section, we will specify the prior distributions of the components of $\Theta = (\alpha, \beta, \sigma^2, \sigma_\theta^2, \sigma_p^2, \eta_1, \eta_2, \eta_3)^T$. The parameter spaces of the each component of Θ are the following: $|\alpha| < 1$, $|\beta| < 1$, and $0 < \sigma^2, \sigma_\theta^2, \sigma_p^2, \eta_1, \eta_2, \eta_3 < \infty$. We make the following transformations on α , β , η_i , for $i = 1, 2, 3$ for better MCMC mixing. Define $\alpha^* = \log\left(\frac{1+\alpha}{1-\alpha}\right)$, $\beta^* = \log\left(\frac{1+\beta}{1-\beta}\right)$, and $\eta_i^* = \log(\eta_i)$, for $i = 1, 2, 3$, so that $\alpha^*, \beta^*, \eta_i^* \in \mathbb{R}$, for $i = 1, 2, 3$. This implies $\alpha = 1 - \frac{2e^{\alpha^*}}{1+e^{\alpha^*}}$, $\beta = 1 - \frac{2e^{\beta^*}}{1+e^{\beta^*}}$, $\eta_i = e^{\eta_i^*}$, $i = 1, 2, 3$, respectively. We assume that the prior distributions are independent. Since the parameter spaces of α^* and β^* are \mathbb{R} and they are involved in the mean function of our proposed model, the prior for α^* and β^* are taken as normal with mean 0 and large variances (of order 100). Particular choices of the prior variances are discussed in Sections 6 and 7. Moreover, the parameter spaces of η_i^* , $i = 1, 2, 3$ are also \mathbb{R} and they are involved in the covariance structure of our proposed model in the sense that they determine the amount of correlations between spatial and temporal points. So, we take the priors for η_i^* , $i = 1, 2, 3$, as normal with means μ_{η_i} and variances 1. Larger variance of the η_i^* made the variances of their posterior distributions unreasonably large due to huge data

variability. The exact values of the hyper-prior means depend upon the data under consideration and is discussed in Sections 6 and 7. Finally, the prior distributions of variance parameters are taken to be inverse-gamma, as they are the conjugate priors, conditionally. It is expected that the variability of the spatio-temporal data is very large, which might possibly render the posterior means and variances of σ_θ^2 , σ_p^2 , σ^2 very large (especially for σ^2). So we decided to choose the hyper-parameters in such a way that the prior means (with some exceptions in the mean in a few cases) and variances are both close to zero. The exact choices of the hyper-parameters of priors of σ_p^2 , σ_θ^2 and σ^2 are mentioned in Sections 6 and 7.

The general forms of the prior distributions of α^* , β^* , σ^2 , σ_θ^2 , σ_p^2 , η_i^* , $i = 1, 2, 3$, are taken as follows:

$$[\alpha^*] \propto N(0, \sigma_\alpha), [\beta^*] \propto N(0, \sigma_\beta^2), [\sigma^2] \propto IG(\alpha_v, \gamma_v/2), [\sigma_\theta^2] \propto IG(\alpha_\theta, \gamma_\theta/2)$$

$$[\sigma_p^2] \propto IG(\alpha_p, \gamma_p/2), [\eta_1^*] \propto N(\mu_{\eta_1}, 1), [\eta_2^*] \propto N(\mu_{\eta_2}, 1), [\eta_3^*] \propto N(\mu_{\eta_3}, 1),$$

where IG stands for inverse gamma distribution.

5 Full conditional distributions

In this section, we will obtain the full conditional distributions of the parameters, which will be used for generating samples from posterior distributions of the parameters using Gibbs sampling or Metropolis-Hastings within Gibbs sampling. The detailed calculations are provided in Appendix D.

Full conditional distribution of β^*

The full conditional density of β^* , is given by $[\beta^* | \dots] \propto \exp\{-\beta^{*2}/2\sigma_{\beta^*}^2\}g_1(\beta^*)$,

where

$$g_1(\beta^*) = \exp \left\{ -\frac{2\beta^2}{\sigma^2} \sum_{t=1}^T \mathbf{y}_{t-1}^T \Sigma_{t-1}^{-1} \mathbf{y}_{t-1} + \frac{4\beta}{\sigma^2} \sum_{t=1}^T \mathbf{y}'_t \Sigma_{t-1}^{-1} \mathbf{y}_{t-1} \right\},$$

with $\beta = 1 - 2e^{\beta^*}/(1 + e^{\beta^*})$.

Full conditional distribution of α^*

The full conditional density of α^* is given by $[\alpha^* | \dots] \propto \exp\{-\alpha^{*2}/2\sigma_{\alpha^*}^2\} g_2(\alpha^*)$,

where

$$g_2(\alpha^*) = \frac{1}{\prod_{t=1}^T |\Omega_t|^{1/2}} \exp \left\{ -\frac{2}{\sigma^2} \sum_{t=1}^T [(\mathbf{x}_t - \alpha^2 \mathbf{x}_{t-1})^T \Omega_t^{-1} (\mathbf{x}_t - \alpha^2 \mathbf{x}_{t-1})] - \frac{2\alpha}{\sigma^2} \sum_{t=1}^T [\alpha \mathbf{x}_{t-1}^T D \Sigma_{t-1}^{-1} D \mathbf{x}_{t-1} - 2 \mathbf{y}_t^T \Sigma_{t-1}^{-1} D \mathbf{x}_{t-1}] \right\},$$

and $\alpha = 1 - 2e^{\alpha^*}/(1 + e^{\alpha^*})$. The closed forms of the full conditionals of α^* and β^* are not available, and hence will be updated using random walk Metropolis.

Full conditional distribution of σ_θ^2

The full conditional distribution of σ_θ^2 is $\text{IG}(\alpha_\theta + n/2, \gamma_\theta + \mathbf{y}_0^T \Delta_0^{-1} \mathbf{y}_0/2)$.

Full conditional distribution of σ_p^2

The full conditional distribution of σ_p^2 is $\text{IG}(\alpha_p + n/2, \gamma_p + \mathbf{x}_0^T \Delta_0^{-1} \mathbf{x}_0/2)$.

Full conditional distribution of σ^2

The full conditional distribution of σ^2 is inverse-Gamma with parameters $\alpha_v + Tn$ and $\gamma_v/2 + 2\zeta$, where $\zeta = \sum_{t=1}^T [(\mathbf{y}_t - \boldsymbol{\mu}_t)^T \Sigma_{t-1}^{-1} (\mathbf{y}_t - \boldsymbol{\mu}_t) + (\mathbf{x}_t - \alpha^2 \mathbf{x}_{t-1})^T \Omega_t^{-1} (\mathbf{x}_t - \alpha^2 \mathbf{x}_{t-1})]$.

Thus, σ_θ^2 , σ_p^2 and σ^2 updated using a Gibbs sampling step.

Full conditional distributions of η_1^* , η_2^* , and η_3^*

The full conditional distributions of η_1^* , η_2^* and η_3^* are $[\eta_1^* | \dots] \propto \pi(\eta_1^*) g_3(\eta_1^*)$, $[\eta_2^* | \dots] \propto$

$\pi(\eta_2^*)g_4(\eta_2^*)$, and $[\eta_3^*|\dots] \propto \pi(\eta_3^*)g_5(\eta_3^*)$, where $\eta_j = \exp\{\eta_j^*\}$, $\pi(\eta_j^*) = \exp\{\eta_j^{*2}/2\}$, for $j = 1, 2, 3$. Finally, $g_3(\cdot)$, $g_4(\cdot)$ and $g_5(\cdot)$ are specified as follows:

$$g_3(\eta_1^*) = \frac{1}{|\Omega_0|^{1/2}} \exp\left\{-\frac{1}{2\sigma_p^2}\mathbf{x}_0^T\Omega_0^{-1}\mathbf{x}_0\right\}, g_4(\eta_2^*) = \frac{1}{|\Delta_0|^{1/2}} \exp\left\{-\frac{1}{2\sigma_\theta^2}\mathbf{y}_0^T\Delta_0^{-1}\mathbf{y}_0\right\}, \text{ and}$$

$$g_5(\eta_3^*) = \frac{1}{\prod_{t=1}^T |\Sigma_{t-1}|^{1/2}|\Omega_t|^{1/2}} \exp\left\{-\frac{2}{\sigma^2}\sum_{t=1}^T [(\mathbf{y}_t - \boldsymbol{\mu}_t)^T\Sigma_{t-1}^{-1}(\mathbf{y}_t - \boldsymbol{\mu}_t) + (\mathbf{x}_t - \alpha^2\mathbf{x}_{t-1})^T\Omega_t^{-1}(\mathbf{x}_t - \alpha^2\mathbf{x}_{t-1})]\right\}$$

None of the full conditional distributions of η_1^* , η_2^* or η_3^* have close form and hence they are updated random walk Metropolis. The detailed calculations of the full conditionals for η_i^* , for $i = 1, 2, 3$, are given in Appendix D.

Full conditional distributions of \mathbf{x}_t , $t = 1, 2, \dots, T$ and \mathbf{x}_0

From the equation (9), we immediately see that $[\mathbf{x}_t|\dots] \sim N_n\left(\alpha^2\mathbf{x}_{t-1}, \frac{\sigma^2}{4}\Omega_t\right)$, for $t = 1, \dots, T$. With $A = \Omega_0^{-1} + 4\sigma_p^2\alpha^4\sigma^{-2}\Omega_1^{-1} + 4\sigma_p^2\alpha^2\sigma^{-2}D\Sigma_0^{-1}D$, $B = 4\sigma_p^2\alpha^2\sigma^{-2}\Omega_1^{-1}$ and $C = 4\sigma_p^2\alpha\sigma^{-2}D\Sigma_0^{-1}$, the full conditional density of \mathbf{x}_0 is found to be a n -variate normal with mean $A^{-1}(B\mathbf{x}_1 + C(\mathbf{y}_1 - \beta\mathbf{y}_0))$ and the variance-covariance matrix $\sigma_p^2A^{-1}$. Hence, \mathbf{x}_t , for $t = 0, 1, \dots, T$ are updated using a Gibbs sampling step.

Remark 6 *We add a ridge parameter to the diagonals of the all dispersion matrices while performing the MCMC runs to make the matrices non-singular. Note that the added ridge parameter to the diagonal of Σ_{t-1} , for $t = 1, \dots, T$ works as nugget in the model. The ridge parameter is fixed to a small value, which is chosen based cross-validation with several pilot runs of MCMC.*

6 Simulation Studies

In order to assess the performance of our model and to compare our findings with those of a well-known non-stationary model based on Gaussian process (described below), we conduct two extensive simulation studies. The first data set is generated from a mixture of three Gaussian process models, and the other from a mixture of two general quadratic nonlinear (GQN) models. The data generation algorithms are described in the relevant subsections (Sections 6.1 and 6.3). First, we describe the model, whose findings are compared with the results of our model applied to the simulated data sets. The model is as follows:

Letting s and s' denote the locations, and t, t' denote the time points, we have

$$\begin{aligned} y_{s,t} &\sim N(\eta_{s,t}, \sigma_\epsilon^2), \\ \eta_{s,t} &= b_0 + \omega_{s,t}, \\ \omega_{s,t} &= a\omega_{s,(t-1)} + \xi_{s,t}, \text{ with } |a| < 1, \\ \xi_{s,t} &\sim NGP(0, C(\cdot, \cdot)), \end{aligned}$$

where *NGP* stands for non-stationary Gaussian process and

$$C(\xi_{s,t}, \xi_{s',t'}) = \begin{cases} 0 & \text{if } t \neq t' \\ \text{cov}(\xi_s, \xi_{s'}) & \text{if } t = t' \end{cases}$$

with $\text{cov}(\xi_s, \xi_{s'})$ being a Matérn covariance kernel with smoothness parameter 2. The other parameters of the Matérn covariance kernel depend on location s , which makes the model non-stationary (Lindgren et al. [2011], Bolin and Lindgren [2011], Ingebrigtsen et al. [2014] and Blangiardo and Cameletti [2015]). For future reference in the

manuscript, we shall denote the above mentioned model as the NGP model. The NGP model is fitted using the SPDE approach as described in Chapter 6 of Blangiardo and Cameletti [2015] (also see Lindgren et al. [2022] for a review on the SPDE approach).

In all the simulation experiments, we chose the number of locations to be $n = 50$ and the number of time points to be $T = 20$. The data vector corresponding to the last time point, which contains observations at 50 locations, is kept aside for the purpose of evaluating model performance (the details of predictive density at a future time point is given in Appendix E). Hence, the data set that we observe is $\mathbb{D} = \{y(s_1, 1), \dots, y(s_{50}, 1), \dots, y(s_1, 19), \dots, y(s_{50}, 19)\}$ and the corresponding latent data is $\mathbb{L} = \{x(s_1, 1), \dots, x(s_{50}, 1), \dots, x(s_1, 19), \dots, x(s_{50}, 19)\}$. The validation set contains $\mathbf{y}_{20} = (y(s_1, 20), \dots, y(s_{50}, 20))^T$ and $\mathbf{x}_{20} = (x(s_1, 20), \dots, x(s_{50}, 20))^T$.

We run our MCMC sampler for 1,75,000 iterations with a burn-in of 1,50,000 for simulation examples. The MCMC computations were carried out in MATLAB R2018a. For each model-fitting it took about 3 hours 49 minutes on a desktop computer having 8GB RAM, 1 TB Hard Drive and 3.8 GHz core_i5.

6.1 Mixture of three Gaussian Processes

6.1.1 Data generation

A data set is simulated from a mixture of three Gaussian process models. Given the number of locations n and the time points T , we obeyed the following steps to simulate the data set.

- a. Generate n locations, s_1, \dots, s_n , uniformly from $[0, 1] \times [0, 1]$.
- b. For $j = 1, 2, 3$, simulate an $m \times n$ matrix ξ_j , where each column is independently simulated from m -variate normal mean $\mathbf{0}$ and covariance C_j . The $m \times m$ matrix

C_j is determined by Matérn covariance kernel(2) with the parameters κ_j and σ_j^2 .

- c. Calculate $\omega_j(s, t)$, for $t = 1, \dots, T$, and $s = s_1, \dots, s_n$, $\omega_j(s, t) = a_j \omega_j(s, t-1) + \xi_j(s, t)$, for $j = 1, 2, 3$. Here we set $\omega(s, 0) = 0$, for $s = s_1, \dots, s_n$.
- d. Set $\mathbf{p} = (1/3, 1/3, 1/3)$, which defines a partition of $[0, 1]$ as $\mathbb{P}_1 = [0, 1/3)$, $\mathbb{P}_2 = [1/3, 2/3)$ and $\mathbb{P}_3 = [2/3, 1]$.
- e. For $s = s_1, \dots, s_n$, simulate $u \sim (0, 1)$. If $u \in \mathbb{P}_j$, generate T -variate observation vector $\mathbf{y}(s) = (y(s, 1), \dots, y(s, T))^T$ from an T -variate normal distribution with mean $b_{0j} \mathbf{1}_T + \boldsymbol{\omega}_j(s)$ and covariance $\sigma_{\epsilon_j}^2 \mathbb{I}_T$, where $\boldsymbol{\omega}_j(s) = (\omega_j(s, 1), \dots, \omega_j(s, T))^T$. Finally, set $\omega_j(s, t) = x(s, t)$, for $t = 1, \dots, T$.

The following values of parameters are provided for the purpose of simulation: $b_{0_1} = 0$, $b_{0_2} = 10$, $b_{0_3} = 20$, $\sigma_{\epsilon_1}^2 = 1.0$, $\sigma_{\epsilon_2}^2 = 0.01$, $\sigma_{\epsilon_3}^2 = 2.0$, $a_1 = -0.75$, $a_2 = 0.75$, $a_3 = 0.25$, $\kappa_1 = 1$, $\kappa_2 = 1.5$, $\kappa_3 = 2$, $\sigma_1^2 = 1$, $\sigma_2^2 = 2$ and $\sigma_3^2 = 0.2$.

6.1.2 Results from our model

With the observed data set \mathbb{D} , we run the MCMC iterations for the proposed model. Based on MCMC iterations, observations from the predictive densities of \mathbf{y}_{20} and \mathbf{x}_{20} given the data set \mathbb{D} are simulated using the algorithm given in Appendix E. For running MCMC iterations, one needs to provide the prior parameters. Although we have chosen a finite prior variance for η_3^* , the posterior variance of η_3 turned out to be very large, which is probably due to huge variability present in the spatio-temporal data. This large posterior variance of η_3 makes the complete system unstable, so, we fix the value of η_3 at its maximum likelihood estimate 2.6889 computed by simulated annealing. Note that it is not very uncommon to fix the decay parameter in Bayesian inference of spatial data analysis, see for example Zhang [2004] and Banerjee [2020]. We give a

complete prior specification for the other parameters in the following.

Choice of prior parameters:

The particular choices of the hyper-prior parameters have been chosen using the leave-one-out cross-validation technique. Specifically, for $t = 1, \dots, 20$, we leave \mathbf{y}_t in turn and compute its posterior predictive distribution using relatively short MCMC runs. We then selected those hyperparameters that yielded the minimum average length of the 95% prediction intervals. The final specifications are as follows:

$$\alpha^* \sim N(0, \sqrt{500}), \beta^* \sim N(0, \sqrt{300}), [\sigma^2] \propto IG(170000, 2/2), [\sigma_\theta^2] \propto IG(5500, 780/2),$$

$$[\sigma_p^2] \propto IG(800, 20/2), [\eta_1^*] \propto N(-3, 1), [\eta_2^*] \propto N(-5, 1).$$

The large values of the shape parameters of the variance parameters are used, otherwise the posterior variance explodes and hence makes the complete model unstable. The plausible reason for such behaviour is the inherent large data variability. To restrict such an unusually large posterior variance, we restrict the prior of variance parameters very close to 0, with a very narrow variance.

Trace plots and posterior analysis:

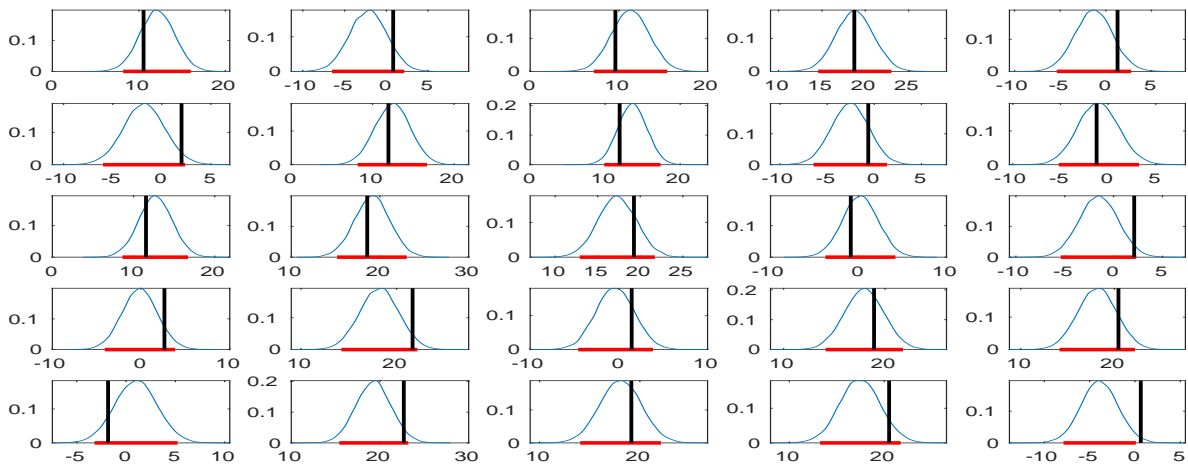
The trace plots of the parameters are given in Figure 17 of Appendix G. The plots do not exhibit lack of convergence of the MCMC runs. The posterior probability densities for the latent variables at 50 locations for 19 time points are shown in Figures 18 and 19 of Appendix G, where higher probability densities are depicted by progressively intense colours. We observe that true latent time series at all the 50 locations always lie in the high probability density regions.

The posterior predictive densities for the response vector \mathbf{y}_{20} and the latent vector

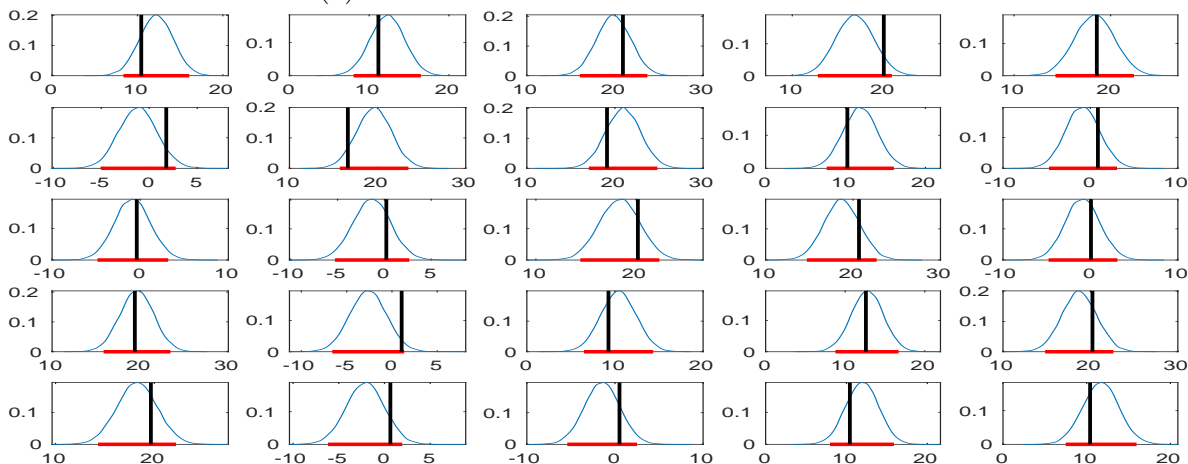
\mathbf{x}_{20} based on our model are provided in Figure 2 (first 25 locations in Figure 2b and next 25 locations in Figure 2b) and Figure 3 (Figure 3a for first 25 locations and Figure 3b for next 25 locations), respectively. Predictive densities for the responses capture the true values within the 95% predictive intervals in all but one location (25th location). The length of the predictive intervals lie between 7.49 to 8.83 with mean being 8.0219 and standard deviation (sd) 0.304879. For the latent vector \mathbf{x}_{20} , all the true values fall within the 95% predictive intervals of the predictive densities. The length of the intervals, in this case, ranges from 9.44 to 9.69 with mean 9.55808 and standard deviation (sd) 0.0582219.

6.2 Comparative study with nonstationary GP model

With the data set as generated above, we fit the NGP model using the SPDE technique. It is implemented using the package INLA in statistical software R. The posterior predictive densities of \mathbf{y}_{20} and \mathbf{x}_{20} , given \mathbb{D} , are provided below for purpose of comparison with the results of our model. It is seen that the 95% predictive intervals of each component of \mathbf{y}_{20} contains the true values of \mathbf{y}_{20} . However, they vary from 1894 to 3364 with mean 2378.483 and standard deviation (sd) = 259.3669 (Figure 4). A similar result is seen for the latent vector \mathbf{x}_{20} as well (Figure 5). All the true latent values are contained within the respective 95% predictive intervals, and the range of the length of the 95% intervals is from 1764 to 3053 with mean 2371.798 and standard deviation (sd) = 217.7212 (Figure 5). Clearly, the performance of our model, in terms of the length of predictive intervals for both response \mathbf{y}_{20} and latent \mathbf{x}_{20} outperformed the NGP model.



(a) Predictive densities for first 25 locations

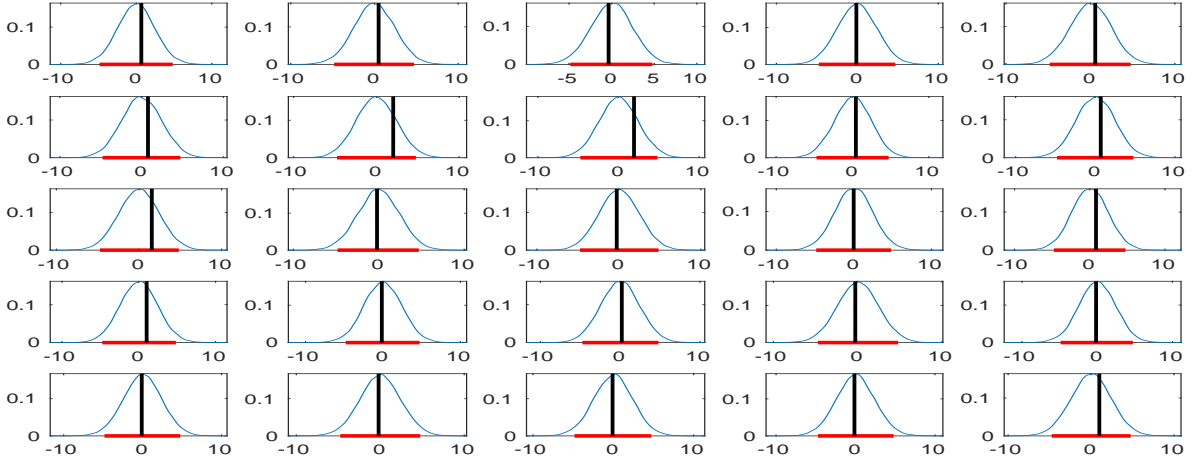


(b) Predictive densities for last 25 locations

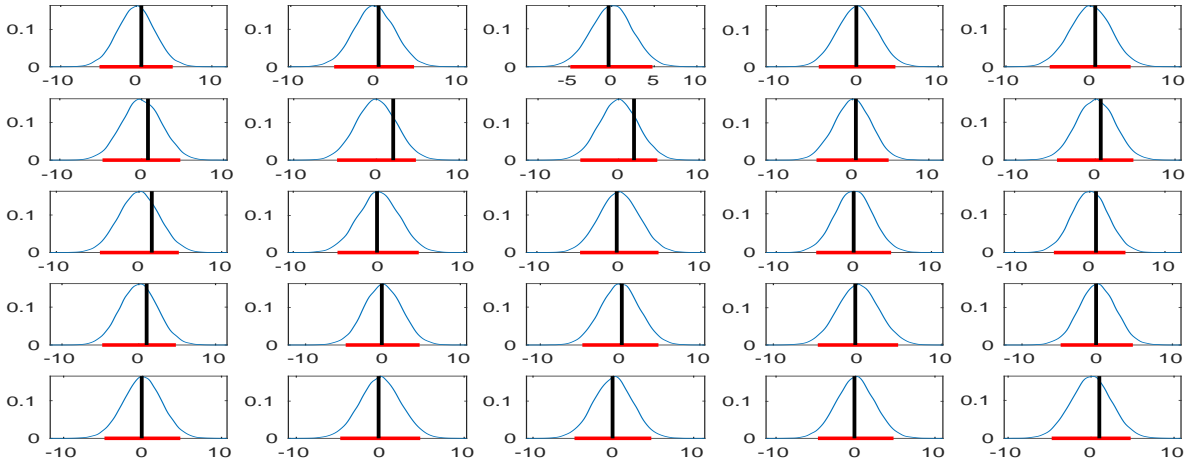
Figure 2: Predictive densities of 50 components of the response vector \mathbf{y}_{20} corresponding to 50 locations for the data set simulated from mixtures of three GPs, using our method. The red horizontal lines denote the 95% predictive intervals. The vertical black lines indicate the true values. All the true values, except one, lie within the 95% predictive intervals. The interval lengths vary from 7.49 to 8.83 units with mean 8.0219 (sd = 0.304879).

6.3 Mixture of two GQNs

For a second comparison study, we choose to simulate from a mixture two highly non-linear models, called general quadratic nonlinear (GQN) model. GQN model has been widely used in the literature of spatial and spatio-temporal modeling, see, for example, Wikle and Hooten [2010], Cressie and Wikle [2015], and Bhattacharya [2021] for a



(a) Predictive densities of latent variable for first 25 locations for 3 component mixture of GPs.



(b) Predictive densities of latent variable for last 25 locations for 3 component mixture of GPs.

Figure 3: Predictive densities of 50 components of the latent vector \mathbf{x}_{20} corresponding to 50 locations for the data set simulated from mixtures of three GPs, using our method. The red horizontal lines denote the 95% predictive interval. The vertical black lines indicate the true values. All the true values lie within the 95% predictive interval. The length of the intervals vary from 9.44 to 9.69 units, with mean 9.55808 (sd = 0.05822192).

significant overview of GQN model. We define the GQN model as

$$Y(s_i, t_k) = \phi_1(t_k, s_i) + \phi_2(t_k, s_i) \tan(X(s_i, t_k)) + \epsilon(s_i, t_k), \quad (12)$$

$$X(s_i, t_k) = \sum_{j=1}^n a_{ij} X(s_j, t_{k-1}) + \sum_{j=1}^n \sum_{l=1}^n b_{ijl} X(s_j, t_{k-1}) [X(s_l, t_{k-1})]^2 + \eta(s_i, t_k), \quad (13)$$

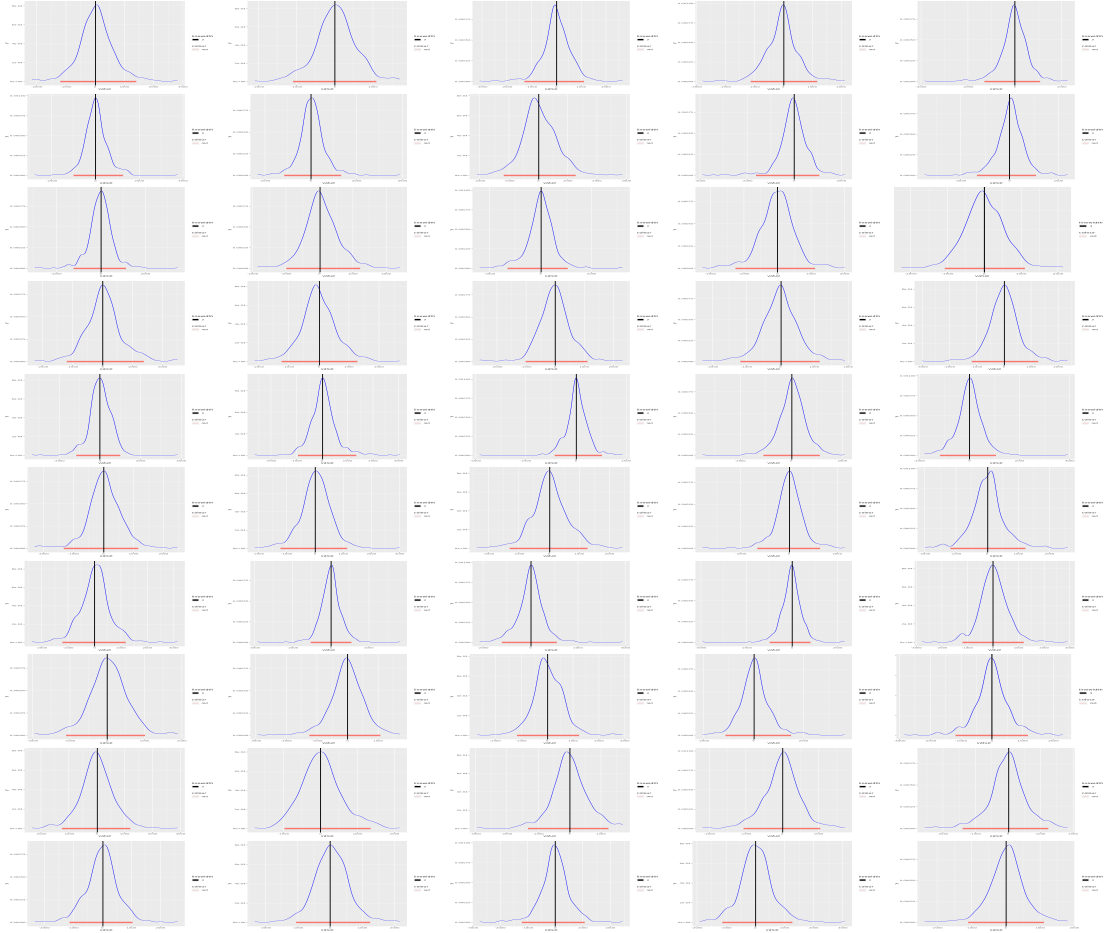


Figure 4: Posterior predictive densities of 50 components of \mathbf{y}_{20} , corresponding to 50 locations, for data simulated from 3 component mixtures of GPs, using NGP model. The vertical black line indicates the true value and the red horizontal line denotes the 95% predictive intervals. All the true values lie within the 95% predictive intervals. The interval lengths vary from 1894 to 3364 with mean 2378.483 (sd = 259.3669).

where $i \in \{1, \dots, n\}$ and $k \in \{1, \dots, T\}$. The coefficients $\phi_1(t_k, \cdot)$, $\phi_2(t_k, \cdot)$, random errors $\epsilon(t_k, \cdot)$, $\eta(t_k, \cdot)$ and the initial latent variable $X(t_0, \cdot)$ are assumed to be independent zero-mean Gaussian processes having covariance structure $c(\mathbf{s}_1, \mathbf{s}_2) = \exp(-\|\mathbf{s}_1 - \mathbf{s}_2\|)$, for $\mathbf{s}_1, \mathbf{s}_2 \in \mathbb{R}^2$, with $\|\cdot\|$ being the Euclidean norm. Moreover, it is assumed that for $i, j, l \in \{1, \dots, n\}$, a_{ij} and b_{ijl} have independent univariate 0 mean normal distributions with variance 0.001^2 .

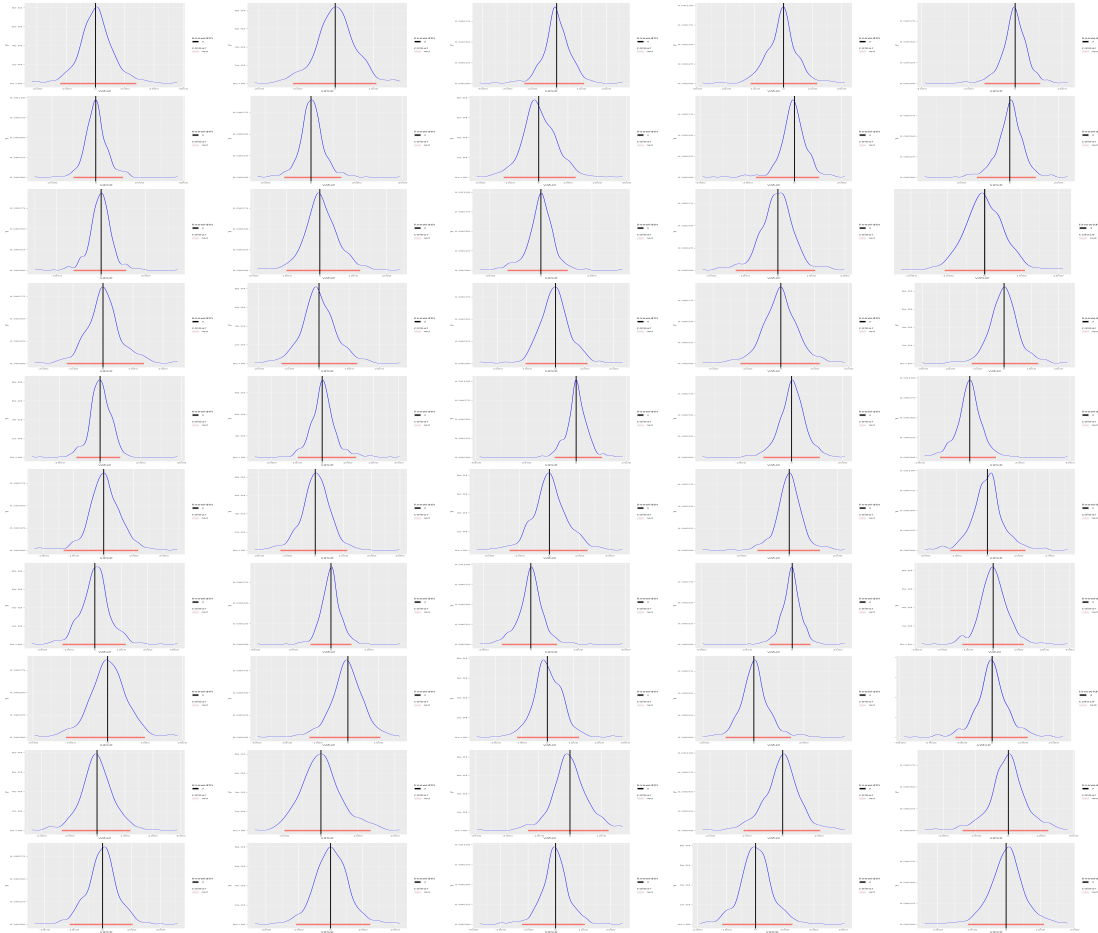


Figure 5: Predictive densities of 50 components of \mathbf{x}_{20} , corresponding to 50 locations, for data simulated from 3 component mixtures of GPs, using NGP model. The vertical black line indicates the true value and the red horizontal line denotes the 95% predictive intervals. All the true values lie within the 95% predictive intervals. The interval lengths vary from 1764 to 3053 with mean 2371.798 (sd = 217.7212).

6.3.1 Data generation

Here, a step-by-step description is provided for generating observations from the mixture of two GQNs. Let n and T denote the number of locations and time points.

- a. Generate n locations s_1, \dots, s_n from $[0, 1] \times [0, 1]$.
- b. Generate $n \times T$ matrix X using equation (13) by taking the coefficients as described above.
- c. $\phi_1(t)$, $\phi_2(t)$ and $\epsilon(t)$ are generated independently for $t = 1, \dots, T$ from zero-mean

m -variate Gaussian with variance-covariance matrix \mathbb{S} , whose (i, j) th element is $\exp(-\|s_i - s_j\|)$. Let the i th element of $\boldsymbol{\phi}_j(t)$, $j = 1, 2$, and $\boldsymbol{\epsilon}(t)$ be $\phi_j(t, s_i)$ and $\epsilon(t, s_i)$, respectively.

- d. Let $u \sim \text{unif}(0, 1)$. Given all the parameters and latent variables, generate $Y(s_i, t)$, for $i = 1, \dots, n$ and $t = 1, \dots, T$, as

$$Y(s_i, t) = \begin{cases} \phi_1(t, s_i) + \phi_2(t, s_i) \tan(X(s_i, t)) + \epsilon(t, s_i) & \text{if } u < 0.6, \\ 5 + \phi_1(t, s_i) + \phi_2(t, s_i) \tan(X(s_i, t)) + \epsilon(t, s_i) & \text{if } u \geq 0.6. \end{cases}$$

6.3.2 Results from our model

For this data set as well, we run the MCMC iterations for simulating observations from the posterior densities of the parameters involved in our model. These MCMC iterations and Monte Carlo averages provide simulated observations from the posterior densities of \mathbf{y}_{20} and \mathbf{x}_{20} , given the data set \mathbb{D} (for the Algorithm see Appendix E). To make the MCMC run feasible one needs to specify the prior parameters. The specific choice of the hyperparameters are mentioned below, except for η_3 , which is kept fixed at its MLE 5.5042, obtained by simulated annealing.

Choice of prior parameters:

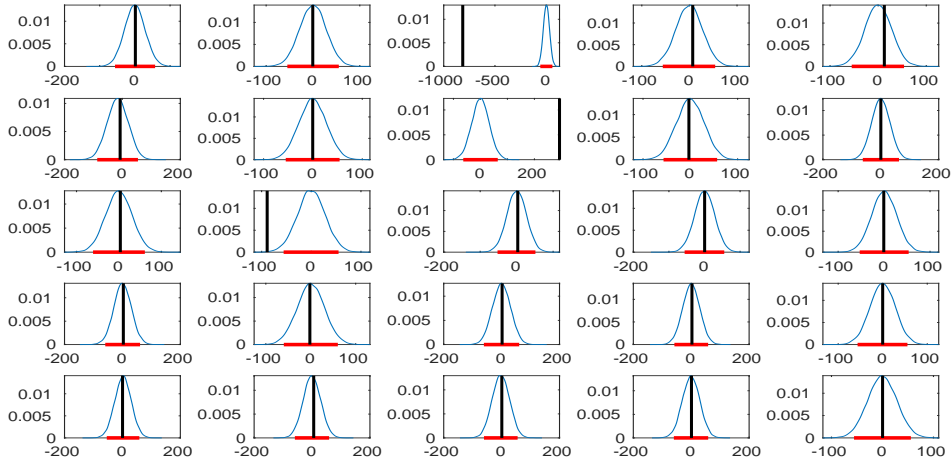
Using the same cross-validation technique as before, we obtain the following prior specifications:

$$\alpha^* \sim N(0, \sqrt{500}), \beta^* \sim N(0, \sqrt{300}), [\sigma^2] \propto IG(780000, 2/2), [\sigma_\theta^2] \propto IG(58900, 770/2), \\ [\sigma_p^2] \propto IG(385, 20/2), [\eta_1^*] \propto N(-3, 1), [\eta_2^*] \propto N(-5, 1).$$

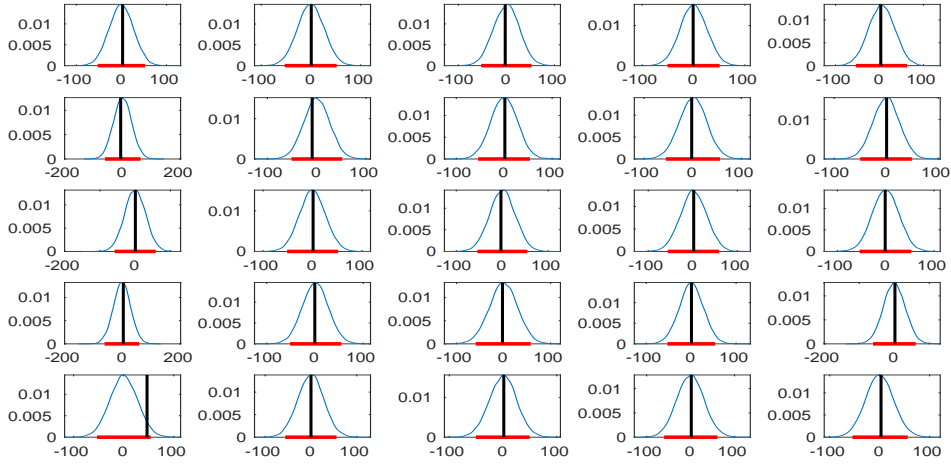
As earlier, here also the shape parameters of the variance parameters are taken large because of the huge inherent data-variability. Unless we restrict the prior mean and variance very close to 0, the posterior variances of the variance parameters become extremely high, making the complete systems unstable.

Trace plots and posterior analysis:

The trace plots of the parameters are provided in the Figure 20, and the posterior density plot of $\mathbf{x}_t, t = 1, \dots, 19$ are displayed in 21 and 21 of Appendix H. The trace plots provide strong evidence of MCMC convergence. Further, the posterior density plots show that the posteriors of the latent variables contain the true latent variable time series at all the 50 locations in the high probability density regions successfully.



(a) Predictive densities for first 25 locations

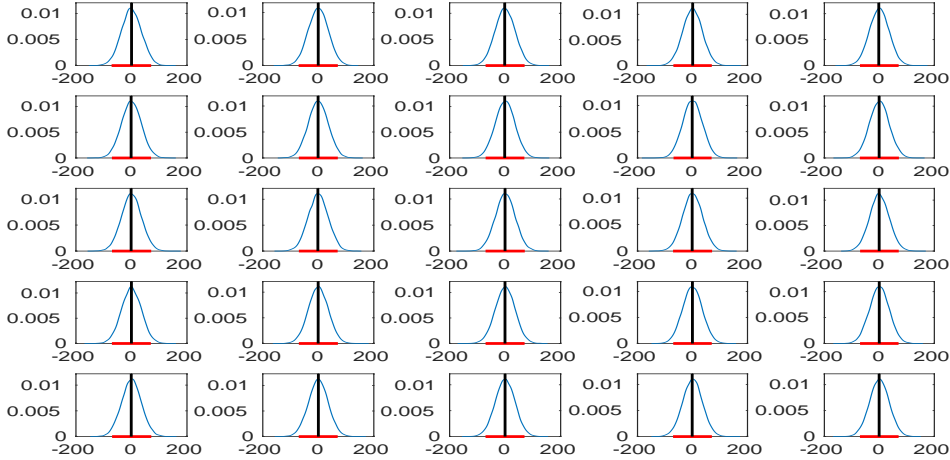


(b) Predictive densities for last 25 locations

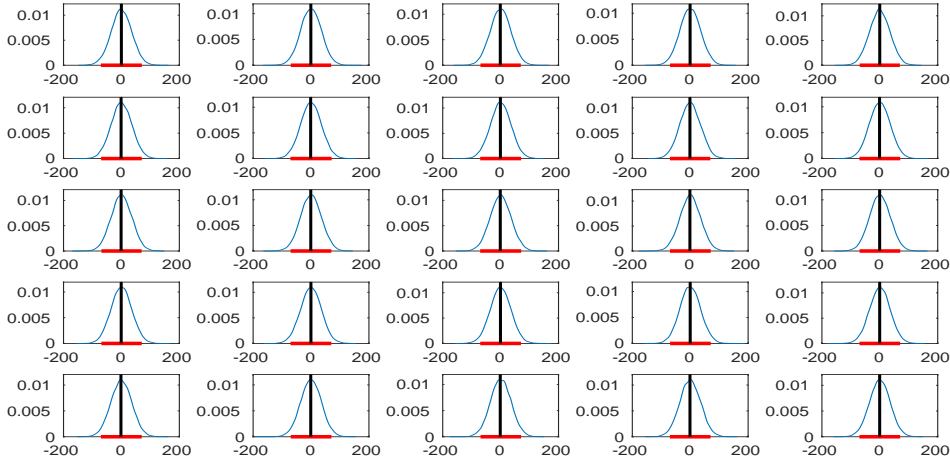
Figure 6: Predictive densities of the 50 components of response vector \mathbf{y}_{20} , corresponding to 50 locations, for data set simulated from mixtures of two GQNs, using our model. The red horizontal lines denote the 95% predictive intervals. The vertical black lines indicate the true values. All the true values, except three, lie within the 95% predictive intervals. The interval lengths vary from 99 to 141 units, with mean 112.9458 (sd = 7.9680).

The posterior predictive densities of 50 components of \mathbf{y}_{20} and \mathbf{x}_{20} are provided in Figures 6 and 7, respectively. For the first 25 components of \mathbf{y}_{20} Figure 6a provides the density plots along with the 95% predictive intervals. They failed to capture true values at locations s_3 , s_8 and s_{13} . The posterior predictive densities along with the 95% predictive intervals for the next 25 locations are provided in 6b. It is seen that all the true values fall within the 95% predictive intervals. Thus, out of 50 locations, except

for 3 places, the true response values are captured by the 95% predictive intervals. The lengths of the intervals vary from 99 to 141 units. The mean length of intervals turned out to be 112 with standard deviation (sd) = 7.9680. In the case of latent vector, \mathbf{x}_{20} , the posterior predictive density plots of first 25 components of \mathbf{x}_{20} are given in 7a and that of next 25 components are provided in 7b.



(a) Predictive densities of latent variable for first 25 locations.



(b) Predictive densities of latent variable for last 25 locations.

Figure 7: Predictive densities of the 50 components of latent vector \mathbf{x}_{20} , corresponding to 50 locations, for data set simulated from mixtures of two GQNs, using proposed model. The red horizontal lines denote the 95% predictive interval. The vertical black lines indicate the true values. All the true values lie within the 95% predictive interval. The length of the intervals vary from 138 to 142.5 units with mean 140.4856 (sd = 0.8524).

All the true values are captured by the respective predictive intervals. The length of the intervals vary from 138 to 142.5 units with mean 140.4856 and standard deviation

(sd) = 0.8524.

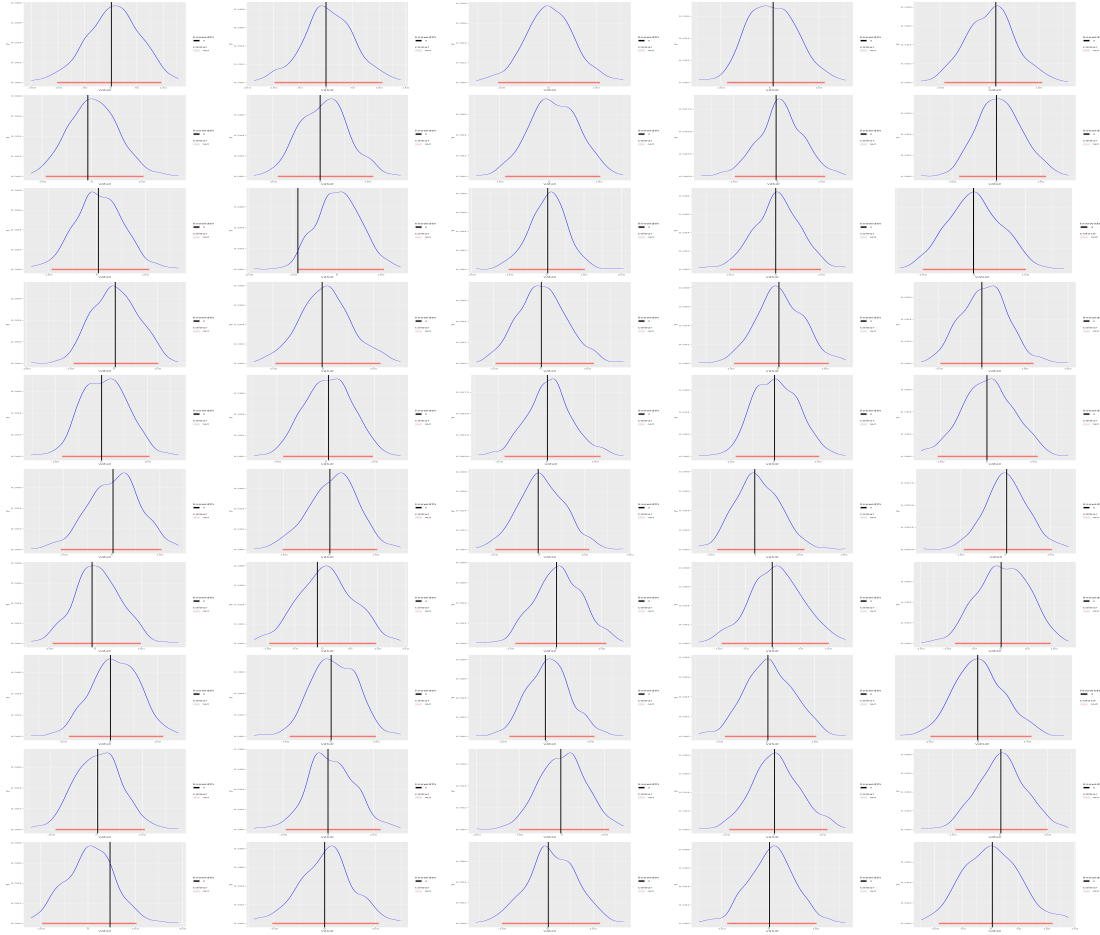


Figure 8: Predictive densities of 50 components of response vector \mathbf{y}_{20} , corresponding to 50 locations, for data simulated from mixtures of two GQNs, using NGP model. The vertical black line indicates the true value and the red horizontal line denotes the 95% predictive intervals. All the true values lie within the 95% predictive intervals. The interval lengths vary from 172 to 233.5 with mean 200.79 (sd = 10.18972).

6.3.3 Comparative study with non-stationary GP model

Similar to the analysis of the mixture of GP models, we fitted the NGP model on the current data set using INLA in R. For the purpose of fitting the NGP model, the same SPDE technique has been implemented. The posterior predictive densities for the components of \mathbf{y}_{20} and \mathbf{x}_{20} are reported in Figures 8 and 9, respectively. The 95% predictive intervals of the components of \mathbf{y}_{20} capture the true values except for the

3rd, 8th and 12th components. The range of the lengths of the predictive intervals is from 172 to 233.5 units. The mean length of the intervals turned out to be 200.79 with standard deviation (sd) = 10.1872. Therefore, the mean length of the predictive intervals is more than 1.75 times the mean length of the predictive intervals our proposed model. It is interesting to see that none of the true values were captured by the 95% predictive intervals of the posterior predictive densities of the components of \boldsymbol{x}_{20} (Figure 9). Interestingly, the lengths of the intervals turned out to be too small, in the order of 10^{-4} . Hence from the analysis of this simulated data set, we observe that the performance of our model is significantly better than that of the NGP model for the mixture of GQN data set.

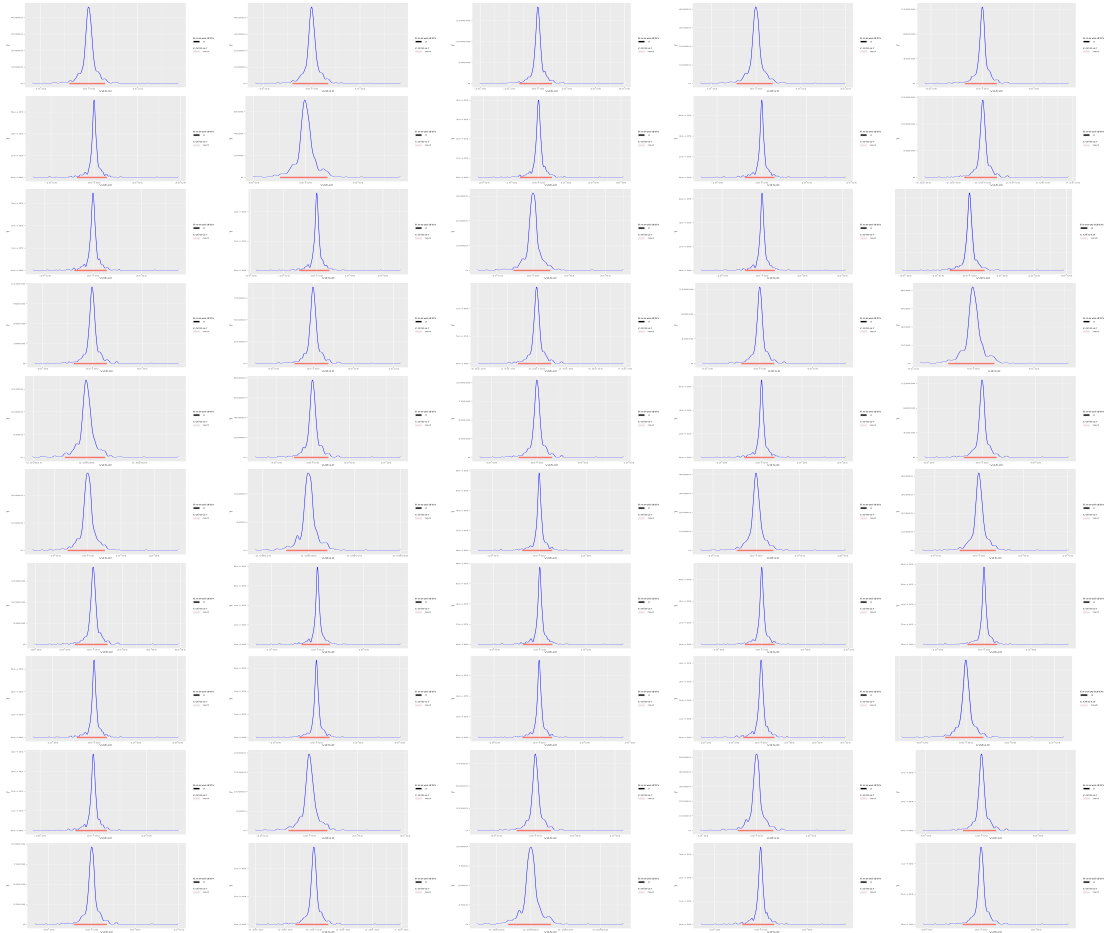


Figure 9: Predictive densities of 50 components of latent vector \mathbf{x}_{20} , corresponding to 50 locations, for data simulated from mixtures of two GQNs, using NGP model. The red horizontal line denotes the 95% predictive intervals. None of the true values lie within the respective predictive interval. The interval lengths are of the order 10^{-4} .

7 Real data analysis

We evaluate our model performance on two real data sets on temperatures. The first spatio-temporal data is the temperature values taken around Alaska recorded for 65-70 years. The second data set consists of sea surface temperatures over a wide range of areas, recorded for 100 months. The details of the data sets are provided in Sections 7.1 and 7.2, respectively.

Before applying our model on these data sets, we first make the following transfor-

mation (Lambert projection, see Guha [2017]) of the locations so that the Euclidean distance make more sense. Let ϕ be longitude and ψ be latitude in radian. Then the following transformation is made:

$$\begin{aligned} s_1 &= 2 \sin \left(\frac{\pi}{4} - \frac{\psi}{2} \right) \sin \phi; \\ s_2 &= -2 \sin \left(\frac{\pi}{4} - \frac{\psi}{2} \right) \cos \phi. \end{aligned} \tag{14}$$

7.1 Alaska temperature data

A real data analysis is done on the temperature data of Alaska and its surroundings. The data set is collected from <https://www.metoffice.gov.uk/hadobs/crutem4/data/download.html> by clicking the link `CRUTEM.4.6.0.0.station_files.zip` given under the heading **Station data**. The details of the data set can be read from <https://crudata.uea.ac.uk/cru/data/temperature/crutem4/station-data.htm>. A total of 30 locations are considered for the analysis. Annual average temperature data for the years 1950 to 2015 are taken after detrending. Of these 30 locations, at four locations many data were missing. So, we decided to construct the complete time series for these four locations. Among these 30 locations, data till 2021 were available for 16 positions. We thus have made multiple time predictions for these 16 locations. The 26 spatial points are indicated in Figure 10 in red and 4 locations (for which the complete time series is reconstructed) are indicated in blue in the same graph. The latitudes and longitudes are provided in Table 1.

Thus, the data set considered here contains 26 locations and 65 time points from 1950 to 2014 (last time point is set aside for the purpose of single time point prediction). We denote the data set by $\mathbb{D} = \{\mathbf{y}_1, \dots, \mathbf{y}_{65}\}$, where \mathbf{y}_t , $t \in \{1, \dots, 65\}$, is a 26 dimensional vector. In this analysis, we have made both temporal and spatial predictions after

Sl. No.	Lat.	Long.	Sl. No.	Lat.	Long.	Sl. No.	Lat.	Long.
1	71.3N	156.8W	11	64.8N	147.9W	21	62.2N	145.5W
2	60.6N	151.3W	12	60.1N	149.5W	22	66.9N	162.6W
3	59.5N	139.7W	13	63N	155.6W	23	58.4N	134.6W
4	55.2N	162.7W	14	63N	141.9W	24	63.7N	149W
5	61.2N	150W	15	55N	131.6W	25	68.2N	135W
6	70.1N	143.6W	16	61.6N	149.3W	26	59.6N	133.7W
7	64.5N	165.4W	17	64N	145.7W	27	62.8N	137.4W
8	66.9N	151.5W	18	60.8N	161.8W	28	64.1N	139.1W
9	59.6N	151.5W	19	57.8N	152.5W	29	67.4N	134.9W
10	60.5N	145.5W	20	58.7N	156.7W	30	60.7N	135.1W

Table 1: Latitude and Longitude (in degrees) of 30 locations in and around Alaska. The locations corresponding to the serial numbers, indicated in bold, are used for multiple predictions. The serial numbers which are denoted in blue, for the corresponding spatial locations, complete time series are reconstructed. These blue serial numbers are indicated by L_{25} , L_{26} , L_{28} and L_{30} for future references.

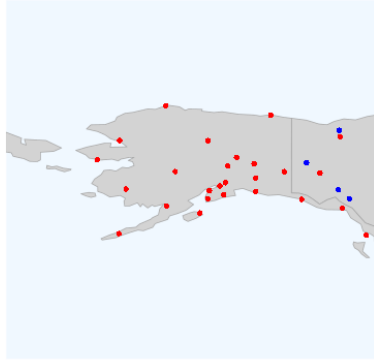


Figure 10: The map of Alaska and its surroundings. The red dots indicate the locations at which the data for the year 1950-2015 are considered. The positions indicated by blue dots at which the spatial prediction are made for the complete time series.

detrending the data. At these 26 locations, we obtained the predictive densities for the year 2015. For 16 locations (indicated by $L_1, \dots, L_7, L_{11}, \dots, L_{13}, L_{18}, \dots, L_{20}, L_{22}, L_{27}, L_{29}$ for references hereafter) we made multiple time point predictions (see Appendix E for the temporal prediction). Along with these temporal predictions, we constructed the 95% predictive intervals for the complete time series for the 4 left out locations (The algorithm for spatial prediction is given in Appendix F). To do this, we augmented the data set \mathbb{D} with the initial values for the 65 time points of the four locations and then updated the values by calculating the conditional densities given the data set \mathbb{D} . That is

to say, we start with $\mathbb{D}^* = \{\mathbf{y}_1^*, \dots, \mathbf{y}_{65}^*\}$, where \mathbf{y}_t^* is a 30 dimensional vector, with the last four values augmented with \mathbf{y}_t , for $t \in \{1, \dots, 65\}$. The parameters of our model, including the latent variables, are updated given \mathbb{D}^* , and then the last four values of \mathbf{y}_t^* are updated given the parameter values and latent variables. This is continued for the complete MCMC run. In Appendix K, we validate that the underlying spatio-temporal process that generated the Alaska data is non-Gaussian, strictly stationary, and the lagged correlations converge to zero as the lags tend to infinity. Besides, there is no reason to assume separability of the spatio-temporal covariance structure. Although our spatio-temporal process is non-stationary, it is endowed with the other desirable features, and the results of analysis of the Alaska data show that it is an appropriate model for this data.

7.1.1 Prior choices for the Alaska temperature data

With the same cross-validation technique as in the simulation experiments, the complete specifications of the priors are obtained as follows:

$$\alpha^* \sim N(0, \sqrt{500}), \beta^* \sim N(0, \sqrt{300}), [\sigma^2] \propto IG(550000, 2/2), [\sigma_\theta^2] \propto IG(700, 780/2),$$

$$[\sigma_p^2] \propto IG(1000, 100/2), [\eta_1^*] \propto N(-3, 1), [\eta_2^*] \propto N(-5, 1).$$

As before, we fix η_3 at its maximum likelihood estimate 4.5579. As in the cases of simulation studies, the shape parameters for the prior distribution of the variance parameters are kept large to make sure that the posterior variances of the variance parameters remain finite; see Bhattacharya [2021] for a similar strategy.

7.1.2 Results of the Alaska temperature data

For the current study, we run 2,50,000 MCMC iterations with the first 1,25,000 iterations as burn-in. Moreover, we make a thinning of width 5 for better mixing of the MCMC samples. The time taken was about 8 hours 12 minutes on our desktop computer. The MCMC trace plots for the parameters, except η_3 , are given in Figure 23 of Appendix I.1. The trace plots do not show signs of non-convergence. The posterior densities of the latent variables are displayed in Figure 24 of Appendix I.2.

The predictive densities for \mathbf{y}_{66} (detrended temperatures of the Alaska temperature data for the year 2015) at 26 locations along with the highest density regions are depicted in Figure 11. The intensity of the colour is proportional to the density of the predictive densities of \mathbf{y}_{66} . The plot shows that most of the true values fall in the highest density regions. The individual predictive densities with 95% prediction intervals and the true values are provided in Figure 25 in Appendix I.3 for further reference. Except one, all the true values lie well within the 95% predictive intervals.

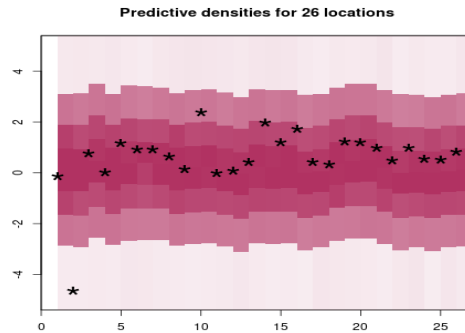


Figure 11: The highest probability density region of the predictive densities and the true values of detrended temperatures (Alaska temperature data) for the year 2015 at 26 locations are depicted in this figure. The x-axis of the figure indicates the locations, and at each location, colour-coded densities are plotted in the vertical axis. The intensity of the colour is proportional to the density. The true values are indicated by the black stars. Majority of the true values fall in the high density regions.

The predictive densities together with highest density regions (the higher the inten-

sity of colour, higher the density) for the years 2016-2021 at the 16 locations, $L_1, \dots, L_7, L_{11}, L_{12}, L_{13}, L_{18}, L_{19}, L_{20}, L_{22}, L_{27}, L_{28}$, are shown in Figure 12. The two figures (Figure 26 and Figure 27) in Appendix I.4, each containing 8 locations, show the predictive densities with 95% prediction intervals. Except for one location, at one time point, in all other scenarios, the true values are captured by the 95% predictive intervals associated with our model.

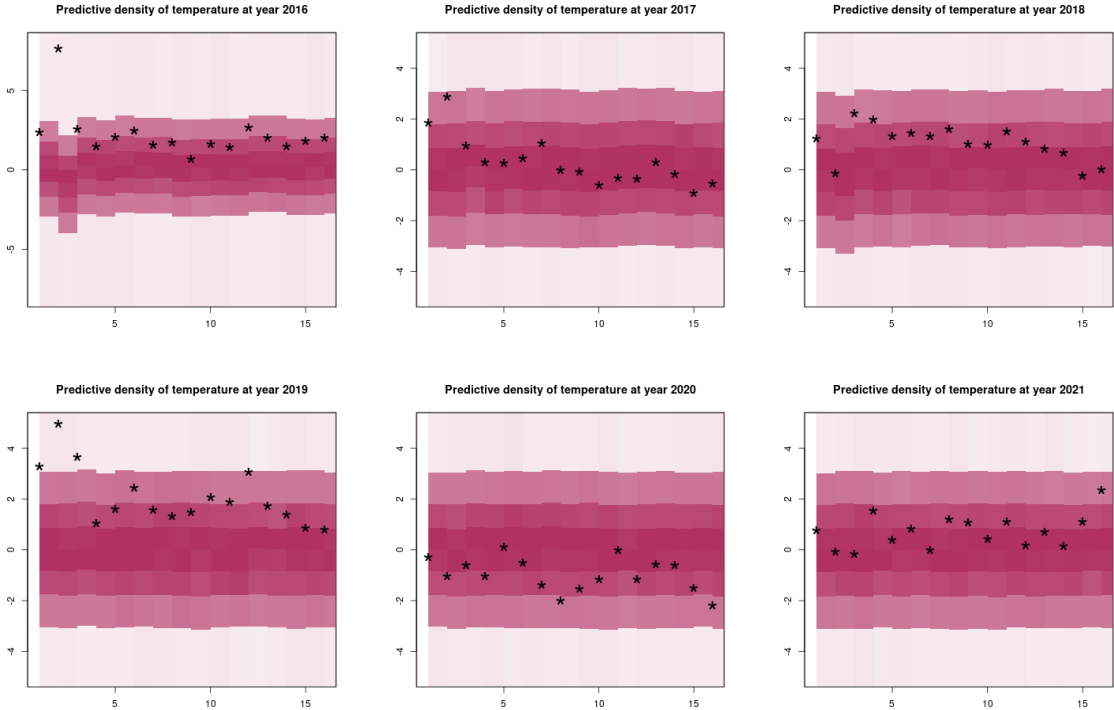


Figure 12: The highest probability density region of the predictive densities and the true values of detrended temperatures (Alaska temperature data) for the years 2016 to 2021 at 16 locations are depicted in this figure. The x-axis of of the figure indicates the locations, and at each location, colour-coded densities are plotted in the vertical axis. The intensity of the colour is proportional to the density. The true values are indicated by the black stars. Majority of the true values for all the 6 years fall in the high density regions.

The complete time series for the four locations, which were indicated as blue dots in Figure 10, are reconstructed using our model. The Bayesian predictive densities at each time point for these locations are shown in Figure 13 using probability plot. Higher the intensity of the color, higher is the density. The available true detrended temperature

values at these locations are plotted and depicted by black stars in Figure 13. Except a very few points at these locations, the detrended true values lie well within the high density regions. Overall, the performance of our model on this particular data set is encouraging.

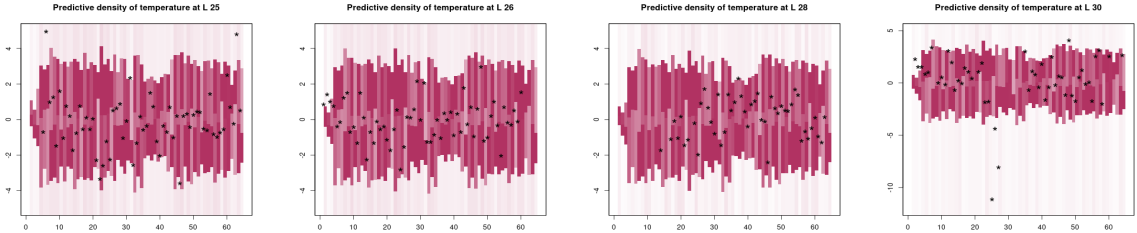


Figure 13: Posterior predictive densities of the reconstructed detrended temperature data of Alaska and its surroundings at 4 locations. Higher the intensity of the colour, higher is the probability density. The black stars represent the available true temperature values (detrended). Except for few points, majority of the true values at each location fall within the high probability density region.

7.2 Sea surface temperature data

The sea surface temperature data is obtained from <http://iridl.ldeo.columbia.edu/SOURCES/.CAC/>. For the purpose of illustration, we have taken spatio-temporal observations of the first 40 locations and the first 100 time points from the complete data set. The locations of the chosen data set varies from 56°W to 110°E and 19°S to 25°N . The locations are given in Table 2. Hundred monthly average temperatures are taken starting from the month of January 1970. Among these 40 locations and 100 time points, observations corresponding to 30 locations and 99 time points are taken as the learning set. The observations corresponding to the last 10 locations and the last time point are kept aside for the prediction purpose (see Appendix E for the algorithm of obtaining observations from predictive densities). Only for the sake of convenience, the time series at each location is referenced to its mean, in the

sense that the mean of the time series at each location is subtracted from the original data. As in the Alaska temperature data analysis, we denote the learning data set by

Sl. No.	Lat.	Long.	Sl. No.	Lat.	Long.	Sl. No.	Lat.	Long.	Sl. No.	Lat.	Long.
1	19S	108E	11	1N	84E	21	13N	30E	31	25N	4E
2	19N	20W	12	19S	14E	22	7S	36E	32	7N	52E
3	19S	42E	13	13N	48E	23	29N	104E	33	11N	18E
4	17N	58E	14	27N	18W	24	15S	24W	34	5N	16W
5	7N	2W	15	5S	110E	25	1N	72E	35	7N	56W
6	11S	76E	16	17S	46W	26	1S	46W	36	19S	106E
7	3S	2E	17	7S	10W	27	13S	64E	37	1S	20W
8	25S	28W	18	23S	14E	28	9N	12E	38	17S	28W
9	25N	100E	19	21S	36W	29	15N	24E	39	19S	0
10	7N	26W	20	1S	28W	30	25S	52E	40	29N	48W

Table 2: Latitude and Longitude (in degrees) of 40 locations for the sea surface temperature data. The locations corresponding to the serial numbers, indicated in bold, are used for complete time series prediction. These bold serial numbers are indicated as L_{31}, \dots, L_{40} for future reference.

$\mathbb{D} = \{\mathbf{y}_1, \dots, \mathbf{y}_{99}\}$, where \mathbf{y}_t is a 30 dimensional spatial observation at time point t .

At these 30 locations, we obtain the posterior predictive densities for the 100th time point and find out the high probability density regions for the entire time series of the locations corresponding to the serial numbers indicated in bold within Table 2. We provide below a plot (Figure 14) which represents the locations of the sea temperature data after we make the Lambert projections (see equation (14)). The blue dots in Figure 14 are used as the test set locations for the complete time series prediction. These locations are referred to as L_{31}, \dots, L_{40} hereafter. For calculating the posterior predictive densities at 99 time points for the above mentioned 10 spatial locations, the data set \mathbb{D} is first augmented with the initial values for 99 time points of the ten locations and then the values are updated by sampling from the corresponding conditional distributions given the data set \mathbb{D} . That is to say, we start with $\mathbb{D}^* = \{\mathbf{y}_1^*, \dots, \mathbf{y}_{99}^*\}$, where $\mathbf{y}_t^* = [\mathbf{y}_t^T : \mathbf{z}_t^T]^T$ is a 40 dimensional vector, with \mathbf{z}_t being the initial guess for the ten locations L_{31}, \dots, L_{40} , $t \in \{1, \dots, 99\}$. The parameters of our

model, including the latent variables, are then updated given \mathbb{D}^* , and then the last ten values of \mathbf{y}_t^* are updated given the parameter values and the latent values. This continues for the entire MCMC run. (The detailed algorithm for spatial predictions is provided in Appendix F). Note that this sea surface temperature data arises from a non-stationary (both weakly and strongly), non-Gaussian spatio-temporal process with lagged correlations tending to zero (refer to Bhattacharya [2021] for further details).

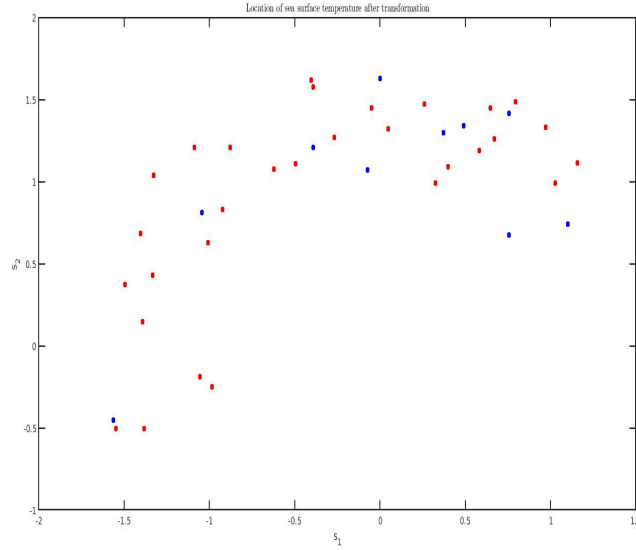


Figure 14: Locations of sea surface temperature data after the transformation given in equations 14. The red points represent the locations of the observations in the learning set. The blue solid dots are the locations of the observations in the test set.

7.2.1 Prior choices for sea surface temperature data

Following our cross-validation technique to obtain the hyper parameters, we completely specify the priors as follows:

$$\alpha^* \sim N(0, \sqrt{500}), \beta^* \sim N(0, \sqrt{300}), [\sigma^2] \propto IG(45000, 2/2), [\sigma_\theta^2] \propto IG(1000, 780/2),$$

$$[\sigma_p^2] \propto IG(100, 100/2), [\eta_1^*] \propto N(-3, 1), [\eta_2^*] \propto N(-3, 1).$$

As before, we fixed η_3 at its maximum likelihood estimate; here the value is 5.8879. The shape parameters for the prior distribution of the variance parameters are kept to be large to ensure that the posterior variances of the variance parameters remain finite, as done in other studies. We performed a total of 2,50,000 MCMC iterations with 1,00,000 burn-in. In addition, for a better mixing, a thinning of width 5 has been done. It took around 12 hours and 53 minutes on our desktop computer.

7.2.2 Controlling M_s

Since the locations are distributed very widely over the space, the value of M_s becomes too large for this data for a given s . Now M_s appears in the denominator of the variance covariance matrix of the predictive densities of the time series at a particular location (see equation (8)). Therefore, the variability becomes too less. So, to control the variability we modify the definition of M_s as $M_s = \exp(c \max\{\|s^2 - u^2\|^2 : u \in S\})$, where c is a positive small constant. Note that it does not hamper the properties of M_s and hence all the theoretical properties of the processes remain unchanged. The constant c controls the spatial variability which can be thought of as a distance scaling factor. The choice of c was also done by cross-validation. It was found that $c = 0.25$ works reasonably well for the sea surface temperature data.

7.2.3 Results of the sea surface temperature data

Figure 28 of Appendix J.1, representing the MCMC trace plots of the parameters, exhibits no evidence of non-convergence of our MCMC algorithm. The posterior predictive colour density plots for the latent variables are shown in Figure 29 of Appendix J.2.

Next, we provide the posterior predictive densities at the 100th month for each of

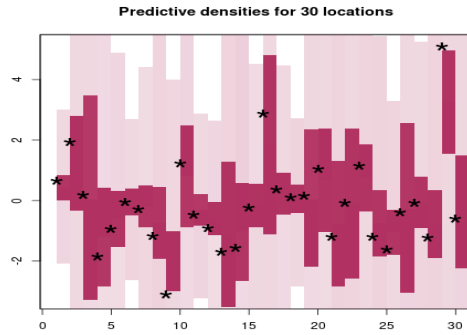


Figure 15: The highest probability density region of the predictive densities and the true values of sea surface temperature data for the 100th month at 30 locations are depicted in this figure. The x-axis of the figure indicates the locations, and at each location, colour-coded densities are plotted in the vertical axis. The intensity of the colour is proportional to the density. The true values are indicated by the black stars. All of the true values (average referenced) fall in the high density regions.

the 30 locations (the algorithm for obtaining the temporal predictive densities is given in the Appendix E). The highest predictive density regions are given for 30 locations and are displayed in Figure 15. All the true values fall in the high probability density region. Further, the individual predictive density plots are shown in Figure 30 of Appendix J. As the plots indicate, the posterior predictive densities for the future time point correctly contains the true values for all of these locations. The results encourage us to use the proposed model for the future time point prediction for a non-stationary spatio-temporal data.

Similar to the other real data analyses, here also we predict at various spatial locations. As mentioned in Section 7.2, we kept aside the complete temporal observations for the ten locations for evaluating the performance of the proposed model. We obtained the posterior predictive densities for each of the 99 time points for a given location (see F for the algorithm). The highest density regions of the predictive densities are depicted in Figure 16. Clearly, most of the true values, indicated by black stars in Figure 16, fall within the high probability density regions.

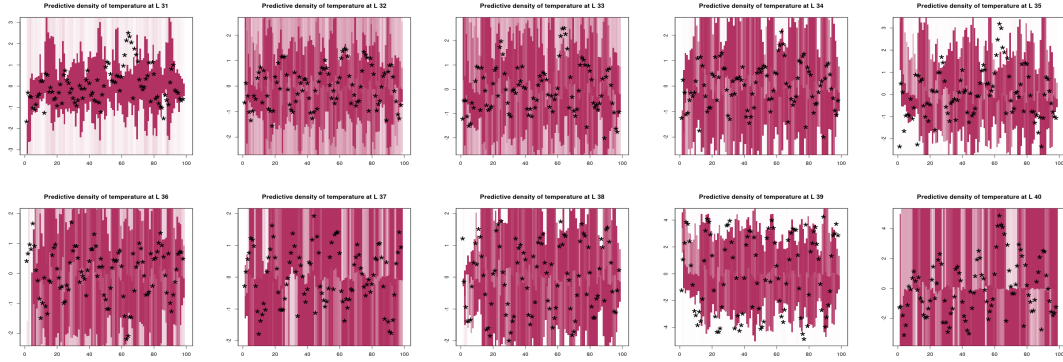


Figure 16: Posterior predictive densities of the reconstructed time series of sea surface temperature data (average referenced) at ten locations. Higher the intensity of the colour, higher is the probability density. The black stars represents the true temperature values (average referenced). Most of the true values fall within the high density regions.

8 Summary and conclusion

Although Hamiltonian equations are very well-known in Physics, its importance in Statistics is mostly confined to Hamiltonian Monte Carlo for approximate simulations from posterior distributions. However, given the success of the Hamiltonian equations in phase-space modeling, it is not difficult to anticipate its usefulness in spatio-temporal statistics, if properly exploited. This key insight motivated us to build a new spatio-temporal model through the leap-frog algorithm for a suitably modified set of Hamiltonian equations, where stochasticity is induced through appropriate Gaussian processes. Our marginal stochastic process is *nonparametric, non-Gaussian, non-stationary, non-separable*, with appropriate dynamic temporal structure, and with time treated as a continuous variable. Additionally, the lagged correlations between the observations tend to zero as the space-time lag goes to infinity. Hence, compared to the existing spatio-temporal processes, our process seems to be the most realistic. Indeed, our simulation experiments reveal that for general spatio-temporal datasets, our model outperforms the popular approach of latent process spatio-temporal modeling based on non-stationary Gaussian processes. Furthermore, suitability and flexibility of our model

is vindicated by the results of our applications to two real data sets. Continuity and smoothness properties add further elegance to our new process. In all the simulation and real data analyses, we have considered the time points to be evenly spaced. For unevenly spaced time points, the model can be applied without much changes.

The way to deal with the unevenly distributed observed time points data using our model is to assume that there are a few missing values in the data set. During the MCMC process, the missing values can be simulated. Assume for the sake of clarity that the data are observed at time points $t_1, t_1 + \delta, t_1 + 3\delta$, and $t_1 + 5\delta$ (in, say, seconds), where $\delta > 0$. The data at time points $t_1, t_1 + \delta, t_1 + 2\delta, t_1 + 3\delta, t_1 + 4\delta$, and $t_1 + 5\delta$ (in seconds) will be taken into consideration. Data at time points $t_1 + 2\delta$ and $t_1 + 4\delta$ (in seconds) should be regarded as missing, and they can be simulated during MCMC runs using the predictive densities.

We did not try to analyse particularly sizable datasets in this article. In our future endeavors, we shall consider application of our ideas to very big datasets using basis representation, and a variable dimensional MCMC technique, called TTMC, which was proposed by Das and Bhattacharya [2019].

Acknowledgment

The authors are thankful to Dr. Moumita Das and Dr. Suman Guha for their valuable remarks which significantly improves the presentation of the manuscript.

A Proofs of the theorems

This appendix contains the proof of all the relevant results presented in subsection 2.3.

Lemma A.1 M_s is infinitely differentiable in $s \in S$.

Proof: Since the exponential function is infinitely differentiable, it is sufficient to show that $\max\{|s^2 - u^2|^2 : u \in S\}$ is infinitely differentiable with respect to s . We first prove the result in one dimension and then will generalize to higher dimension. Let S be a compact set in \mathbb{R} . We consider different cases as follows.

Case 1: Let $S = [a, b]$, where $0 < a < b$. Then $\max\{|s^2 - u^2|^2 : u \in [a, b]\} = s^4 + \max(a^4, b^4) - 2s^2a^2$, which is an infinitely smooth function of s .

Case2: Let $S = [a, b]$, where $a < b < 0$. Then $\max\{|s^2 - u^2|^2 : u \in [a, b]\} = s^4 + \max(a^4, b^4) - 2s^2b^2$, which is also infinitely differentiable function of s .

Case 3: Let $S = [-a, b]$, where $a, b > 0$. Then

$$\max\{|s^2 - u^2|^2 : u \in [-a, b]\} = s^4 + \max(a^4, b^4) - 2s^2 \min(a^2, b^2) \quad (15)$$

Clearly, $\max\{|s^2 - u^2|^2 : u \in [-a, b]\}$ is infinitely differentiable function of s , for any $s \in [-a, b]$.

Now suppose that $S = [-a_1, b_1] \times [-a_2, b_2]$, where a_i, b_i are positive for each $i = 1, 2$. Let $s \in S$. Define $f_s : S \rightarrow \mathbb{R}$, such that $f_s(u) = \|s^2 - u^2\|^2 = (s_1^2 - u_1^2)^2 + (s_2^2 - u_2^2)^2$. Define $f_{1s}(u_1) = (s_1^2 - u_1^2)^2$ and $f_{2s}(u_2) = (s_2^2 - u_2^2)^2$. Therefore, $f_s(u) = f_{1s}(u_1) + f_{2s}(u_2)$ and $\max_{u \in S} f_s(u) = \max_{u \in S} [f_{1s}(u_1) + f_{2s}(u_2)] = \max_{u_1 \in [-a_1, b_1]} f_{1s}(u_1) + \max_{u_2 \in [-a_2, b_2]} f_{2s}(u_2)$. The equality follows as $u = (u_1, u_2) \in S$, with $u_1 \in [-a_1, b_1]$ and $u_2 \in [-a_2, b_2]$. We have already proved that (Case 3, equation (15)) $\max_{u_i \in [-a_i, b_i]} f_{is}(u_i) = s_i^4 + \max(a_i^4, b_i^4) - 2s_i^2 \min(a_i^2, b_i^2)$ for $i = 1, 2$. Hence $\max_{u \in S} f_s(u) = \sum_{i=1}^2 s_i^4 + \max(a_i^4, b_i^4) - 2s_i^2 \min(a_i^2, b_i^2)$, which is infinitely differentiable with respect to s_1 and s_2 .

If $S = [a_1, b_1] \times [a_2, b_2]$ where (i) $0 < a_1 < b_1$ and $0 < a_2 < b_2$ or (ii) $a_1 < b_1 < 0$ and $a_2 < b_2 < 0$ or (iii) $0 < a_1 < b_1$ and $a_2 < b_2 < 0$ or (iv) $a_1 < b_1 < 0$ and $0 < a_2 < b_2$, the proof goes in a similar manner as above except that now we have to use Case 1 and

Case 2 for one dimension, instead of Case 3. \square

Theorem A.1 *Under assumptions A1 to A3, $\text{cov}(Y(s, h\delta t), Y(s'h'\delta t))$ converges to 0 as $\|s - s'\| \rightarrow \infty$ and/or $|h - h'| \rightarrow \infty$.*

Proof: Let us denote $Y(s, \cdot)$ by $\theta_s(\cdot)$, $Y(s', \cdot)$ by $\theta_{s'}(\cdot)$ and $X(s, t)$ by $p(s, t)$, for any $s \in S$, and $t \in [0, \infty)$. First we shall show that

$$\text{cov} \left(\theta_s(h\delta t), \theta_{s'}(h'\delta t) \middle| p \rightarrow 0 \right),$$

as $\|s - s'\| \rightarrow \infty$ and/or $|h - h'| \rightarrow \infty$. Without loss of generality let us assume that $h > h'$. Now

$$\begin{aligned} & \text{cov} \left(\theta_s(h\delta t), \theta_{s'}(h'\delta t) \middle| p \right) \\ &= \text{cov} \left(\beta\theta_s((h-1)\delta t) + \frac{\delta t}{M_s} \left\{ \alpha p_s((h-1)\delta t) - \frac{\delta t}{2} \frac{\partial}{\partial \theta_s} V(\theta_s((h-1)\delta t)) \right\}, \theta_{s'}(h'\delta t) \middle| p \right) \\ &= \text{cov}(\beta\theta_s((h-1)\delta t), \theta_{s'}(h'\delta t) \middle| p) - \frac{1}{2} \frac{(\delta t)^2}{M_s} \text{cov} \left(\frac{\partial}{\partial \theta_s} V(\theta_s((h-1)\delta t)), \theta_{s'}(h'\delta t) \middle| p \right) \\ &= \dots \\ &= \beta^{h-h'} \text{cov}(\theta_s(h'\delta t), \theta_{s'}(h'\delta t) \middle| p) - \frac{1}{2} \frac{(\delta t)^2}{M_s} \sum_{k=1}^{h-h'} \beta^{k-1} \text{cov} \left[\frac{\partial}{\partial \theta_s} V(\theta_s((h-k)\delta t)), \theta_{s'}(h'\delta t) \middle| p \right]. \end{aligned} \tag{16}$$

Since, for any $1 \leq \ell \leq h - h'$,

$$\begin{aligned} & \text{cov} \left(\frac{\partial}{\partial \theta_s} V(\theta_s((h-\ell)\delta t)), \theta_{s'}(h'\delta t) \middle| p \right) \\ &= \text{cov} \left(\frac{\partial}{\partial \theta_s} V(\theta_s((h-\ell)\delta t)), \beta\theta_{s'}((h'-1)\delta t) + \frac{\delta t}{M_{s'}} \left\{ \alpha p_{s'}((h'-1)\delta t) - \frac{\delta t}{2} \frac{\partial}{\partial \theta_{s'}} V(\theta_{s'}((h'-1)\delta t)) \right\} \middle| p \right) \\ &= \beta \text{cov} \left(\frac{\partial}{\partial \theta_s} V(\theta_s((h-\ell)\delta t)), \theta_{s'}((h'-1)\delta t) \middle| p \right) - \frac{(\delta t)^2}{2M_{s'}} \text{cov} \left(\frac{\partial}{\partial \theta_s} V(\theta_s((h-\ell)\delta t)), \frac{\partial}{\partial \theta_{s'}} \right. \\ & \quad \left. V(\theta_{s'}((h-1)\delta t)) \middle| p \right) \end{aligned}$$

= ...

$$= \beta^{h'} \text{cov} \left(\frac{\partial}{\partial \theta_s} V(\theta_s((h-\ell)\delta t)), \theta_{s'}(0) \middle| p \right) - \frac{(\delta t)^2}{2M_{s'}} \sum_{k=1}^{h'} \beta^{k-1} \text{cov} \left(\frac{\partial}{\partial \theta_s} V(\theta_s((h-\ell)\delta t)), \frac{\partial}{\partial \theta_{s'}} V(\theta_{s'}((h-k)\delta t)) \middle| p \right),$$

we have,

$$\begin{aligned} & \left| \text{cov} \left(\frac{\partial}{\partial \theta_s} V(\theta_s((h-\ell)\delta t)), \theta_{s'}(h'\delta t) \middle| p \right) \right| \\ & \leq \left| \beta^{h'} \text{cov} \left(\frac{\partial}{\partial \theta_s} V(\theta_s((h-\ell)\delta t)), \theta_{s'}(0) \middle| p \right) \right| + \frac{(\delta t)^2}{2M_{s'}} \sum_{k=1}^{h'} \left| \beta^{k-1} \text{cov} \left[\frac{\partial}{\partial \theta_s} V(\theta_s((h-\ell)\delta t)), \frac{\partial}{\partial \theta_{s'}} V(\theta_{s'}((h-k)\delta t)) \right] \right| \\ & \leq |\beta|^{h'} \sigma_\theta \sigma + \frac{1 - |\beta|^{h'}}{1 - |\beta|} \frac{(\delta t)^2}{2M_{s'}} \sigma^2 = \epsilon, \text{ say,} \end{aligned} \quad (17)$$

where σ^2 and σ_θ^2 are the variance terms of the processes $\frac{\partial}{\partial \theta_s} V(\theta_s(h-1)\delta t)$ and $\theta_s(0)$, respectively (see A2 and A3). Therefore, from Equation (16) we obtain

$$\begin{aligned} & \left| \text{cov} \left(\theta_s(h\delta t), \theta_{s'}(h'\delta t) \middle| p \right) - \beta^{h-h'} \text{cov} \left(\theta_s(h'\delta t), \theta_{s'}(h'\delta t) \middle| p \right) \right| \\ & \leq \frac{1}{2} \frac{(\delta t)^2}{M_s} \sum_{k=1}^{h-h'} |\beta|^{k-1} \left| \text{cov} \left[\frac{\partial}{\partial \theta_s} V(\theta_s((h-k)\delta t)), \theta_{s'}(h'\delta t) \middle| p \right] \right| \\ & \leq \frac{1}{2} \frac{(\delta t)^2}{M_s} \frac{1 - |\beta|^{h-h'}}{1 - |\beta|} \epsilon, \end{aligned} \quad (18)$$

using equation (17). Now from the first term of the right hand side of equation (16), we obtain

$$\begin{aligned} & \text{cov} \left(\theta_s(h'\delta t), \theta_{s'}(h'\delta t) \middle| p \right) \\ & = \text{cov} \left(\beta \theta_s((h'-1)\delta t) + \frac{\delta t}{M_s} \left\{ \alpha p_s((h'-1)\delta t) - \frac{\delta t}{2} \frac{\partial}{\partial \theta_s} V(\theta_s((h'-1)\delta t)) \right\}, \right. \end{aligned}$$

$$\begin{aligned}
& \beta \theta_{s'}((h' - 1)\delta t) + \frac{\delta t}{M_{s'}} \left\{ \alpha p_s((h' - 1)\delta t) - \frac{\delta t}{2} \frac{\partial}{\partial \theta_{s'}} V(\theta_s((h' - 1)\delta t)) \right\} \Big| p \Big) \\
&= \beta^2 \text{cov} \left(\theta_s((h' - 1)\delta t), \theta_{s'}((h' - 1)\delta t) \Big| p \right) - \beta \frac{1}{2} \frac{(\delta t)^2}{M_{s'}} \text{cov} \left(\theta_s((h' - 1)\delta t), \frac{\partial}{\partial \theta_{s'}} V(\theta_{s'}((h' - 1)\delta t)) \Big| p \right) \\
&\quad - \beta \frac{1}{2} \frac{(\delta t)^2}{M_s} \text{cov} \left(\theta_{s'}((h' - 1)\delta t), \frac{\partial}{\partial \theta_s} V(\theta_s((h' - 1)\delta t)) \Big| p \right) + \frac{1}{4} \frac{(\delta t)^4}{M_s M_{s'}} \text{cov} \left(\frac{\partial}{\partial \theta_s} V(\theta_s((h' - 1)\delta t)), \right. \\
&\quad \left. \frac{\partial}{\partial \theta_{s'}} V(\theta_{s'}((h' - 1)\delta t)) \Big| p \right) \\
&= \dots \\
&= \beta^{2h'} \text{cov} \left(\theta_s(0), \theta_{s'}(0) \Big| p \right) - \frac{(\delta t)^2}{2M_{s'}} \sum_{k=1}^{h'} \beta^{2k-1} \text{cov} \left(\theta_s((h' - k)\delta t), \frac{\partial}{\partial \theta_{s'}} V(\theta_{s'}((h' - k)\delta t)) \Big| p \right) \\
&\quad - \frac{(\delta t)^2}{2M_s} \sum_{k=1}^{h'} \beta^{2k-1} \text{cov} \left(\theta_{s'}((h' - k)\delta t), \frac{\partial}{\partial \theta_s} V(\theta_s((h' - k)\delta t)) \Big| p \right) + \frac{1}{4} \frac{(\delta t)^4}{M_s M_{s'}} \sum_{k=1}^{h'} \beta^{2(k-1)} \times \\
&\quad \text{cov} \left(\frac{\partial}{\partial \theta_s} V(\theta_s((h' - k)\delta t)), \frac{\partial}{\partial \theta_{s'}} V(\theta_{s'}((h' - k)\delta t)) \Big| p \right),
\end{aligned}$$

which in turn implies

$$\begin{aligned}
& \left| \text{cov} \left(\theta_s(h'\delta t), \theta_{s'}(h'\delta t) \Big| p \right) - \beta^{2h'} \text{cov} \left(\theta_s(0), \theta_{s'}(0) \Big| p \right) \right| \\
&\leq \frac{(\delta t)^2}{2M_{s'}} \sum_{k=1}^{h'} |\beta|^{2k-1} \left| \text{cov} \left(\theta_s((h' - k)\delta t), \frac{\partial}{\partial \theta_{s'}} V(\theta_{s'}((h' - k)\delta t)) \Big| p \right) \right| + \frac{(\delta t)^2}{2M_s} \sum_{k=1}^{h'} |\beta|^{2k-1} \times \\
&\quad \left| \text{cov} \left(\theta_{s'}((h' - k)\delta t), \frac{\partial}{\partial \theta_s} V(\theta_s((h' - k)\delta t)) \Big| p \right) \right| + \frac{1}{4} \frac{(\delta t)^4}{M_s M_{s'}} \sum_{k=1}^{h'} |\beta|^{2(k-1)} \left| \text{cov} \left(\frac{\partial}{\partial \theta_s} V(\theta_s((h' - k)\delta t)), \right. \right. \\
&\quad \left. \left. \frac{\partial}{\partial \theta_{s'}} V(\theta_{s'}((h' - k)\delta t)) \Big| p \right) \right| \leq \frac{(\delta t)^2}{2M_{s'}} \sum_{k=1}^{h'} |\beta|^{2k-1} \epsilon + \frac{(\delta t)^2}{2M_s} \sum_{k=1}^{h'} |\beta|^{2k-1} \epsilon + \frac{1}{4} \frac{(\delta t)^4}{M_s M_{s'}} \sum_{k=1}^{h'} |\beta|^{2(k-1)} \sigma^2 \\
&\leq \frac{(\delta t)^2}{2M_{s'}} |\beta| \frac{1 - |\beta|^{2h'}}{1 - |\beta|^2} \epsilon + \frac{(\delta t)^2}{2M_s} |\beta| \frac{1 - |\beta|^{2h'}}{1 - |\beta|^2} \epsilon + \frac{1}{4} \frac{(\delta t)^4}{M_s M_{s'}} \frac{1 - |\beta|^{2h'}}{1 - |\beta|^2} \sigma^2. \tag{19}
\end{aligned}$$

From equations (18) and (19), we get

$$\begin{aligned}
& \left| \text{Cov} \left[\theta_s(h\delta t), \theta_{s'}(h'\delta t) \Big| p \right] - \beta^{(h-h')+2h'} \text{cov} \left(\theta_s(0), \theta_{s'}(0) \Big| p \right) \right| \\
&\leq \left| \text{Cov} \left[\theta_s(h\delta t), \theta_{s'}(h'\delta t) \Big| p \right] - \beta^{h-h'} \text{Cov} \left[\theta_s(h'\delta t), \theta_{s'}(h'\delta t) \Big| p \right] \right| + |\beta|^{h-h'} \left| \text{Cov} \left[\theta_s(h'\delta t), \theta_{s'}(h'\delta t) \Big| p \right] - \right.
\end{aligned}$$

$$\begin{aligned}
& \left| \beta^{2h'} \text{cov} \left(\theta_s(0), \theta_{s'}(0) \middle| p \right) \right| \\
& \leq \frac{1}{2} \frac{(\delta t)^2}{M_s} \frac{1 - |\beta|^{h-h'}}{1 - |\beta|} \epsilon + |\beta|^{h-h'} \left\{ \frac{(\delta t)^2}{2M_{s'}} |\beta| \frac{1 - |\beta|^{2h'}}{1 - |\beta|^2} \epsilon + \frac{(\delta t)^2}{2M_s} |\beta| \frac{1 - |\beta|^{2h'}}{1 - |\beta|^2} \epsilon + \frac{1}{4} \frac{(\delta t)^4}{M_s M_{s'}} \frac{1 - |\beta|^{2h'}}{1 - |\beta|^2} \sigma^2 \right\},
\end{aligned} \tag{20}$$

which goes to 0 as $|h - h'| \rightarrow \infty$ and/or $\|s - s'\| \rightarrow \infty$, under assumptions A1-A3 in conjunction with Remark 3. Writing $\left| \text{Cov} \left[\theta_s(h\delta t), \theta_{s'}(h'\delta t) \middle| p \right] \right|$ as $\left| \text{Cov} \left[\theta_s(h\delta t), \theta_{s'}(h'\delta t) \middle| p \right] - \beta^{(h-h')+2h'} \text{Cov} \left[\theta_s(0), \theta_{s'}(0) \middle| p \right] + \beta^{(h-h')+2h'} \text{Cov} \left[\theta_s(0), \theta_{s'}(0) \middle| p \right] \right|$ and noting that $\left| \beta^{(h-h')+2h'} \text{Cov} \left[\theta_s(0), \theta_{s'}(0) \middle| p \right] \right|$ is $|\beta|^{(h-h')} |\beta|^{2h'} \sigma_\theta^2 \exp \{-\eta_2 \|s_1 - s_2\|^2\}$ (by assumption A2), we have

$$\text{cov} \left(\theta_s(h\delta t), \theta_{s'}(h'\delta t) \middle| p \right) \rightarrow 0,$$

as $\|s - s'\| \rightarrow \infty$ and/or $|h - h'| \rightarrow \infty$. Now the dominated convergence theorem indicates that the unconditional covariance $\text{cov} (Y(s, h\delta t), Y(s', h'\delta t)) \rightarrow 0$ as $\|s - s'\| \rightarrow \infty$ and $|h - h'| \rightarrow \infty$. \square

Theorem A.2 *If the assumptions A1-A3 hold true, then $Y(s, h\delta t)$ and $X(s, h\delta t)$ are continuous in s , for all $h \geq 1$, with probability 1.*

Proof: Let us denote $Y(s, \cdot)$ by $\theta_s(\cdot)$ and $X(s, \cdot)$ by $p_s(\cdot)$. Note that, for $h \geq 1$,

$$\theta_s(h\delta t) = \beta \theta_s((h-1)\delta t) + \frac{\delta t}{M_s} \left\{ \alpha p_s((h-1)\delta t) - \frac{\delta t}{2} \frac{\partial}{\partial \theta_s} V(\theta_s((h-1)\delta t)) \right\} \text{ and} \tag{21}$$

$$p_s(h\delta t) = \alpha^2 p_s((h-1)\delta t) - \frac{\delta t}{2} \left\{ \alpha \frac{\partial}{\partial \theta_s} V(\theta_s((h-1)\delta t)) + \frac{\partial}{\partial \theta_s} V(\theta_s(h\delta t)) \right\}. \tag{22}$$

Putting $h = 1$ in equations (21) and (22), we get

$$\theta_s(\delta t) = \beta \theta_s(0) + \frac{\delta t}{M_s} \left\{ \alpha p_s(0) - \frac{\delta t}{2} \frac{\partial}{\partial \theta_s} V(\theta_s(0)) \right\} \text{ and}$$

$$p_s(\delta t) = \alpha^2 p_s(0) - \frac{\delta t}{2} \left\{ \alpha \frac{\partial}{\partial \theta_s} V(\theta_s(0)) + \frac{\partial}{\partial \theta_s} V(\theta_s(\delta t)) \right\}.$$

Now $p_s(0)$ and $\theta_s(0)$ are Gaussian processes with continuous sample paths with probability 1 under assumptions A1 and A2 (also see Remark 1), and Lemma 2.1 shows that M_s is continuous in s . Furthermore, assumption A3 implies that the derivative of $V(\cdot)$ is also Gaussian process with continuous sample paths (see Remark 2). Since composition of two continuous function is also a continuous function therefore, $\frac{\partial}{\partial \theta_s} V(\theta_s(0))$ is also continuous in s with probability 1. This implies $\theta_s(\delta t)$ is continuous in s with probability 1 as it is a linear combination of three almost sure continuous functions in s . This immediately implies that $p_s(\delta t)$ is also continuous in s with probability 1.

Assume that $\theta_s(h\delta t)$ and $p_s(h\delta)$ are continuous in s with probability 1, for $h = k + 1$. We will show that $\theta_s(h\delta t)$ and $p_s(h\delta)$ are almost surely continuous in s for $h = k + 2$. Now

$$\begin{aligned} \theta_s((k+2)\delta t) &= \beta \theta_s((k+1)\delta t) + \frac{\delta t}{M_s} \left\{ p_s((k+1)\delta t) - \frac{\delta t}{2} \frac{\partial}{\partial \theta_s} V(\theta_s((k+1)\delta t)) \right\} \text{ and} \\ p_s((k+2)\delta t) &= \alpha^2 p_s((k+1)\delta t) - \frac{\delta t}{2} \left\{ \alpha \frac{\partial}{\partial \theta_s} V(\theta_s((k+1)\delta t)) + \frac{\partial}{\partial \theta_s} V(\theta_s((k+2)\delta t)) \right\}. \end{aligned}$$

Since $\theta_s((k+1)\delta t)$ and $p_s((k+1)\delta t)$ are assumed to be continuous in s with probability 1, derivative of a Gaussian process is also a Gaussian process, composition of two continuous functions is also a continuous function, and linear combinations of continuous functions is a continuous function, we have $\theta_s((k+2)\delta t)$ is continuous in s with probability 1. Similar arguments show that $p_s((k+2)\delta t)$ is also continuous in s with probability 1. Hence using the argument of induction, we claim that $\theta_s(h\delta t)$ and $p_s(h\delta t)$ are continuous in s for any $h \geq 1$, with probability 1. \square

Theorem A.3 *Under the assumptions A1-A3, $Y(s, h\delta t)$ and $X(s, h\delta t)$ are continuous*

in s in the mean square sense, for all $h \geq 1$.

Proof: Let us denote $Y(s, \cdot)$ by $\theta_s(\cdot)$ and $X(s, \cdot)$ by $p_s(\cdot)$. We follow similar steps as in Lemma 2.2. From equation (21) we have

$$\theta_s(\delta t) = \beta\theta_s(0) + \frac{\delta t}{M_s} \left\{ \alpha p_s(0) - \frac{\delta t}{2} \frac{\partial}{\partial \theta_s} V(\theta_s(0)) \right\}.$$

Under assumptions A1 and A2, $p_s(0)$ and $\theta_s(0)$ are continuous in s in the mean square sense, and by Lemma 2.1, M_s is continuous in s . Now since the random function $V(\cdot)$ is twice differentiable under assumption A3 (see Remark 2 also), the partial derivative process of V is Lipschitz and hence the composition function $\frac{\partial}{\partial \theta_s} V(\theta_s(0))$ is also mean square continuous in s (see page 416 of Banerjee et al. [2015]). Now using the fact the linear combination of mean square continuous processes is also mean-square continuous, we have $\theta_s(\delta t)$ is mean square continuous in s . This, in turn implies that, $\frac{\partial}{\partial \theta_s} V(\theta_s(\delta t))$ is also mean square continuous in s using the same argument as above. Therefore,

$$p_s(\delta t) = \alpha^2 p_s(0) - \frac{\delta t}{2} \left\{ \alpha \frac{\partial}{\partial \theta_s} V(\theta_s(0)) + \frac{\partial}{\partial \theta_s} V(\theta_s(\delta t)) \right\}$$

is mean square continuous in s .

Now applying the similar argument of induction as in Lemma 2.2, we have the desired result. \square

Theorem A.4 *Under the assumptions A1-A3, $Y(s, h\delta t)$ and $X(s, h\delta t)$ have differentiable sample paths with respect to s , almost surely.*

Proof: Let us denote $Y(s, \cdot)$ by $\theta_s(\cdot)$ and $X(s, \cdot)$ by $p_s(\cdot)$. The proof goes in the same line as that of Lemma 2.2. We start with $\theta_s(\delta t)$ which is a linear combination of $\theta_s(0)$, $p_s(0)$ and $\frac{\partial}{\partial \theta_s} V(\theta_s(0))$. Note that $\theta_s(0)$, $p_s(0)$ have differentiable sample paths in s

by assumptions A1 and A2 (see Remark 1). Now using the fact that composition of two differentiable function is also differentiable (see the Lemma 3.4 of Guha [2017]), $\frac{\partial}{\partial \theta_s} V(\theta_s(0))$ has differentiable sample paths in s (refer to assumption A3 and Remark 2). Moreover, since M_s is differentiable (Lemma 2.1) and since the linear combination of differentiable functions is a differentiable function, $\theta_s(\delta t)$ has differentiable sample paths in s . The existence of differentiable sample paths of $\theta_s(\delta t)$ implies that $p_s(\delta t)$ will have differentiable sample paths in s . The rest of the proof is similar to that of Lemma 2.2. \square

Lemma A.2 *Let $f : \mathbb{R} \rightarrow \mathbb{R}$ be a zero mean Gaussian random function with covariance function $c_f(x_1, x_2)$, $x_1, x_2 \in \mathbb{R}$, which is four times continuously differentiable. Let $\{Z(s) : s \in S\}$ be a random process with the following properties*

1. $E(Z(s)) = 0$,
2. *The covariance function $c_Z(s_1, s_2)$, $s_1, s_2 \in S$, where S is a compact subspace of \mathbb{R}^2 , is four times continuously differentiable, and*
3. $\frac{\partial Z(s)}{\partial s_i}$ *has finite fourth moment.*

Then the process $\{g(s) : s \in S\}$, where $g(s) = f(Z(s))$, is mean square differentiable in s .

Proof: To show that $\{g(s) : s \in S\}$ is mean square differentiable in s we have to show that, for any $p \in S$, there exists a function $L_s(p)$, linear in p , such that

$$g(s + p) = g(s) + L_s(p) + R(s, p),$$

where

$$\frac{R(s, p)}{\|p\|} \xrightarrow{L_2} 0.$$

Let $s_0 \in S$ be any point in S . Using multivariate Taylor series expansion we have

$$g(s_0 + p) = g(s_0) + p^T \nabla g(s_0) + R(s_0, p),$$

where $\nabla g(s_0) = \left(\frac{\partial f(Z(s))}{\partial s_1}, \frac{\partial f(Z(s))}{\partial s_2} \right)^T$, with $\frac{\partial f(Z(s))}{\partial s_i} = \frac{df(Z(s))}{d(Z(s))} \frac{\partial Z(s)}{\partial s_i}$, for $i = 1, 2$. Therefore, $L_{s_0}(p) = p^T \nabla g(s_0)$, a linear function in p . To complete the proof we note that, from multivariate Taylor series expansion, $|R(s_0, p)| \leq M^* \|p\|^2$, where

$$M^* = \max \left\{ \left| \frac{\partial^2 f(Z(s))}{\partial s_1^2} \right|, \left| \frac{\partial^2 f(Z(s))}{\partial s_1 \partial s_2} \right|, \left| \frac{\partial^2 f(Z(s))}{\partial s_2 \partial s_1} \right|, \left| \frac{\partial^2 f(Z(s))}{\partial s_2^2} \right| \right\},$$

with

$$\frac{\partial^2 f(Z(s))}{\partial s_i^2} = \frac{d^2 f(Z(s))}{d((Z(s)))^2} \left(\frac{\partial Z(s)}{\partial s_i} \right)^2 + \frac{df(Z(s))}{dZ(s)} \frac{\partial^2 Z(s)}{\partial s_i^2}, \text{ for } i = 1, 2,$$

and

$$\frac{\partial^2 f(Z(s))}{\partial s_1 \partial s_2} = \frac{\partial^2 f(Z(s))}{\partial s_2 \partial s_1} = \frac{d^2 f(Z(s))}{d(Z(s))^2} \frac{\partial Z(s)}{\partial s_1} \frac{\partial Z(s)}{\partial s_2} + \frac{df(Z(s))}{d(Z(s))} \frac{\partial^2 Z(s)}{\partial s_1 \partial s_2}.$$

Since we have assumed that $Z(\cdot)$ and $f(\cdot)$ have covariance functions which are four times continuously differentiable, $Z(\cdot)$ and $f(\cdot)$ are twice differentiable (in the mean square sense) and hence the above terms involving first and second derivatives of $f(\cdot)$ and $Z(\cdot)$ are well-defined.

We will now show that the second moment of $\frac{\partial^2 f(Z(s))}{\partial s_i^2}$, for $i = 1, 2$, and $\frac{\partial^2 f(Z(s))}{\partial s_1 \partial s_2}$ are finite. To prove the above fact, we first show that $\text{var} \left(\frac{d^2 f(Z(s))}{d((Z(s)))^2} \right) < \infty$. Note that

$$\text{var} \left(\frac{d^2 f(Z(s))}{d((Z(s)))^2} \right) = \text{var} \left(E \left\{ \frac{d^2 f(Z(s))}{d((Z(s)))^2} \middle| Z(s) \right\} \right) + E \left(\text{var} \left\{ \frac{d^2 f(Z(s))}{d((Z(s)))^2} \middle| Z(s) \right\} \right). \quad (23)$$

Moreover, since $f''(x)$ is a Gaussian function with 0 mean and a constant variance, we have

$$E \left\{ \frac{d^2 f(Z(s))}{d((Z(s)))^2} \middle| Z(s) \right\} = 0 \text{ and } \text{var} \left\{ \frac{d^2 f(Z(s))}{d((Z(s)))^2} \middle| Z(s) \right\} = \text{constant} < \infty. \text{ Thus}$$

$$\text{var} \left(E \left\{ \frac{d^2 f(Z(s))}{d((Z(s)))^2} \middle| Z(s) \right\} \right) = 0 \text{ and} \quad (24)$$

$$E \left(\text{var} \left\{ \frac{d^2 f(Z(s))}{d((Z(s)))^2} \middle| Z(s) \right\} \right) = \text{constant}. \quad (25)$$

Therefore, combining equations (24) and (25), and using equation (23) we see that $\text{var} \left(\frac{d^2 f(Z(s))}{d((Z(s)))^2} \right) < \infty$. Similar argument shows that $\text{var} \left(\frac{df(Z(s))}{dZ(s)} \right) < \infty$. Now to show that $E \left(\frac{\partial^2 f(Z(s))}{\partial s_i^2} \right)^2 < \infty$, we use $(a + b)^2 \leq 2(a^2 + b^2)$ and have

$$\begin{aligned} E \left(\frac{\partial^2 f(Z(s))}{\partial s_i^2} \right)^2 &\leq 2 \left\{ E \left(\left[\frac{d^2 f(Z(s))}{d((Z(s)))^2} \right]^2 \left[\frac{\partial Z(s)}{\partial s_i} \right]^4 \right) + E \left(\left[\frac{df(Z(s))}{dZ(s)} \right]^2 \left[\frac{\partial^2 Z(s)}{\partial s_i^2} \right]^2 \right) \right\} \\ &= 2E \left(E \left(\left[\frac{d^2 f(Z(s))}{d((Z(s)))^2} \right]^2 \middle| Z(s) \right) \left[\frac{\partial Z(s)}{\partial s_i} \right]^4 \right) \\ &\quad + 2E \left(E \left(\left[\frac{df(Z(s))}{dZ(s)} \right]^2 \middle| Z(s) \right) \left[\frac{\partial^2 Z(s)}{\partial s_i^2} \right]^2 \right). \end{aligned} \quad (26)$$

Again using the fact that $f'(x)$ and $f''(x)$ are Gaussian with 0 mean and constant variance, we have $E \left(\left[\frac{d^2 f(Z(s))}{d((Z(s)))^2} \right]^2 \middle| Z(s) \right) = \text{constant}$ and $E \left(\left[\frac{df(Z(s))}{dZ(s)} \right]^2 \middle| Z(s) \right) = \text{constant}$.

Further, since the covariance function of $Z(s)$ is assumed to be four times continuously differentiable (2nd assumption of the Lemma), the first two derivatives of $Z(s)$, $\frac{\partial Z(s)}{\partial s_i}, i = 1, 2$ and $\frac{\partial^2 Z(s)}{\partial s_i^2}, i = 1, 2$ will also exist in the mean square sense, with zero means. Thus, $E \left[\frac{\partial^2 Z(s)}{\partial s_1^2} \right]^2 = \text{constant}$. Also by the 3rd assumption of the Lemma,

the fourth moment of $\frac{\partial Z(s)}{\partial s_i}$, for $i = 1, 2$, are finite. That is, $E \left[\frac{\partial Z(s)}{\partial s_i} \right]^4 = \text{constant}$. Therefore, from equation (26) we see that $E \left(\frac{\partial^2 f(Z(s))}{\partial s_1^2} \right)^2 < M_1 < \infty$, for some $M_1 \in \mathbb{R}$.

Next we show that $E \left(\frac{\partial^2 f(Z(s))}{\partial s_1 \partial s_2} \right)^2 < \infty$. Using the same inequality, $(a + b)^2 \leq 2(a^2 + b^2)$, we have

$$\begin{aligned} E \left(\frac{\partial^2 f(Z(s))}{\partial s_1 \partial s_2} \right)^2 &\leq 2 \left[E \left\{ \frac{d^2 f(Z(s))}{d(Z(s))^2} \frac{\partial Z(s)}{\partial s_1} \frac{\partial Z(s)}{\partial s_2} \right\}^2 + E \left\{ \frac{df(Z(s))}{d(Z(s))} \frac{\partial^2 Z(s)}{\partial s_1 \partial s_2} \right\}^2 \right] \\ &= 2E \left[E \left(\left[\frac{d^2 f(Z(s))}{d((Z(s)))^2} \right]^2 \middle| Z(s) \right) \left(\frac{\partial Z(s)}{\partial s_1} \right)^2 \left(\frac{\partial Z(s)}{\partial s_2} \right)^2 \right] \\ &\quad + 2E \left[E \left\{ \left(\frac{df(Z(s))}{d(Z(s))} \right)^2 \middle| Z(s) \right\} \left(\frac{\partial^2 Z(s)}{\partial s_1 \partial s_2} \right)^2 \right]. \end{aligned} \quad (27)$$

Since $f'(x)$ and $f''(x)$ are Gaussian functions with mean 0 and constant variance, therefore, $E \left(\left[\frac{d^2 f(Z(s))}{d((Z(s)))^2} \right]^2 \middle| Z(s) \right) = \text{constant}$ and $E \left\{ \left(\frac{df(Z(s))}{d(Z(s))} \right)^2 \middle| Z(s) \right\} = \text{constant}$. Moreover, since by our assumption, the fourth moment of $\frac{\partial Z(s)}{\partial s_i}$, for $i = 1, 2$, are finite, we have $E \left[\left(\frac{\partial Z(s)}{\partial s_1} \right)^2 \left(\frac{\partial Z(s)}{\partial s_2} \right)^2 \right] \leq \sqrt{E \left(\frac{\partial Z(s)}{\partial s_1} \right)^4 E \left(\frac{\partial Z(s)}{\partial s_2} \right)^4} = \text{constant}$. Since the covariance function of $Z(s)$ is four times continuously differentiable, $E \left(\frac{\partial^2 Z(s)}{\partial s_1 \partial s_2} \right)^2 = \text{constant}$. Thus we have, from equation (27), $E \left(\frac{\partial^2 f(Z(s))}{\partial s_1 \partial s_2} \right)^2 < M_2$, for some $M_2 \in \mathbb{R}$. Hence each term in $M^* = \max \left\{ \left| \frac{\partial^2 f(Z(s))}{\partial s_1^2} \right|, \left| \frac{\partial^2 f(Z(s))}{\partial s_1 \partial s_2} \right|, \left| \frac{\partial^2 f(Z(s))}{\partial s_2 \partial s_1} \right|, \left| \frac{\partial^2 f(Z(s))}{\partial s_2^2} \right| \right\}$ has bounded second moment.

Next we have to show that $E(M^*)^2 < \infty$. Denote $M^* = \max\{A, B, C, D\}$, where $A = \left| \frac{\partial^2 f(Z(s))}{\partial s_1^2} \right|$, $B = \left| \frac{\partial^2 f(Z(s))}{\partial s_1 \partial s_2} \right|$, $C = \left| \frac{\partial^2 f(Z(s))}{\partial s_2 \partial s_1} \right|$ and $D = \left| \frac{\partial^2 f(Z(s))}{\partial s_2^2} \right|$. Note that it is sufficient to show that $X = \max\{A, B\}$ has finite second moment, because then with the same argument $Y = \max\{C, D\}$ will have finite second moment, and finally $Z = \max\{X, Y\}$ ($= \max\{A, B, C, D\}$) will have finite second moment.

Now $X = \max\{A, B\} = \frac{A+B+|A-B|}{2} \leq \frac{A+B+|A|+|B|}{2}$. Therefore,

$$\begin{aligned} EX^2 &\leq \frac{1}{4}2 [E \{(A+B)^2 + (|A|+|B|)^2\}] \\ &\leq E\{A^2 + B^2 + |A|^2 + |B|^2\} = 2E(A^2 + B^2). \end{aligned}$$

Since $EA^2 < \infty$ and $EB^2 < \infty$, therefore, $EX^2 < \infty$. Now exactly same arguments imply that $EY^2 < \infty$ and $EZ^2 < \infty$. Hence, $\frac{R(s_0, p)}{\|p\|} \xrightarrow{L_2} 0$. Since s_0 is any point in S , the proof is complete. \square

Theorem A.5 *Let the assumptions A1-A3 hold true, with the covariance functions of all the assumed Gaussian processes being square exponentials. Then $Y(s, h\delta t)$ and $X(s, h\delta t)$ are mean square differentiable in s , for every $h \geq 1$.*

Proof: Let us denote $Y(s, \cdot)$ by $\theta_s(\cdot)$ and $X(s, \cdot)$ by $p_s(\cdot)$. The proof will follow the similar argument of induction as done in Lemma 2.2. For $h = 1$, we have

$$\theta_s(\delta t) = \beta\theta_s(0) + \frac{\delta t}{M_s} \left\{ \alpha p_s(0) - \frac{1}{2}\delta t \frac{\partial}{\partial \theta_s} V(\theta_s(0)) \right\}.$$

Since, under the assumption A2 and the assumption of the theorem, $\theta_s(0)$ is a centered Gaussian process with squared exponential covariance function, the fourth moment of $\frac{\partial \delta_s(0)}{\partial s_i}$, $i = 1, 2$ are finite, and by assumption A3, $V(\cdot)$ is a zero-mean Gaussian random function with squared exponential covariance. Therefore, using lemma 2.2, $\frac{\partial}{\partial \theta_s} V(\theta_s(0))$ is mean square differentiable. Under the assumptions A1 and A2, and using the fact the covariance functions are assumed to squared exponential, $p_s(0)$ and $\theta_s(0)$ are mean squared differentiable. Using the fact that M_s is differentiable in s (see Lemma 2.1), $\theta_s(\delta t)$, being a linear combination of mean square differentiable functions, is also mean square differentiable.

Next we show that $E(\theta_s(\delta t)) = 0$ and $\text{cov}(\theta_{s_1}(\delta t), \theta_{s_2}(\delta t))$ is 4-times differentiable.

Denoting the first derivative of V by V' , we obtain

$$E(\theta_s(\delta t)) = \beta E(\theta_s(0)) + \frac{\delta t}{M_s} \left\{ \alpha E(p_s(0)) - \frac{1}{2} \delta t E(V'(\theta_s(0))) \right\} = 0,$$

where we have used the fact that $E(V'(\theta_s(0))) = E[E(V'(\theta_s(0))) | \theta_s(0)] = E(0) = 0$.

Therefore, $\text{cov}(\theta_{s_1}(\delta t), \theta_{s_2}(\delta t)) = E(\theta_{s_1}(\delta t)\theta_{s_2}(\delta t))$. Since the processes are assumed to be independent, we have

$$E(\theta_{s_1}(\delta t)\theta_{s_2}(\delta t)) = \beta^2 \sigma_\theta^2 e^{-\eta_2 \|s_1 - s_2\|^2} + \frac{(\delta t)^2 \alpha^2}{M_{s_1} M_{s_2}} \sigma_p^2 e^{-\eta_1 \|s_1 - s_2\|^2} + \frac{(\delta t)^4}{4M_{s_1} M_{s_2}} E[V'(\theta_{s_1}(0))V'(\theta_{s_2}(0))]. \quad (28)$$

Now according to our assumption, $\text{cov}(V(x_1), V(x_2)) = \sigma^2 e^{-\eta_3 \|x_1 - x_2\|^2}$, that is, the covariance function of $V(\cdot)$ can be written as $\kappa(h) = \sigma^2 e^{-\eta_3 h^2}$, where $h = \|x_1 - x_2\|$. The second derivative of $\kappa(h)$ is given by $-2\sigma^2 \eta_3 e^{-\eta_3 h^2} (1 - 2\eta_3 h^2)$. Hence the covariance function of $V'(\cdot)$ will be $\text{cov}(V'(x_1), V'(x_2)) = 2\sigma^2 \eta_3 e^{-\eta_3 h^2} (1 - 2\eta_3 h^2)$ (see Stein [1999b], page 21). Therefore, the last term of the right hand side of equation (28) can be computed as

$$\begin{aligned} E[V'(\theta_{s_1}(0))V'(\theta_{s_2}(0))] &= EE[V'(\theta_{s_1}(0))V'(\theta_{s_2}(0)) | \theta_{s_1}(0)\theta_{s_2}(0)] \\ &= E \left[2\sigma^2 \eta_3 e^{-\eta_3 (\theta_{s_1}(0) - \theta_{s_2}(0))^2} (1 - 2\eta_3 (\theta_{s_1}(0) - \theta_{s_2}(0))^2) \right] \\ &= 2\sigma^2 \eta_3 \left[E e^{-\eta_3 (\theta_{s_1}(0) - \theta_{s_2}(0))^2} - 2\eta_3 E \left\{ (\theta_{s_1}(0) - \theta_{s_2}(0))^2 e^{-\eta_3 (\theta_{s_1}(0) - \theta_{s_2}(0))^2} \right\} \right]. \end{aligned} \quad (29)$$

Since $(\theta_{s_1}(0), \theta_{s_2}(0))^T \sim N_2 \left(\mathbf{0}, \begin{pmatrix} \sigma_\theta^2 & \sigma_\theta^2 e^{-\eta_2 \|s_1 - s_2\|^2} \\ \sigma_\theta^2 e^{-\eta_2 \|s_1 - s_2\|^2} & \sigma_\theta^2 \end{pmatrix} \right)$, therefore, $\theta_{s_1}(0) -$

$\theta_{s_2}(0) \sim N(0, 2\sigma_\theta^2 - 2\sigma_\theta^2 e^{-\eta_2 \|s_1 - s_2\|^2})$, which in turn implies that

$$\frac{(\theta_{s_1}(0) - \theta_{s_2}(0))^2}{\nu} \sim \chi_{(1)}^2,$$

where $\nu = 2\sigma_\theta^2 - 2\sigma_\theta^2 e^{-\eta_2 \|s_1 - s_2\|^2}$. Using the fact that the moment generating function (mgf) of a $\chi_{(1)}^2$ random variable is $(1 - 2t)^{-1/2}$, we have

$$E \left[e^{-\eta_3 (\theta_{s_1}(0) - \theta_{s_2}(0))^2} \right] = \left(1 + 4\eta_3 \sigma_\theta^2 \left(1 - e^{\eta_2 \|s_1 - s_2\|^2} \right) \right)^{-1/2}. \quad (30)$$

Differentiating equation (30) with respect to η_3 and cancelling the minus sign from both sides yield

$$E \left[(\theta_{s_1}(0) - \theta_{s_2}(0))^2 e^{-\eta_3 (\theta_{s_1}(0) - \theta_{s_2}(0))^2} \right] = 2\sigma_\theta^2 (1 - e^{\eta_2 \|s_1 - s_2\|^2}) \left(1 + 4\eta_3 \sigma_\theta^2 (1 - e^{\eta_2 \|s_1 - s_2\|^2}) \right)^{-3/2}. \quad (31)$$

Combining equations (29), (30), (31), we get

$$E [V'(\theta_{s_1}(0))V'(\theta_{s_2}(0))] = 2\sigma^2 \eta_3 \left[\frac{1}{(1 + 4\eta_3 \sigma_\theta^2 (1 - e^{\eta_2 \|s_1 - s_2\|^2}))^{1/2}} - \frac{4\eta_3 \sigma_\theta^2 (1 - e^{\eta_2 \|s_1 - s_2\|^2})}{(1 + 4\eta_3 \sigma_\theta^2 (1 - e^{\eta_2 \|s_1 - s_2\|^2}))^{3/2}} \right]. \quad (32)$$

Then inserting the value of $E [V'(\theta_{s_1}(0))V'(\theta_{s_2}(0))]$ from equation (32) to equation (28)

we obtain

$$E(\theta_{s_1}(\delta t)\theta_{s_2}(\delta t)) = \beta^2 \sigma_\theta^2 e^{-\eta_2 \|s_1 - s_2\|^2} + \frac{(\delta t)^2 \alpha^2}{M_{s_1} M_{s_2}} \sigma_p^2 e^{-\eta_1 \|s_1 - s_2\|^2} + \frac{(\delta t)^4}{4M_{s_1} M_{s_2}} 2\sigma^2 \eta_3 \left[\frac{1}{(1 + 4\eta_3 \sigma_\theta^2 (1 - e^{\eta_2 \|s_1 - s_2\|^2}))^{1/2}} - \frac{4\eta_3 \sigma_\theta^2 (1 - e^{\eta_2 \|s_1 - s_2\|^2})}{(1 + 4\eta_3 \sigma_\theta^2 (1 - e^{\eta_2 \|s_1 - s_2\|^2}))^{3/2}} \right].$$

Clearly, the covariance function of $\theta_s(\delta t)$ is four times differentiable, provided M_s is

also four times differentiable. To apply Lemma 1.6 on $V'(\theta_s(\delta t))$ we have to show that the fourth moment of $\frac{\partial}{\partial s_1}\theta_s(\delta t)$ finitely exists. From

$$\theta_s(\delta t) = \beta\theta_s(0) + \frac{\delta t}{M_s} \left\{ \alpha p_s(0) - \frac{\delta t}{2} \frac{\partial}{\partial \theta_s} V(\theta_s(0)) \right\}$$

we obtain

$$\begin{aligned} \frac{\partial \theta_s(\delta t)}{\partial s_1} &= \beta \frac{\partial \theta_s(0)}{\partial s_1} + \frac{\delta t}{M_s} \left\{ \frac{\partial p_s(0)}{\partial s_1} - \frac{\delta t}{2} \frac{\partial}{\partial s_1} V'(\theta_s(0)) \right\} - \frac{\delta t}{M_s^2} \frac{\partial M_s}{\partial s_1} \left\{ p_s(0) - \frac{1}{2} \delta t \frac{\partial}{\partial \theta_s} V(\theta_s(0)) \right\} \\ &= \beta \frac{\partial \theta_s(0)}{\partial s_1} + \frac{\delta t}{M_s} \left\{ \frac{\partial p_s(0)}{\partial s_1} - \frac{\delta t}{2} V''(\theta_s(0)) \frac{\partial \theta_s(0)}{\partial s_1} \right\} - \frac{\delta t}{M_s^2} \frac{\partial M_s}{\partial s_1} \left\{ p_s(0) - \frac{1}{2} \delta t \frac{\partial}{\partial \theta_s} V(\theta_s(0)) \right\}. \end{aligned} \quad (33)$$

Now the fourth moment of $\frac{\partial \theta_s(\delta t)}{\partial s_1}$ will be finite if individually each term of equation (33) has finite fourth moment, because

$$\begin{aligned} \left(\frac{\partial \theta_s(\delta t)}{\partial s_1} \right)^4 &\leq \kappa \left[\beta^4 \left(\frac{\partial \theta_s(0)}{\partial s_1} \right)^4 + \left(\frac{\delta t}{M_s} \right)^4 \left\{ \left(\frac{\partial p_s(0)}{\partial s_1} \right)^4 + \left(\frac{\delta t}{2} \right)^4 \left(V''(\theta_s(0)) \frac{\partial \theta_s(0)}{\partial s_1} \right)^4 \right\} + \right. \\ &\quad \left. \left(\frac{\delta t}{M_s^2} \frac{\partial M_s}{\partial s_1} \right)^4 \left\{ (p_s(0))^4 + \left(\frac{1}{2} \delta t \right)^4 \left(\frac{\partial}{\partial \theta_s} V(\theta_s(0)) \right)^4 \right\} \right], \end{aligned}$$

where κ is a suitable constant. Note that due to assumptions A1-A2 and squared exponential covariance functions, $\frac{\partial \theta_s(0)}{\partial s_1}$, $\frac{\partial p_s(0)}{\partial s_1}$, and $p_s(0)$ are Gaussian processes with 0 mean and constant variances. Hence they have finite fourth moments. Therefore, we just need to show that $V''(\theta_s(0)) \frac{\partial \theta_s(0)}{\partial s_1}$ and $\frac{\partial}{\partial \theta_s} V(\theta_s(0))$ have finite 4th moments.

Observe that

$$\begin{aligned} E \left[V''(\theta_s(0)) \frac{\partial \theta_s(0)}{\partial s_1} \right]^4 &= EE \left\{ \left[V''(\theta_s(0)) \frac{\partial \theta_s(0)}{\partial s_1} \right]^4 \middle| \theta_s(0) \right\} \\ &= E \left[E \left\{ [V''(\theta_s(0))]^4 \middle| \theta_s(0) \right\} \left(\frac{\partial \theta_s(0)}{\partial s_1} \right)^4 \right] \end{aligned} \quad (34)$$

Now since $V''(\theta_s(0))$, given $\theta_s(0)$, is Gaussian with mean 0 and constant variance, $E \left\{ [V''(\theta_s(0))]^4 \middle| \theta_s(0) \right\}$ is constant (independent of $\theta_s(0)$), say κ_1 . Hence from equation (34) we obtain

$$E \left[V''(\theta_s(0)) \frac{\partial \theta_s(0)}{\partial s_1} \right]^4 = \kappa_1 E \left(\frac{\partial \theta_s(0)}{\partial s_1} \right)^4. \quad (35)$$

Now note that $\frac{\partial \theta_s(0)}{\partial s_1}$ is also Gaussian with mean 0 and constant variance, so that $E \left(\frac{\partial \theta_s(0)}{\partial s_1} \right)^4$ is also constant. Thus, combining equations (34) and (35) we have

$$E \left[V''(\theta_s(0)) \frac{\partial \theta_s(0)}{\partial s_1} \right]^4 < \infty. \quad (36)$$

Next to show that $\frac{\partial}{\partial \theta_s} V(\theta_s(0))$ has finite 4th moment, we notice that

$$E(V'(\theta_s(0)))^4 = E \left[E(V'(\theta_s(0)))^4 \middle| \theta_s(0) \right] = \text{constant} = \kappa_2, \text{ say.}$$

The last equality follows because $V'(\theta_s(0))$, given $\theta_s(0)$, is a Gaussian process with 0 mean and constant variance.

Therefore, the fourth moment of $\frac{\partial}{\partial s_1} \theta_s(\delta t)$ exists finitely. So, by Lemma 2.2, $V'(\theta_s(\delta t))$ is mean square differentiable, and hence under assumptions A1, A2, for $h = 1$,

$$p_s(\delta t) = \alpha^2 p_s(0) - \frac{\delta t}{2} \left\{ \alpha \frac{\partial}{\partial \theta_s} V(\theta_s(0)) + \frac{\partial}{\partial \theta_s} V(\theta_s(\delta t)) \right\},$$

a linear combination of mean square differentiable function, is also mean square differentiable. Before, applying the steps of induction, we show that $\frac{\partial p_s(\delta t)}{\partial s_i}$, $i = 1, 2$, have finite 4th moment as it has to be used for the next step of induction. Note that, for

$i = 1, 2$,

$$\frac{\partial p_s(\delta t)}{\partial s_i} = \alpha^2 \frac{\partial p_s(0)}{\partial s_i} - \frac{\delta t}{2} \left\{ \alpha V''(\theta_s(0)) \frac{\partial \theta_s(0)}{\partial s_i} + V''(\theta_s(\delta t)) \frac{\partial \theta_s(\delta t)}{\partial s_i} \right\}.$$

From equation (36), $E \left(V''(\theta_s(0)) \frac{\partial \theta_s(0)}{\partial s_i} \right)^4 < \infty$. We have already shown that $\frac{\partial \theta_s(\delta t)}{\partial s_i}$ has finite fourth moment, for $i = 1, 2$. Thus, each term in the expression of $\frac{\partial p_s(\delta t)}{\partial s_i}$ has finite fourth moment. Hence $E \left(\frac{\partial p_s(\delta t)}{\partial s_i} \right)^4 < \infty$.

Thereafter, using the argument of induction as in the proof of Lemma 2.2, we have the desired result. \square

B Calculation of joint conditional density of the observed data

Here we will find the data model, that is, the conditional distribution of Data given Latent, \mathbf{y}_0 , \mathbf{x}_0 and the parameter $\boldsymbol{\theta}$.

First, we will find the conditional distribution of \mathbf{y}_1 given \mathbf{y}_0 , \mathbf{x}_0 and the parameter $\boldsymbol{\theta}$. We have, for $i = 1, 2, \dots, n$,

$$y(s_i, 1) = \beta y(s_i, 0) + \frac{\alpha x(s_i, 0)}{M_{s_i}} - \frac{1}{2} \frac{V'(y(s_i, 0))}{M_{s_i}},$$

and

$$\frac{1}{2} \left[\frac{V'(y(s_1, 0))}{M_{s_1}}, \dots, \frac{V'(y(s_n, 0))}{M_{s_n}} \right]' \sim N_n \left(\mathbf{0}, \frac{\sigma^2}{4} \Sigma_0 \right),$$

where Σ_0 is the $n \times n$ covariance matrix with (i, j) th element $\frac{2\eta_3 e^{-\eta_3 h_{ij}^2(0)} (1 - 2\eta_3 h_{ij}^2(0))}{M_{s_i} M_{s_j}}$.

Therefore,

$$\left[\mathbf{y}_1 \middle| \mathbf{y}_0; \mathbf{x}_0; \boldsymbol{\theta} \right] \sim N_n \left(\boldsymbol{\mu}_0, \frac{\sigma^2}{4} \Sigma_0 \right). \quad (37)$$

Similarly,

$$\left[\mathbf{y}_2 \middle| \mathbf{y}_1; \mathbf{x}_1; \mathbf{y}_0; \mathbf{x}_0; \boldsymbol{\theta} \right] \sim N_n \left(\boldsymbol{\mu}_1, \frac{\sigma^2}{4} \Sigma_1 \right), \quad (38)$$

where the (i, j) th element of the $n \times n$ covariance matrix Σ_1 is $\frac{2\eta_3 e^{-\eta_3 h_{ij}^2(1)} (1 - 2\eta_3 h_{ij}^2(1))}{M_{s_i} M_{s_j}}$.

Following the same argument, we can write down the likelihood as

$$\begin{aligned} L &= [\mathbb{D} \middle| \mathbf{x}_0; \dots; \mathbf{x}_{T-1}; \mathbf{y}_0; \boldsymbol{\theta}] \\ &\propto [\mathbf{y}_1 \middle| \mathbf{y}_0; \mathbf{x}_0; \boldsymbol{\theta}] \dots [\mathbf{y}_T \middle| \mathbf{y}_{T-1}, \dots, \mathbf{y}_0; \mathbf{x}_{T-1}, \dots, \mathbf{x}_0; \boldsymbol{\theta}] \\ &\propto \frac{(\sigma^2)^{-nT/2}}{\prod_{t=1}^T |\Sigma_{t-1}|^{1/2}} e^{-\frac{2}{\sigma^2} \sum_{t=1}^T (\mathbf{y}_t - \boldsymbol{\mu}_{t-1})^T \Sigma_{t-1}^{-1} (\mathbf{y}_t - \boldsymbol{\mu}_{t-1})}, \end{aligned}$$

where, for $j = 1, 2, \dots, T$, the (k, ℓ) th element of Σ_{j-1} is

$$\frac{2\eta_3 e^{-\eta_3 h_{k\ell}^2(j-1)} (1 - 2\eta_3 h_{k\ell}^2(j-1))}{M_{s_k} M_{s_\ell}}.$$

C Calculation of the conditional joint density of latent data

Here we will derive the conditional distribution of the \mathbb{L} given \mathbb{D} , \mathbf{y}_0 , \mathbf{x}_0 and the parameter $\boldsymbol{\theta}$.

First, we shall find the conditional distribution of \mathbf{x}_1 given \mathbf{x}_0 , \mathbf{y}_0 , and \mathbf{y}_1 . For

$i = 1, \dots, n$, we have

$$x(s_i, 1) = \alpha^2 x(s_i, 0) - \frac{1}{2} \{ \alpha V'(y(s_i, 0)) + V'(y(s_i, 1)) \}.$$

Since $V'(\cdot)$ is a random Gaussian function with zero mean and covariance function given in equation (7) and $\mathbb{W}_0 = (\mathbf{W}'_0 \mathbf{W}'_1)'$ is a $2n \times 1$ vector, $\mathbb{W}_0 \sim N_{2n}(\mathbf{0}, \sigma^2 \Sigma)$, where Σ is the $2n \times 2n$ covariance matrix partitioned as

$$\begin{pmatrix} \alpha^2 \Sigma_{00} & \alpha \Sigma_{01} \\ \alpha \Sigma_{10} & \Sigma_{11} \end{pmatrix},$$

where the (i, k) th element of Σ_{jj} is $2\eta_3 e^{-\eta_3 h_{ik}^2(j)} (1 - 2\eta_3 h_{ik}^2(j))$, for $j = 0, 1$, and the (i, k) th element of $\Sigma_{01} = \Sigma'_{10}$ is $2\eta_3 e^{-\eta_3 \ell_{ik}^2(0,1)} (1 - 2\eta_3 \ell_{ik}^2(0,1))$. Therefore,

$$\mathbf{W}_0 + \mathbf{W}_1 = [I_n; I_n] \mathbb{W}_0 \sim N_n(\mathbf{0}, \sigma^2 (\alpha^2 \Sigma_{00} + \alpha \Sigma_{01} + \alpha \Sigma_{10} + \Sigma_{11})).$$

Let $\Omega_1 = \alpha^2 \Sigma_{00} + \alpha \Sigma_{01} + \alpha \Sigma_{10} + \Sigma_{11}$. Then

$$[\mathbf{x}_1 | \mathbf{x}_0; \mathbf{y}_0; \mathbf{y}_1; \boldsymbol{\theta}] \sim N_n(\alpha^2 \mathbf{x}_0, \frac{\sigma^2}{4} \Omega_1). \quad (39)$$

Similarly,

$$[\mathbf{x}_2 | \mathbf{x}_1; \mathbf{x}_0; \mathbf{y}_0; \mathbf{y}_1; \mathbf{y}_2; \boldsymbol{\theta}] \sim N_n(\alpha^2 \mathbf{x}_1, \frac{\sigma^2}{4} \Omega_2), \quad (40)$$

where $\Omega_2 = \alpha^2 \Sigma_{11} + \alpha \Sigma_{12} + \alpha \Sigma_{21} + \Sigma_{22}$. For $j = 1, 2$, the (i, k) th element of Σ_{jj} is $2\eta_3 e^{-\eta_3 h_{ik}^2(j)} (1 - 2\eta_3 h_{ik}^2(j))$, and the (i, k) th element of $\Sigma_{12} = \Sigma'_{21}$ is $2\eta_3 e^{-\eta_3 \ell_{ik}^2(1,2)} (1 - 2\eta_3 \ell_{ik}^2(1,2))$.

Now with the help of equations (39) and (40) we write down the conditional latent pro-

cess model as

$$\begin{aligned}
& \left[\mathbb{L} \left| \mathbf{y}_0; \dots; \mathbf{y}_T; \mathbf{x}_0; \boldsymbol{\theta} \right. \right] \\
& \propto [\mathbf{x}_1 | \mathbf{x}_0; \mathbf{y}_0; \mathbf{y}_1; \boldsymbol{\theta}] \dots [\mathbf{x}_T | \mathbf{x}_{T-1}; \dots; \mathbf{x}_0; \mathbf{y}_0; \dots; \mathbf{y}_T; \boldsymbol{\theta}] \\
& \propto \frac{(\sigma^2)^{-nT/2}}{\prod_{t=1}^T |\Omega_t|^{1/2}} e^{-\frac{2}{\sigma^2} \sum_{t=1}^T (\mathbf{x}_t - \alpha^2 \mathbf{x}_{t-1})^T \Omega_t^{-1} (\mathbf{x}_t - \alpha^2 \mathbf{x}_{t-1})},
\end{aligned}$$

where, for $m \in \{1, 2, \dots, T\}$, $\Omega_t = \alpha^2 \Sigma_{t-1, t-1} + \alpha \Sigma_{t-1, t} + \alpha \Sigma_{t, t-1} + \Sigma_{t, t}$, where the (i, k) th element of Σ_{jj} , for $j = t-1, t$, is $2\eta_3 e^{-\eta_3 h_{ik}^2(j)} (1 - 2\eta_3 h_{ik}^2(j))$, and the (i, k) th element of $\Sigma_{t-1, t} = \Sigma'_{t, t-1}$ is $2\eta_3 e^{-\eta_3 \ell_{ik}^2(t-1, t)} (1 - 2\eta_3 \ell_{ik}^2(t-1, t))$.

D Calculation of full conditional distributions of the parameters and the latent variables, given the observed data

D.1 Full conditional distribution of β^*

Before finding the full conditional distribution of β (hence β^*), we note that the only term that depends on β in equation (11) is $\exp \left\{ -\frac{2}{\sigma^2} \sum_{t=1}^T [\boldsymbol{\mu}_{t-1}^T \Sigma_{t-1}^{-1} \boldsymbol{\mu}_{t-1} - 2\mathbf{y}_t^T \Sigma_{t-1}^{-1} \boldsymbol{\mu}_{t-1}] \right\}$.

Further notice that $\boldsymbol{\mu}_t = \beta \mathbf{y}_{t-1} + \text{constant}$ (with respect to β). Therefore, the term which depends on β (hence on β^*) simplifies to $e^{-\frac{2\beta^2}{\sigma^2} \sum_{t=1}^T \mathbf{y}'_{t-1} \Sigma_{t-1}^{-1} \mathbf{y}_{t-1}} \times e^{\frac{4\beta}{\sigma^2} \sum_{t=1}^T \mathbf{y}'_{t-1} \Sigma_{t-1}^{-1} \mathbf{y}_{t-1}}$,

where $\beta = -1 + \frac{2e^{\beta^*}}{1+2e^{\beta^*}}$. The full conditional density of β^* , therefore, is given by

$$\begin{aligned}
[\beta^* | \dots] & \propto [\beta^*] e^{-\frac{2\beta^2}{\sigma^2} \sum_{t=1}^T \mathbf{y}'_{t-1} \Sigma_{t-1}^{-1} \mathbf{y}_{t-1} + \frac{4\beta}{\sigma^2} \sum_{t=1}^T \mathbf{y}'_{t-1} \Sigma_{t-1}^{-1} \mathbf{y}_{t-1}} \\
& \propto e^{-\frac{\beta^{*2}}{2\sigma^2}} e^{-\frac{2\beta^2}{\sigma^2} \sum_{t=1}^T \mathbf{y}'_{t-1} \Sigma_{t-1}^{-1} \mathbf{y}_{t-1} + \frac{4\beta}{\sigma^2} \sum_{t=1}^T \mathbf{y}'_{t-1} \Sigma_{t-1}^{-1} \mathbf{y}_{t-1}}
\end{aligned}$$

$$= \pi(\beta^*)g_1(\beta^*),$$

where $\pi(\beta^*) = e^{-\frac{\beta^{*2}}{2\sigma_\beta^2}}$ and $g_1(\beta^*) = e^{-\frac{2\beta^2}{\sigma^2} \sum_{t=1}^T \mathbf{y}'_{t-1} \Sigma_{t-1}^{-1} \mathbf{y}_{t-1} + \frac{4\beta}{\sigma^2} \sum_{t=1}^T \mathbf{y}'_t \Sigma_{t-1}^{-1} \mathbf{y}_{t-1}}$.

D.2 Full conditional distribution of α^*

The full conditional density of α^* will be given by $[\alpha^*] \times [\text{Data, Latent} | \boldsymbol{\theta}]$. Now the term that depends on α (hence on α^*) in $[\text{Data, Latent} | \boldsymbol{\theta}]$, that is, in equation (11), is given by

$$g_2(\alpha^*) = \frac{1}{\prod_{t=1}^T |\Omega_t|^{1/2}} e^{-\frac{2}{\sigma^2} \sum_{t=1}^T [(\mathbf{x}_t - \alpha^2 \mathbf{x}_{t-1})^T \Omega_t^{-1} (\mathbf{x}_t - \alpha^2 \mathbf{x}_{t-1})]} \times e^{-\frac{2\alpha}{\sigma^2} \sum_{t=1}^T [\alpha \mathbf{x}_{t-1}^T D \Sigma_{t-1}^{-1} D \mathbf{x}_{t-1} - 2 \mathbf{y}_t^T \Sigma_{t-1}^{-1} D \mathbf{x}_{t-1}]},$$

where D is the $n \times n$ diagonal matrix containing the diagonal elements $\frac{1}{M_{s_i}}, i = 1, \dots, n$.

In the above calculation we use $\boldsymbol{\mu}_t = \beta \mathbf{y}_t + \alpha D \mathbf{x}_t$. Thus the full conditional density of α^* is given by

$$[\alpha^* | \dots] \propto e^{-\frac{\alpha^{*2}}{2\sigma_{\alpha^*}^2}} g_2(\alpha^*).$$

D.3 Full conditional distribution of σ_θ^2

The only term that depends on σ_θ^2 in equation (11) is $\left(\frac{1}{\sigma_\theta^2}\right)^{n/2} \exp\left\{-\frac{1}{2\sigma_\theta^2} \mathbf{y}'_0 \Delta_0^{-1} \mathbf{y}_0\right\}$, and therefore, the full conditional distribution of σ_θ^2 is

$$\begin{aligned} [\sigma_\theta^2 | \dots] &\propto [\sigma_\theta^2] \left(\frac{1}{\sigma_\theta^2}\right)^{n/2} \exp\left\{-\frac{1}{2\sigma_\theta^2} \mathbf{y}'_0 \Delta_0^{-1} \mathbf{y}_0\right\} \\ &\propto \left(\frac{1}{\sigma_\theta^2}\right)^{\alpha_\theta + n/2 + 1} \exp\left\{-\frac{1}{\sigma_\theta^2} \left(\frac{\gamma_\theta + \mathbf{y}'_0 \Delta_0^{-1} \mathbf{y}_0}{2}\right)\right\}. \end{aligned}$$

That is, the full conditional distribution of σ_θ^2 is $\text{IG}\left(\alpha_\theta + n/2, \frac{\gamma_\theta + \mathbf{y}'_0 \Delta_0^{-1} \mathbf{y}_0}{2}\right)$.

D.4 Full conditional distribution of σ_p^2

Since the only term that depends on σ_p^2 in equation (11) is $\left(\frac{1}{\sigma_p^2}\right)^{n/2} \exp\left\{-\frac{1}{2\sigma_p^2} \mathbf{x}'_0 \Omega_0^{-1} \mathbf{x}_0\right\}$

and we have assumed inverse gamma with parameters α_p and γ_p ,

$$[\sigma_p^2 | \dots] \propto \left(\frac{1}{\sigma_p^2}\right)^{\alpha_p+1} \left(\frac{1}{\sigma_p^2}\right)^{n/2} \exp\left\{-\frac{1}{\sigma_p^2} \left(\frac{\gamma_p + \mathbf{x}'_0 \Omega_0^{-1} \mathbf{x}_0}{2}\right)\right\}.$$

This implies that the full conditional distribution of σ_p^2 is $\text{IG}\left(\alpha_p + n/2, \frac{\gamma_p + \mathbf{x}'_0 \Delta_0^{-1} \mathbf{x}_0}{2}\right)$.

D.5 Full conditional distribution of σ^2

Note that $[\text{Data} | \text{Latent}, \mathbf{x}_0, \mathbf{y}_0, \boldsymbol{\theta}]$ and $[\text{Latent} | \text{Data}, \mathbf{x}_0, \mathbf{y}_0, \boldsymbol{\theta}]$ depend on σ^2 . Therefore,

the full conditional distribution of σ^2 can be achieved as follows:

$$\begin{aligned} [\sigma^2 | \dots] &\propto [\sigma^2] \prod_{t=1}^T [\mathbf{y}_t | \mathbf{y}_{t-1}, \mathbf{x}_{t-1}, \boldsymbol{\theta}] [\mathbf{x}_t | \mathbf{y}_t, \mathbf{y}_{t-1}, \mathbf{x}_{t-1}, \boldsymbol{\theta}] \\ &\propto [\sigma^2] (\sigma^2)^{-Tn} \exp\left\{-\frac{2}{\sigma^2} \sum_{t=1}^T [(\mathbf{y}_t - \boldsymbol{\mu}_t)^T \Sigma_{t-1}^{-1} (\mathbf{y}_t - \boldsymbol{\mu}_t) + (\mathbf{x}_t - \alpha^2 \mathbf{x}_{t-1})^T \Omega_t^{-1} (\mathbf{x}_t - \alpha^2 \mathbf{x}_{t-1})]\right\} \\ &\propto \left(\frac{1}{\sigma^2}\right)^{\alpha_v + Tn+1} \exp\left\{-\frac{1}{\sigma^2} \left[\frac{\gamma_v}{2} + 2\zeta\right]\right\}, \end{aligned}$$

where $\zeta = \sum_{t=1}^T [(\mathbf{y}_t - \boldsymbol{\mu}_t)^T \Sigma_{t-1}^{-1} (\mathbf{y}_t - \boldsymbol{\mu}_t) + (\mathbf{x}_t - \alpha^2 \mathbf{x}_{t-1})^T \Omega_t^{-1} (\mathbf{x}_t - \alpha^2 \mathbf{x}_{t-1})]$. Hence the

full conditional distribution of σ^2 is inverse-Gamma with parameters $\alpha_v + Tm$ and

$\gamma_v/2 + 2\zeta$.

D.6 Full conditional distributions of η_1^* , η_2^* , and η_3^*

We observe that only $[\mathbf{x}_0|\boldsymbol{\theta}]$ depends η_1 (hence on η_1^*) and $[\mathbf{Y}_0|\boldsymbol{\theta}]$ depends on η_2 (hence on η_2^*). Therefore, the full conditional densities of η_1^* and η_2^* are given by

$$\begin{aligned} [\eta_1^*|\dots] &\propto [\eta_1^*][\mathbf{x}_0|\boldsymbol{\theta}] \\ &\propto e^{-\eta_1^{*2}/2} \frac{1}{|\Omega_0|^{1/2}} e^{-\frac{1}{2\sigma_p^2} \mathbf{x}_0^T \Omega_0^{-1} \mathbf{x}_0} \\ &= \pi(\eta_1^*) g_3(\eta_1^*) \end{aligned} \quad (41)$$

and

$$\begin{aligned} [\eta_2^*|\dots] &\propto [\eta_2^*][\mathbf{y}_0|\boldsymbol{\theta}] \\ &\propto e^{-\eta_2^{*2}/2} \frac{1}{|\Delta_0|^{1/2}} e^{-\frac{1}{2\sigma_\theta^2} \mathbf{y}_0^T \Delta_0^{-1} \mathbf{y}_0} \\ &= \pi(\eta_2^*) g_4(\eta_2^*), \end{aligned} \quad (42)$$

respectively, where $\eta_1 = e^{\eta_1^*}$, $\eta_2 = e^{\eta_2^*}$, $\pi(\eta_1^*) = e^{-\eta_1^{*2}/2}$, $\pi(\eta_2^*) = e^{-\eta_2^{*2}/2}$, $g_3(\eta_1^*) = \frac{1}{|\Omega_0|^{1/2}} e^{-\frac{1}{2\sigma_p^2} \mathbf{x}_0^T \Omega_0^{-1} \mathbf{x}_0}$ and $g_4(\eta_2^*) = \frac{1}{|\Delta_0|^{1/2}} e^{-\frac{1}{2\sigma_\theta^2} \mathbf{y}_0^T \Delta_0^{-1} \mathbf{y}_0}$.

On the other hand, the joint conditional distribution of (Data, Latent) given $\mathbf{x}_0, \mathbf{y}_0, \boldsymbol{\theta}$ depends on η_3 (hence on η_3^*). Thus, the full conditional distribution of η_3^* is given by

$$\begin{aligned} [\eta_3^*] &\propto [\eta_3^*] \prod_{t=1}^T [\mathbf{y}_t|\mathbf{y}_{t-1}, \mathbf{x}_{t-1}, \boldsymbol{\theta}] [\mathbf{x}_t|\mathbf{y}_t, \mathbf{y}_{t-1}, \mathbf{x}_{t-1}, \boldsymbol{\theta}] \\ &\propto e^{-\eta_3^{*2}/2} \frac{1}{\prod_{t=1}^T |\Sigma_{t-1}|^{1/2} |\Omega_t|^{1/2}} e^{-\frac{2}{\sigma^2} \sum_{t=1}^T [(\mathbf{y}_t - \boldsymbol{\mu}_t)^T \Sigma_{t-1}^{-1} (\mathbf{y}_t - \boldsymbol{\mu}_t) + (\mathbf{x}_t - \alpha^2 \mathbf{x}_{t-1})^T \Omega_t^{-1} (\mathbf{x}_t - \alpha^2 \mathbf{x}_{t-1})]} \\ &= \pi(\eta_3^*) g_5(\eta_3^*), \end{aligned} \quad (43)$$

where $\eta_3 = e^{\eta_3^*}$, $\pi(\eta_3^*) = e^{-\eta_3^{*2}/2}$ and

$$g_5(\eta_3^*) = \frac{1}{\prod_{t=1}^T |\Sigma_{t-1}|^{1/2} |\Omega_t|^{1/2}} e^{-\frac{2}{\sigma^2} \sum_{t=1}^T [(\mathbf{y}_t - \boldsymbol{\mu}_t)^T \Sigma_{t-1}^{-1} (\mathbf{y}_t - \boldsymbol{\mu}_t) + (\mathbf{x}_t - \alpha^2 \mathbf{x}_{t-1})^T \Omega_t^{-1} (\mathbf{x}_t - \alpha^2 \mathbf{x}_{t-1})]}.$$

D.7 Full conditional distribution of \mathbf{x}_0

Using the fact that only \mathbf{x}_1 and \mathbf{y}_1 depend on \mathbf{x}_0 and writing $\boldsymbol{\mu}_0 = \beta \mathbf{y}_0 + \alpha D \mathbf{x}_0$, we have

$$\begin{aligned} [\mathbf{x}_0 | \dots] &\propto [\mathbf{x}_0 | \boldsymbol{\theta}] [\mathbf{x}_1 | \mathbf{y}_1, \mathbf{y}_0, \mathbf{x}_0, \boldsymbol{\theta}] [\mathbf{y}_1 | \mathbf{y}_0, \mathbf{x}_0, \boldsymbol{\theta}] \\ &\propto e^{-\frac{1}{2\sigma_p^2} \mathbf{x}_0^T \Omega_0^{-1} \mathbf{x}_0} e^{-\frac{2}{\sigma^2} (\mathbf{x}_1 - \alpha^2 \mathbf{x}_0)^T \Omega_1^{-1} (\mathbf{x}_1 - \alpha^2 \mathbf{x}_0)} e^{-\frac{2}{\sigma^2} (\mathbf{y}_1 - \beta \mathbf{y}_0 - \alpha D \mathbf{x}_0)^T \Sigma_0^{-1} (\mathbf{y}_1 - \beta \mathbf{y}_0 - \alpha D \mathbf{x}_0)} \\ &\propto e^{-\frac{1}{2\sigma_p^2} \left[\mathbf{x}_0^T \Omega_0^{-1} \mathbf{x}_0 + \frac{4\sigma_p^2 \alpha^4}{\sigma^2} \mathbf{x}_0^T \Omega_1^{-1} \mathbf{x}_0 + \frac{4\sigma_p^2 \alpha^2}{\sigma^2} \mathbf{x}_0^T D \Sigma_0^{-1} D \mathbf{x}_0 - \frac{8\sigma_p^2 \alpha^2}{\sigma^2} \mathbf{x}_0^T \Omega_1^{-1} \mathbf{x}_1 - \frac{8\sigma_p^2 \alpha}{\sigma^2} \mathbf{x}_0^T D \Sigma_0^{-1} (\mathbf{y}_1 - \beta \mathbf{y}_0) \right]} \\ &\propto e^{-\frac{1}{2\sigma_p^2} [\mathbf{x}_0^T A \mathbf{x}_0 - 2\mathbf{x}_0^T B \mathbf{x}_1 - 2\mathbf{x}_0^T C (\mathbf{y}_1 - \beta \mathbf{y}_0)]} \\ &\propto e^{-\frac{1}{2\sigma_p^2} (\mathbf{x}_0 - A^{-1} B \mathbf{x}_1 - A^{-1} C (\mathbf{y}_1 - \beta \mathbf{y}_0))^T A (\mathbf{x}_0 - A^{-1} B \mathbf{x}_1 - A^{-1} C (\mathbf{y}_1 - \beta \mathbf{y}_0))}, \end{aligned} \quad (44)$$

where $A = \Omega_0^{-1} + \frac{4\sigma_p^2 \alpha^4}{\sigma^2} \Omega_1^{-1} + \frac{4\sigma_p^2 \alpha^2}{\sigma^2} D \Sigma_0^{-1} D$, $B = \frac{4\sigma_p^2 \alpha^2}{\sigma^2} \Omega_1^{-1}$, $C = \frac{4\sigma_p^2 \alpha}{\sigma^2} D \Sigma_0^{-1}$. We note here that D ($= \text{diag}(1/M_{s_i})_{i=1}^n$) is a positive definite matrix as all the diagonal entries are strictly positive, A being a sum of three positive definite matrices is also positive definite and hence invertible. Thus, from equation (44), we get $[\mathbf{x}_0 | \dots] \sim N_n(A^{-1}(B \mathbf{x}_1 + C(\mathbf{y}_1 - \beta \mathbf{y}_0)), \sigma_p^2 A^{-1})$.

E Algorithm for temporal prediction

We provide the algorithms for simulating observations from the posterior predictive densities for single-time point and multiple-time point predictions. Let $\mathbf{Y}_{T+1} = (Y(s_1, T+1), \dots, Y(s_n, T+1))^T$ and $\mathbf{x}_{T+1} = (x(s_1, T+1), \dots, x(s_n, T+1))^T$ be the response and latent variable at time point $T+1$. The aim is simulate observation from the predic-

tive density of \mathbf{Y}_{T+L} , for $L = 1, 2, \dots$. For $k = 1, \dots, N$, where N is the number of iterations after the burn-in period B , do the following.

- S1. simulate from $[\mathbb{L}, \boldsymbol{\theta} | \mathbb{D}]$ using Gibbs, and Metropolis Hastings within Gibbs via the full conditionals as outlined in section 5. Let the simulated value at the k th iteration be denoted by $\boldsymbol{\theta}^{(k)}$ and $\mathbb{L}^{(k)}$.
- S2. Given $\boldsymbol{\theta}^{(k)}$ and $\mathbb{L}^{(k)}$, simulate n -variate observation from normal distribution with the mean $\boldsymbol{\mu}_T$, where the i th element of $\boldsymbol{\mu}_T$ is as mentioned in section 3 with m replaced with T , β replaced with $\beta^{(k)}$, α replaced with $\alpha^{(k)}$, and the covariance matrix Σ_T . The elements of Σ_T is the same as given in subsection 3.1 after equation 8, with η_3 , α and j replaced with $\eta_3^{(k)}$, $\alpha^{(k)}$ and $T + 1$, respectively. Let the simulated observations be denoted by $\mathbf{y}_{T+1}^{(k)}$.
- S4. Then simulate \mathbf{x}_{T+1} from n -variate normal distribution with the mean $\alpha^{(k)^2} \mathbf{x}_T$ and covariance matrix Ω_{T+1} . The elements of the Ω_T , is the same as described in subsection 3.2 with t replaced by $T + 1$, α replaced by $\alpha^{(k)}$ and η_3 replaced by $\eta_3^{(k)}$.
- S5. Update the data \mathbb{D} to $\mathbb{D}_1^{(k)} = \mathbb{D} \cup \{\mathbf{y}_{T+1}^{(k)}\}$ and the latent $\mathbb{L}^{(k)}$ to $\mathbb{L}_1^{(k)} = \mathbb{L} \cup \{\mathbf{x}_{T+1}^{(k)}\}$.
- S6. Given $\mathbb{D}_1^{(k)}, \mathbb{L}_1^{(k)}$ and $\boldsymbol{\theta}^{(k)}$, simulate $\mathbf{y}_{T+2}^{(k)}$ from n -variate normal with the mean $\boldsymbol{\mu}_{T+1}$ and covariance matrix Σ_{T+1} , where the i th element of $\boldsymbol{\mu}_{T+1}$ is as mentioned in section 3 with m , β and α replaced with $T + 1$, $\beta^{(k)}$ and $\alpha^{(k)}$, respectively, and the covariance matrix Σ_{T+1} . The elements of Σ_{T+1} is the same as given in subsection 3.1 after equation 8, with η_3 , α and j replaced with $\eta_3^{(k)}$, $\alpha^{(k)}$ and $T + 2$, respectively. Let the simulated observations be denoted by $\mathbf{y}_{T+2}^{(k)}$.
- S7. Then simulate \mathbf{x}_{T+2} from n -variate normal distribution with the mean $\alpha^{(k)^2} \mathbf{x}_{T+1}^{(k)}$

and covariance matrix Ω_{T+1} . The elements of the Ω_{T+1} , is the same as described in subsection 3.2 with t replaced by $T + 2$, α replaced by $\alpha^{(k)}$ and η_3 replaced by $\eta_3^{(k)}$.

S8. Continue the procedure to get a simulated value $\mathbf{y}_{T+L}^{(k)}$.

F Algorithm for prediction of time series at a spatial point

Let s^* be a spatial location at which we want to get prediction for the time points t_1, \dots, t_T . Therefore, it is required to get observations from the distribution given by

$[y(s^*, t), t = 1, \dots, T, |\mathbb{D}]$. Let us denote $(y(s^*, t), t = 1, \dots, T)$ by \mathbf{y}^* and $(x(s^*, t), t = 1, \dots, T)$

by \mathbf{x}^* . Notice that $(y(s_1, t), \dots, y(s_n, t), y(s^*, t))$ given $\mathbb{L}, \mathbf{x}^*, \boldsymbol{\theta}$ and $(y(s_1, t-1), \dots, y(s_n, t-1), y(s^*, t-1))$

is a $(n+1)$ -variate normal with the mean $\boldsymbol{\mu}_{t-1}^* = \left(\beta y(s_1, t-1) + \frac{\alpha x(s_1, t-1)}{M_{s_1}}, \dots, \beta y(s_n, t-1) + \frac{\alpha x(s_n, t-1)}{M_{s_n}} \right)$,

and covariance matrix Σ_{t-1}^* of order $n+1 \times n+1$. The elements of Σ_{t-1}^* are the same

as given in the Section 3.1. Let Σ_{t-1}^* be partitioned as $\Sigma_{t-1}^* = \begin{pmatrix} \Sigma_{t-1} & \mathbf{S}_{1,t-1} \\ \mathbf{S}_{1,t-1}^T & s_{n+1,n+1} \end{pmatrix}$,

where Σ_{t-1} is $n \times n$ matrix, $\mathbf{S}_{1,t-1}$ is $n \times 1$ vector. Therefore, $[y(s^*, t) | \dots]$ follows a

univariate normal with the mean $\beta y(s^*, t-1) + \frac{\alpha x(s^*, t-1)}{M_{s^*}} - \mathbf{S}_{1,t-1}^T \Sigma_{t-1}^{-1} (\mathbf{y}_t - \boldsymbol{\mu}_t)$ and vari-

ance $s_{n+1,n+1} - \mathbf{S}_{1,t-1}^T \Sigma_{t-1}^{-1} \mathbf{S}_{1,t-1}$. We use this fact to simulate $y(s^*, t)$, for $t = 1, \dots, T$, sequentially.

Initialize \mathbf{y}^* and \mathbf{x}^* by $\mathbf{y}^{*(0)}$ and $\mathbf{x}^{*(0)}$, and all the other unknowns. For $k = 1, \dots, N+B$, do the following.

S1. For $t = 1, \dots, T$,

S2. Define $\mathbb{D}^{(k-1)} = [\mathbb{D}, \mathbf{y}^{*(k-1)}]$ and $\mathbb{L}^{(k-1)} = [\mathbb{L}, \mathbf{x}^{*(k-1)}]$.

- S3. Simulate $\boldsymbol{\theta}^{(k)}$ from $[\boldsymbol{\theta}|\mathbb{D}^{(k-1)}, \mathbb{L}^{(k-1)}]$ using Gibbs and MH within Gibbs via full conditionals as given in Section 5. Let the simulated value be $\boldsymbol{\theta}^{(k)}$.
- S4. Given, $\boldsymbol{\theta}^{(k)}$ and $\mathbb{D}^{(k-1)}$, simulate the latent variables from their full conditionals as given in Section 5. Let the simulated value be $\mathbb{L}^{(k)}$.
- S5. Given $\boldsymbol{\theta}^{(k)}$ and $\mathbb{L}^{(k)}$, simulate $y(s^*, t)$ from $[y(s^*, t)|L^{(k)}, \boldsymbol{\theta}^{(k)}, \mathbb{D}]$, say $y(s^*, t)^{(k)}$.

Store N observations after discarding B observations as burn-in.

G Supplementary plots for 3 component mixture of GPs

In this appendix, we provide the trace plots and the posterior densities of the complete time series of the latent variables for the simulated data used in subsection 6.1.

G.1 Trace plots

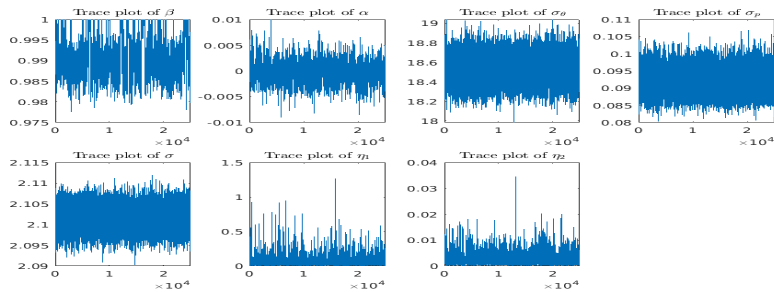


Figure 17: Trace plots for the parameters for data simulated from 3-component GP mixtures.

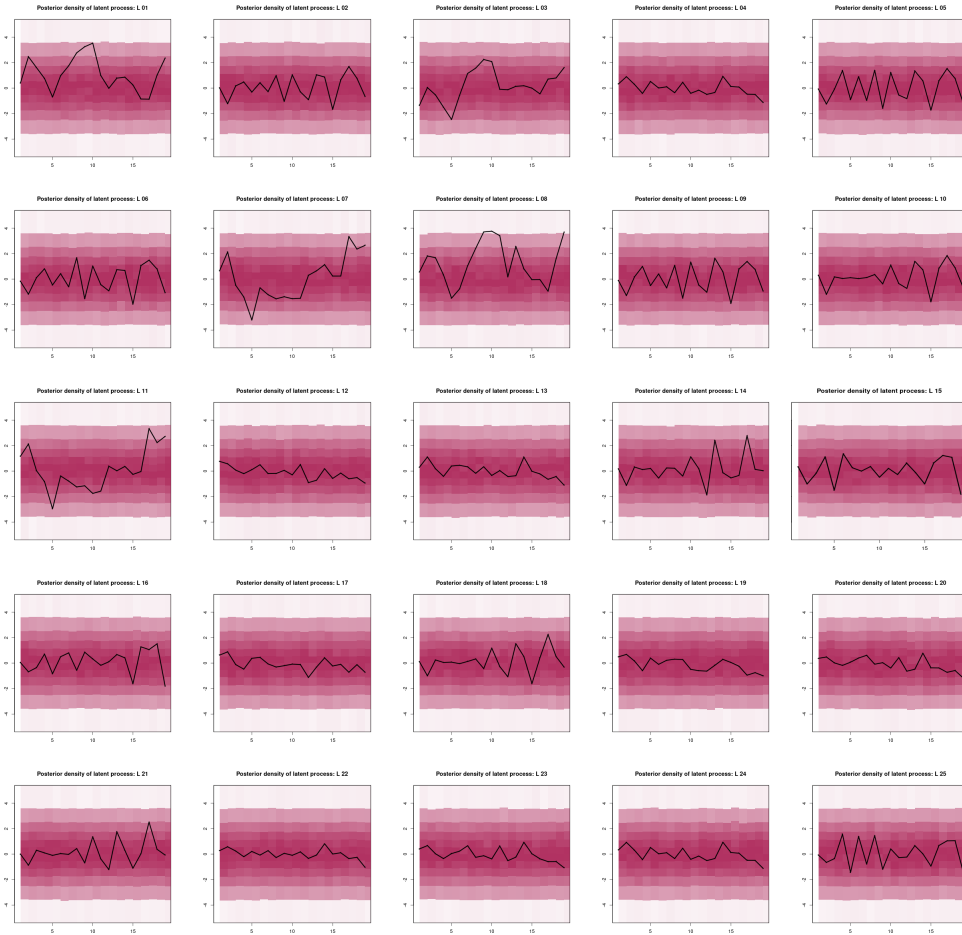


Figure 18: Posterior densities of latent variables for the first 25 locations for data simulated from 3-component mixture of GPs. Higher the intensity of the colour, higher is the probability density. The black line represents the true values of the latent variables. $L_i, i = 1, \dots, 25$, denote the locations.

G.2 Posterior densities of the complete time series of the latent variables

H Supplementary plots for mixture of GQNs

Trace plots of the parameters and the posterior densities of the complete time series of the latent variables for two component mixture of GQNs are depicted below. The details of the data is given in the subsection 6.3.

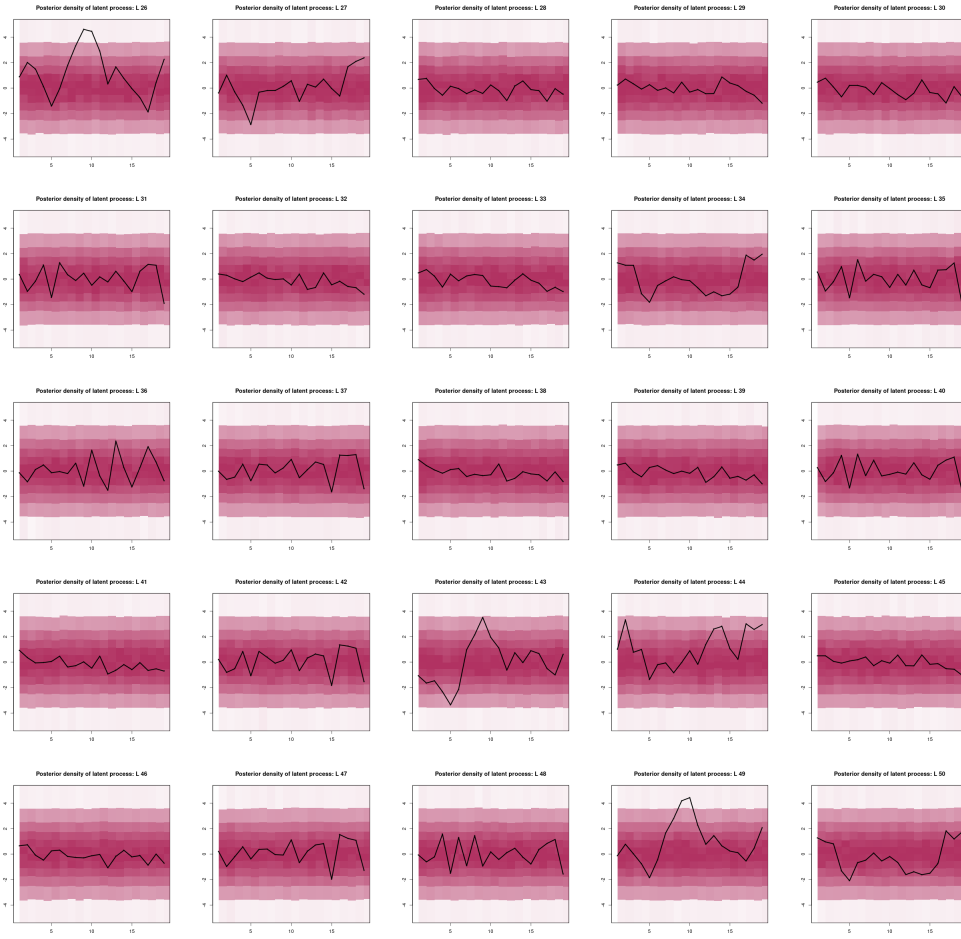


Figure 19: Posterior densities of latent variables for the last 25 locations for data simulated from 3-component mixture of GPs. Higher the intensity of the colour, higher is the probability density. The black line represents the true values of the latent variables. $L_i, i = 26, \dots, 50$, denote the locations.

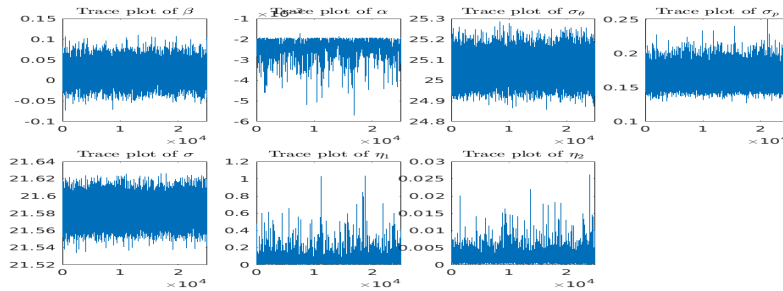


Figure 20: Trace plots for the parameters for data simulated from mixture of GQNs.

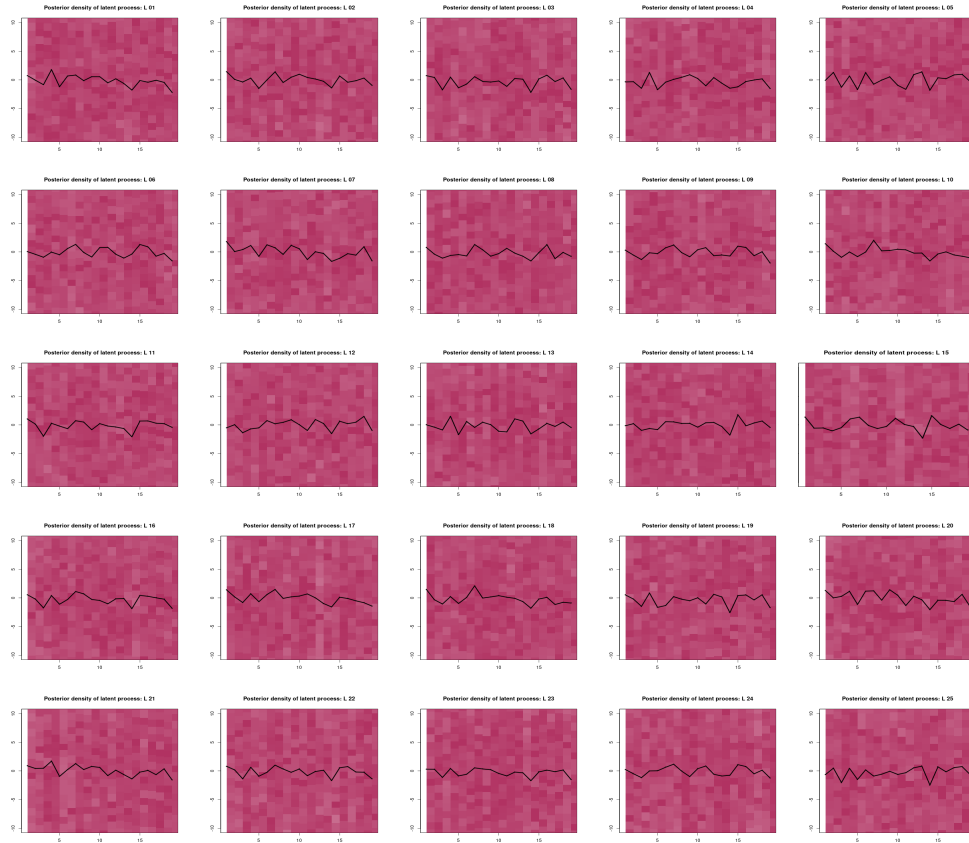


Figure 21: Posterior densities of latent variables for the first 25 locations for data simulated from mixture of two GQNs. Higher the intensity of the colour, higher is the probability density. The black line represents the true values of the latent variables. $L_i, i = 1, \dots, 25$, denote the locations.

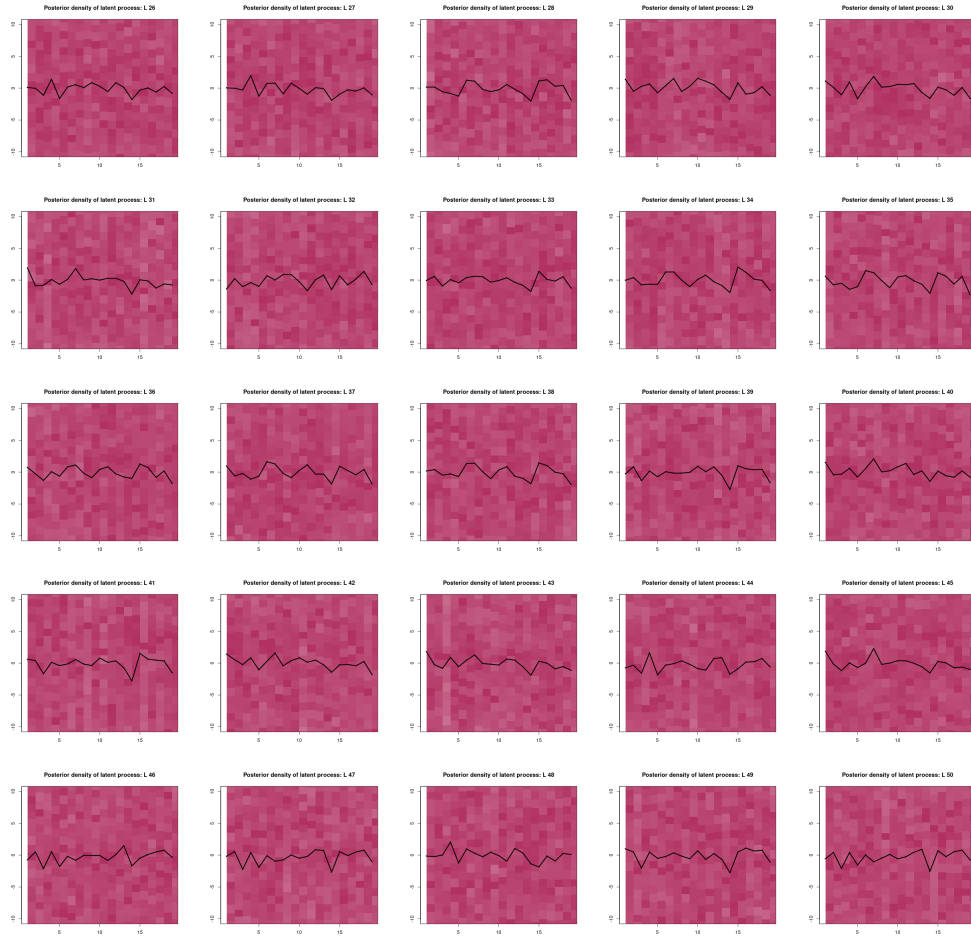


Figure 22: Posterior densities of latent variables for the last 25 locations for data simulated from mixture of two GQNs. Higher the intensity of the colour, higher is the probability density. The black line represents the true values of the latent variables. $L_i, i = 26, \dots, 50$, denote the locations.

I Supplementary plots for Alaska temperature data

I.1 Trace plots

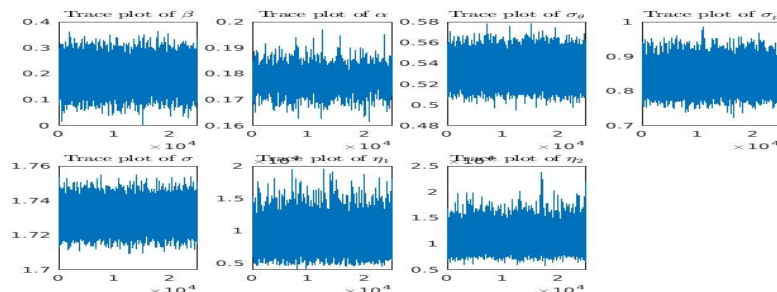


Figure 23: Trace plot for the parameters except for η_3 corresponding to the Alaska temperature data.

I.2 Posterior densities of the complete time series of the latent variables

I.3 Posterior predictive densities for the year 2015 at 26 locations

I.4 Posterior predictive densities for the years 2016–2021 at 16 locations

J Supplementary plots for sea temperature data

J.1 Trace plots

J.2 Predictive densities: latent variables

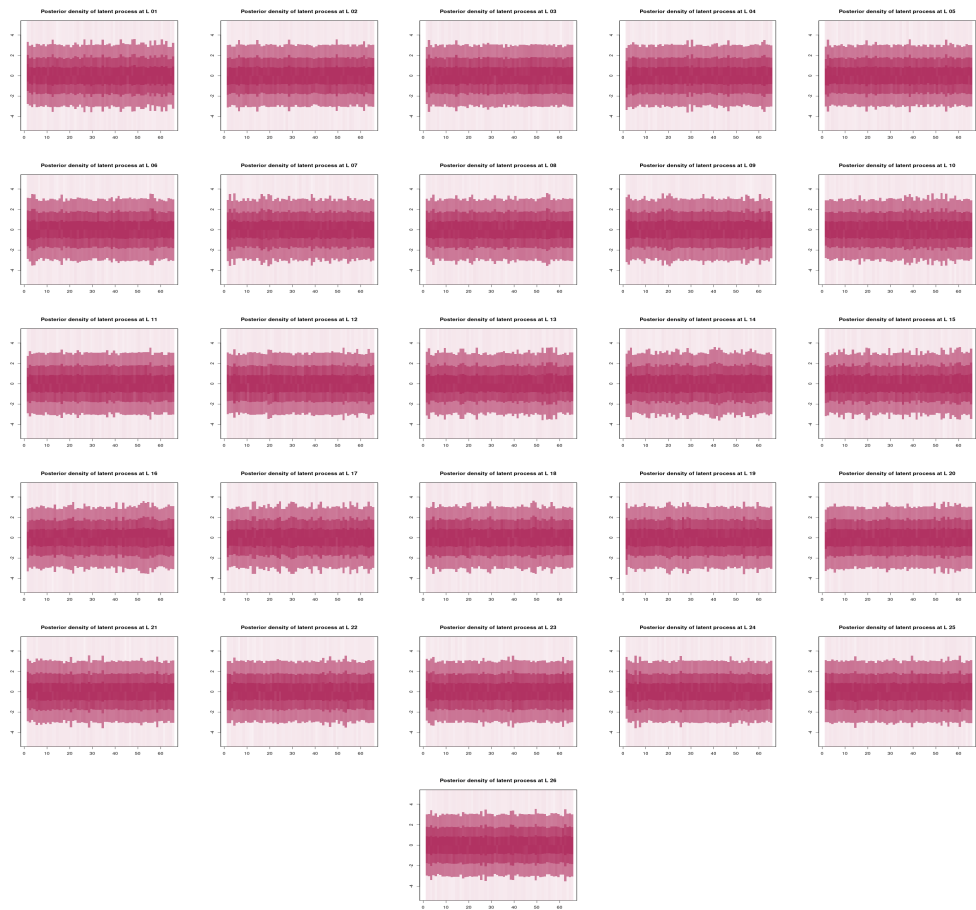


Figure 24: Posterior densities of the latent variables at 26 locations in Alaska and its surroundings corresponding to the annual detrended temperature data. Higher the intensity of the colour, higher is the probability density.

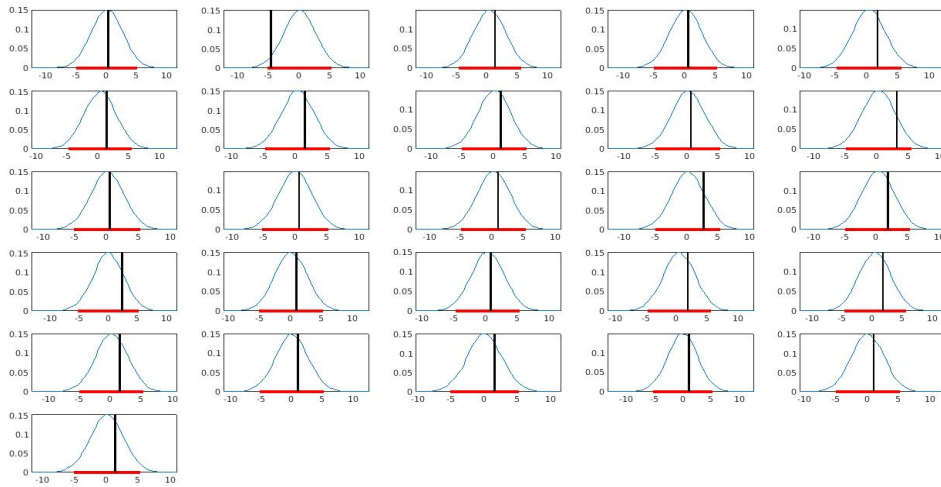


Figure 25: Posterior predictive densities of the detrended temperatures for the year 2015 at 26 locations for the Alaska temperature data. The red horizontal lines denote the 95% predictive intervals. The vertical black lines indicate the true values. All the true values lie within the 95% posterior predictive intervals.

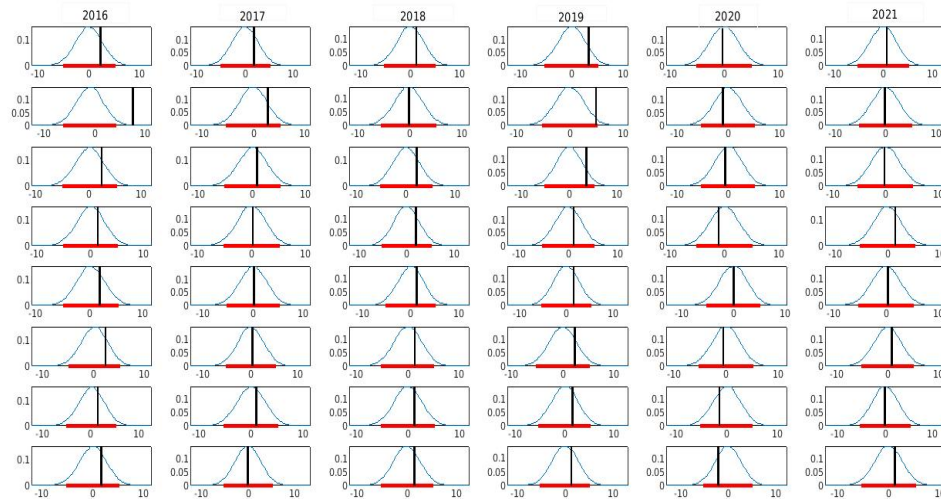


Figure 26: Predictive densities of the detrended temperatures for the years 2016-2021 at 8 locations for the Alaska temperature data. The eight locations are indicated by $L_1 \dots, L_7$, and L_{11} at the left side of the figure corresponding to the rows. The years are shown at the top of the figure corresponding to the columns. The red horizontal line in each plot denotes the 95% posterior predictive interval. The vertical black lines indicate the true values. All the true values, except one, lie within the 95% posterior predictive intervals.

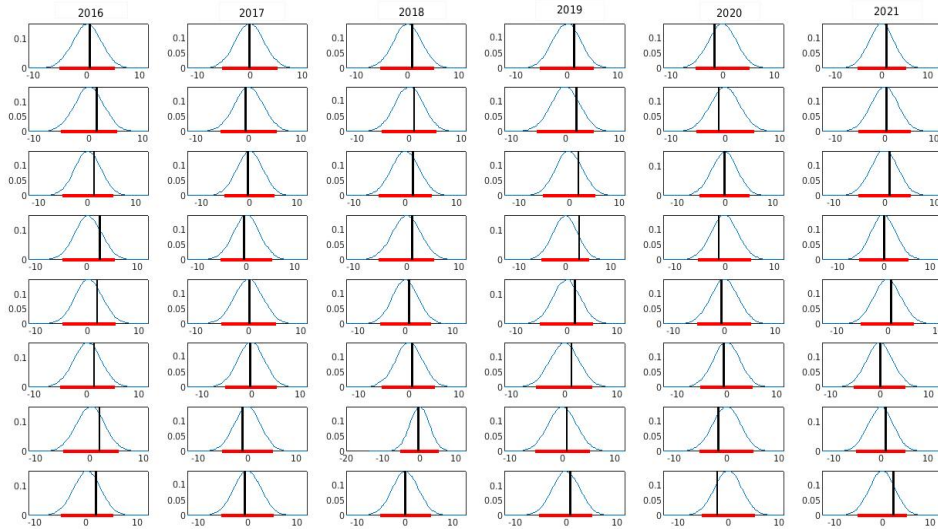


Figure 27: Predictive densities of the detrended temperatures for the years 2016-2021 at *other* 8 locations for the Alaska temperature data. The eight locations are indicated by L_{12} , L_{13} , L_{18} , L_{19} , L_{20} , L_{22} , L_{27} and L_{29} at the left side of the figure corresponding to the rows. The years are shown at the top of the figure corresponding to the columns. The red horizontal line in each plot denotes the 95% posterior predictive interval. The vertical black lines indicate the true values. All the true values lie within the 95% posterior predictive interval.

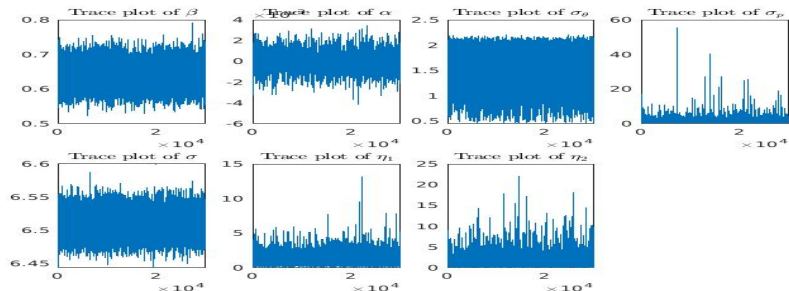


Figure 28: Trace plots of the parameters except for η_3 for the sea surface temperature data.

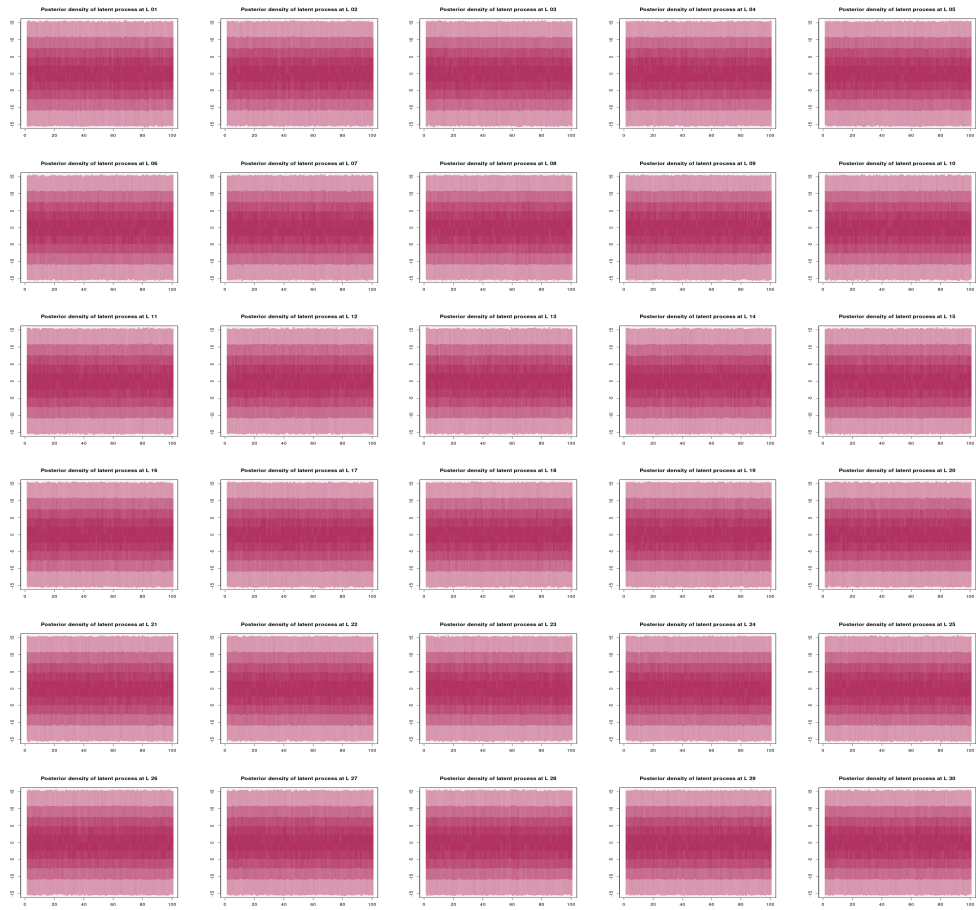


Figure 29: Posterior densities of the latent variables at 30 locations of the sea surface temperature data. Higher the intensity of the colour, higher is the probability density.

J.3 Predictive densities for 100th month for 30 locations

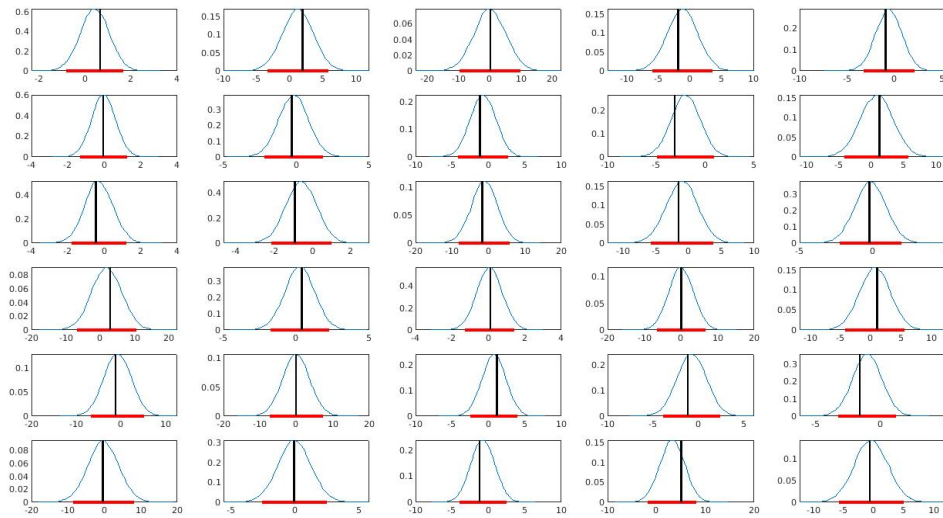


Figure 30: Predictive densities of averaged referenced temperatures for the 100th month at 30 locations for the sea surface temperature data. The red horizontal lines denote the 95% predictive interval. The vertical black lines indicate the true values. All the true values lie within the 95% predictive interval.

K Stationarity, convergence of lagged correlations to zero and non-Gaussianity of the detrended Alaska data process

This appendix shows that the data set analyzed in subsection 7.1 arises from a non-stationary and non-Gaussian process. Further the analysis shows that the sample lagged correlation tends to 0 as the distance between time and/or space tends to infinity.

K.1 Stationarity of the detrended Alaska data process

To check if the data arrived from a stationary or non-stationary process, we resorted to the recursive Bayesian theory and methods developed by Roy and Bhattacharya [2020]. In a nutshell, their key idea is to consider the Kolmogorov-Smirnov distance between distributions of data associated with local and global space-times. Associated with the j -th local space-time region is an unknown probability p_j of the event that the underlying process is stationary when the observed data corresponds to the j -th local region and the Kolmogorov-Smirnov distance falls below c_j , where c_j is any non-negative sequence tending to zero as j tends to infinity. With suitable priors for p_j , Roy and Bhattacharya [2020] constructed recursive posterior distributions for p_j and proved that the underlying process is stationary if and only if for sufficiently large number of observations in the j -th region, the posterior of p_j converges to one as $j \rightarrow \infty$. Nonstationarity is the case if and only if the posterior of p_j converges to zero as $j \rightarrow \infty$.

In our implementation of the ideas of Roy and Bhattacharya [2020], we set the j -th local region to be the entire time series for the spatial location \mathbf{s}_j , for $j = 1, \dots, 29$. Thus, the size of each local region is 65. We choose c_j to be of the same nonparametric,

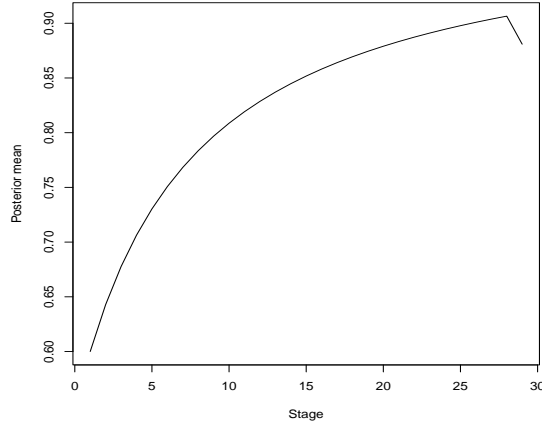


Figure 31: Alaska data analysis: detection of strict stationarity.

dynamic and adaptive form as detailed in Roy and Bhattacharya [2020]. The dynamic form requires an initial value for the sequence. In practice, the choice of the initial value usually has significant effect on the convergence of the posteriors of p_j , and so, the choice must be carefully made. However, in our case, for all initial values that we experimented with, lying between 0.05 and 1, the recursive Bayesian procedure led to the conclusion of stationarity of the underlying spatio-temporal process.

We implemented the idea with our parallelised C code on 29 parallel processors of a VMWare of Indian Statistical Institute; the time taken is less than a second. For the initial value 0.05, Figure 31 displays the means of the posteriors of p_j ; $j = 1, \dots, 29$, showing convergence to 1. The respective posterior variances are negligibly small and hence not shown. Thus, the detrended spatio-temporal process that generated the Alaska data, can be safely regarded as stationary.

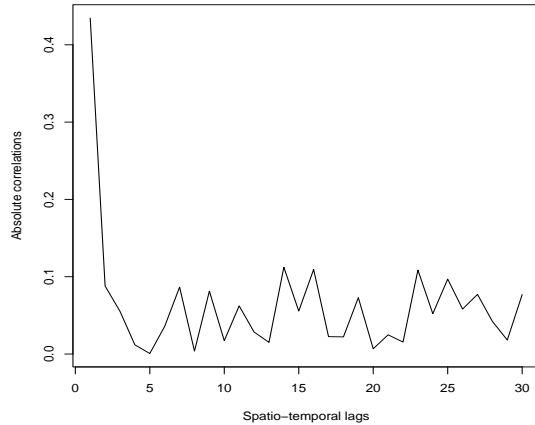


Figure 32: Alaska data analysis: lagged spatio-temporal correlations converging to zero.

K.2 Convergence of lagged spatio-temporal correlations to zero for the Alaska data

Recall that one major purpose of our Hamiltonian spatio-temporal model is to emulate the property of most real datasets that the lagged spatio-temporal correlations tend to zero as the spatio-temporal lag tends to infinity, irrespective of stationarity or nonstationarity. Here we compute the lagged correlations on 30 parallel processors on our VMWare, each processor computing the correlation for a partitioned interval of lag $\|\mathbf{h}\|$ such that the interval is associated with sufficient data making the correlation well-defined. The time taken for this exercise are a few seconds. Figure 32 demonstrates convergence of the lagged spatio-temporal correlations to zero; with larger amount of data such demonstration would have been more convincing.

K.3 Non-Gaussianity of the Alaska data

Simple quantile-quantile plots (not shown for brevity) revealed that the distributions of the time series data at the spatial locations, distributions of the spatial data at the time points, and the overall distribution of the entire data set, are far from normal. Thus,

traditional Gaussian process based models of the underlying spatio-temporal process are ruled out. Since the temporal distributions at the spatial locations and the spatial distributions at different time points are also much different, it does not appear feasible to consider parametric stochastic process models for the data. These seem to make the importance of our nonparametric Hamiltonian process more pronounced.

References

- Mikyoung Jun, Reto Knutti, and Douglas W Nychka. Spatial analysis to quantify numerical model bias and dependence: how many climate models are there? *Journal of the American Statistical Association*, 103(483):934–947, 2008.
- Reinhard Furrer and Stephan R Sain. Spatial model fitting for large datasets with applications to climate and microarray problems. *Statistics and Computing*, 19(2):113–128, 2009.
- Claudia Tebaldi and Bruno Sansó. Joint projections of temperature and precipitation change from multiple climate models: a hierarchical bayesian approach. *Journal of the Royal Statistical Society: Series A (Statistics in Society)*, 172(1):83–106, 2009.
- Stephan R Sain, Reinhard Furrer, and Noel Cressie. A spatial analysis of multivariate output from regional climate models. *The Annals of Applied Statistics*, pages 150–175, 2011.
- Richard L Smith, Claudia Tebaldi, Doug Nychka, and Linda O Mearns. Bayesian modeling of uncertainty in ensembles of climate models. *Journal of the American Statistical Association*, 104(485):97–116, 2009.
- Huiyan Sang, Mikyoun Jun, and Jianhua Z Huang. Covariance approximation for large multivariate spatial data sets with an application to multiple climate model errors. *The Annals of Applied Statistics*, pages 2519–2548, 2011.
- David Roxbee Cox and Valerie Isham. A simple spatial-temporal model of rainfall. *Proceedings of the Royal Society of London. A. Mathematical and Physical Sciences*, 415(1849):317–328, 1988.

- Bruno Sanso and Lelys Guenni. Venezuelan rainfall data analysed by using a bayesian space–time model. *Journal of the Royal Statistical Society: Series C (Applied Statistics)*, 48(3):345–362, 1999.
- Sujit K Sahu, Alan E Gelfand, and David M Holland. Fusing point and areal level space–time data with application to wet deposition. *Journal of the Royal Statistical Society: Series C (Applied Statistics)*, 59(1):77–103, 2010.
- Peter Guttorp, Wendy Meiring, and Paul D Sampson. A space-time analysis of ground-level ozone data. *Environmetrics*, 5(3):241–254, 1994.
- Gabriel Huerta, Bruno Sansó, and Jonathan R Stroud. A spatiotemporal model for mexico city ozone levels. *Journal of the Royal Statistical Society: Series C (Applied Statistics)*, 53(2):231–248, 2004.
- Francesca Bruno, Peter Guttorp, Paul D Sampson, and Daniela Cocchi. A simple non-separable, non-stationary spatiotemporal model for ozone. *Environmental and ecological statistics*, 16(4):515–529, 2009.
- Yiping Dou, Nhu D Le, and James V Zidek. Modeling hourly ozone concentration fields. *The Annals of applied statistics*, 4(3):1183–1213, 2010.
- Christopher J Paciorek, Jeff D Yanosky, Robin C Puett, Francine Laden, and Helen H Suh. Practical large-scale spatio-temporal modeling of particulate matter concentrations. *The Annals of Applied Statistics*, pages 370–397, 2009.
- David M Holland, Oliveira Victor De, Lawrence H Cox, and Richard L Smith. Estimation of regional trends in sulfur dioxide over the eastern united states. *Environmetrics: The official journal of the International Environmetrics Society*, 11(4):373–393, 2000.

- Marco Giannitrapani, Adrian Bowman, Marian Scott, and Ron Smith. Sulphur dioxide in europe: Statistical relationships between emissions and measured concentrations. *Atmospheric Environment*, 40(14):2524–2532, 2006.
- Rob Beelen, Gerard Hoek, Danielle Vienneau, Marloes Eeftens, Konstantina Dimakopoulou, Xanthi Pedeli, Ming-Yi Tsai, Nino Künzli, Tamara Schikowski, Alessandro Marcon, T. Kirsten Eriksen, et al. Development of no₂ and no_x land use regression models for estimating air pollution exposure in 36 study areas in europe—the escape project. *Atmospheric Environment*, 72:10–23, 2013.
- Heresh Amini, Seyed-Mahmood Taghavi-Shahri, Sarah B Henderson, Vahid Hosseini, Hossein Hassankhany, Maryam Naderi, Solmaz Ahadi, Christian Schindler, Nino Künzli, and Masud Yunesian. Annual and seasonal spatial models for nitrogen oxides in tehran, iran. *Scientific reports*, 6(1):1–11, 2016.
- Jin S Deng, Ke Wang, Yang Hong, and Jia G Qi. Spatio-temporal dynamics and evolution of land use change and landscape pattern in response to rapid urbanization. *Landscape and urban planning*, 92(3-4):187–198, 2009.
- Avishek Chakraborty, Alan E Gelfand, Adam M Wilson, Andrew M Latimer, and John A Silander Jr. Modeling large scale species abundance with latent spatial processes. *The Annals of Applied Statistics*, 4(3):1403–1429, 2010.
- Sudipto Banerjee, Bradley P Carlin, and Alan E Gelfand. *Hierarchical modeling and analysis for spatial data*. CRC press, 2014.
- Paul D Sampson and Peter Guttorp. Nonparametric estimation of nonstationary spatial covariance structure. *Journal of the American Statistical Association*, 87(417):108–119, 1992.

- Moumita Das and Sourabh Bhattacharya. A kernel-enriched order-dependent nonparametric spatio-temporal process. *Spatial Statistics*, 55:100751, 2023.
- Sucharita Roy and Sourabh Bhattacharya. Bayesian characterizations of properties of stochastic processes with applications. *arXiv preprint arXiv:2005.00035*, 2020.
- Sourabh Bhattacharya. Bayesian lévy-dynamic spatio-temporal process: Towards big data analysis. *Journal of the Indian Statistical Association*, 59(2):145–195, 2021. Special Issue on Spatio Temporal Modelling.
- Christopher Joseph Paciorek. *Nonstationary Gaussian processes for regression and spatial modelling*. PhD thesis, Carnegie Mellon University, 2003.
- Alan E Gelfand, Peter Diggle, Peter Guttorp, and Montserrat Fuentes. *Handbook of spatial statistics*. CRC press, 2010.
- Doris Damian, Paul D Sampson, and Peter Guttorp. Bayesian estimation of semi-parametric non-stationary spatial covariance structures. *Environmetrics: The official journal of the International Environmetrics Society*, 12(2):161–178, 2001.
- Alexandra M Schmidt and Anthony O’Hagan. Bayesian inference for non-stationary spatial covariance structure via spatial deformations. *Journal of the Royal Statistical Society: Series B (Statistical Methodology)*, 65(3):743–758, 2003.
- David Higdon. A process-convolution approach to modelling temperatures in the north atlantic ocean. *Environmental and Ecological Statistics*, 5(2):173–190, 1998.
- D Higdon, J Swall, and J Kern. Non-stationary spatial modeling. In J Bernardo, J Berger, A Dawid, and A Smith, editors, *Bayesian Statistics 6*, pages 761–768. Oxford University Press, Oxford, U.K., 1999.

- M. Fuentes and R.L. Smith. A new class of nonstationary spatial model. Technical report, North Carolina State University, 2001.
- Dave Higdon. Space and space-time modeling using process convolutions. In W. Anderson Clive, Barnett Vic, C. Chatwin Philip, and Abdel H. El-Shaarawi, editors, *Quantitative methods for current environmental issues*, pages 37–56. Springer, 2002.
- Montserrat Fuentes. Spectral methods for nonstationary spatial processes. *Biometrika*, 89(1):197–210, 2002.
- Christopher J Paciorek and Mark J Schervish. Spatial modelling using a new class of nonstationary covariance functions. *Environmetrics: The official journal of the International Environmetrics Society*, 17(5):483–506, 2006.
- Christopher K Wikle and Mevin B Hooten. A general science-based framework for dynamical spatio-temporal models. *Test*, 19(3):417–451, 2010.
- Finn Lindgren, Håvard Rue, and Johan Lindström. An explicit link between gaussian fields and gaussian markov random fields: the stochastic partial differential equation approach. *Journal of the Royal Statistical Society Series B: Statistical Methodology*, 73(4):423–498, 2011.
- Marta Blangiardo and Michela Cameletti. *Spatial and spatio-temporal Bayesian models with R-INLA*. John Wiley & Sons, 2015.
- David Bolin and Finn Lindgren. Spatial models generated by nested stochastic partial differential equations, with an application to global ozone mapping. *The Annals of Applied Statistics*, pages 523–550, 2011.

- Rikke Ingebrigtsen, Finn Lindgren, and Ingelin Steinsland. Spatial models with explanatory variables in the dependence structure. *Spatial Statistics*, 8:20–38, 2014.
- Finn Lindgren, David Bolin, and Håvard Rue. The spde approach for gaussian and non-gaussian fields: 10 years and still running. *Spatial Statistics*, 50:100599, 2022.
- Finn Lindgren and Håvard Rue. Bayesian spatial modelling with r-inla. *Journal of statistical software*, 63(19), 2015.
- Virgilio Gómez-Rubio. *Bayesian inference with INLA*. CRC Press, 2020.
- Alan E Gelfand, Athanasios Kottas, and Steven N MacEachern. Bayesian nonparametric spatial modeling with dirichlet process mixing. *Journal of the American Statistical Association*, 100(471):1021–1035, 2005.
- Montserrat Fuentes and Brian Reich. Multivariate spatial nonparametric modelling via kernel processes mixing. *Statistica Sinica*, 23(1), 2013.
- Jason A Duan, Alan E Gelfand, and CF Sirmans. Modeling space-time data using stochastic differential equations. *Bayesian analysis*, 4(4):733–758, 2009.
- Charles C Driver and Manuel C Voelkle. Hierarchical bayesian continuous time dynamic modeling. *Psychological methods*, 23(4):774, 2018.
- Noel Cressie and Christopher K Wikle. *Statistics for spatio-temporal data*. John Wiley & Sons, 2015.
- Suman Guha. *Some Theoretical and Methodological Contributions to the Dynamic Modeling of Discrete-Time Spatial Time Series Data*. PhD thesis, Indian Statistical Institute, Kolkata, 2017.

- Michael Betancourt. A conceptual introduction to hamiltonian monte carlo. *arXiv preprint arXiv:1701.02434*, 2017.
- Sai Hung Cheung and James L Beck. Bayesian model updating using hybrid monte carlo simulation with application to structural dynamic models with many uncertain parameters. *Journal of engineering mechanics*, 135(4):243–255, 2009.
- Joan-Andreu Lázaro-Camí and Juan-Pablo Ortega. Stochastic hamiltonian dynamical systems. *arXiv preprint math/0702787*, 2007.
- Jialin Hong, Baohui Hou, Qiang Li, and Liying Sun. Three kinds of novel multi-symplectic methods for stochastic hamiltonian partial differential equations. *Journal of Computational Physics*, 467:111453, 2022.
- Peter Young. The leapfrog method and other symplectic algorithms for integrating newton’s laws of motion. *Lecture notes in University of california, santa cruz*, 2014.
- M. L. Stein. *Interpolation of Spatial Data: Some Theory for Kriging*. Springer-Verlag, New York, Inc, 1999a.
- CE Rasmussen and CKI Williams. *Gaussian process for machine learning*. the MIT Press, 2006.
- Michael L. Stein. *Interpolation of Spatial Data*. Springer, New York, 1999b.
- Hao Zhang. Inconsistent estimation and asymptotically equal interpolations in model-based geostatistics. *Journal of the American Statistical Association*, 99(465):250–261, 2004.
- Sudipto Banerjee. Modeling massive spatial datasets using a conjugate bayesian linear modeling framework. *Spatial Statistics*, 37:100417, 2020.

Moumita Das and Sourabh Bhattacharya. Transdimensional transformation based markov chain monte carlo. *Brazilian Journal of Probability and Statistics*, 33(1): 87–138, 2019.

Sudipto Banerjee, Bradley P Carlin, and Alan E Gelfand. *Hierarchical Modeling and Analysis for Spatial Data*. CRC press, Boca Raton, Florida, 2nd edition, 2015.